

## AN ABSTRACT OF THE THESIS OF

Stephanie R. Wafforn for the degree of Master of Science in Geology presented on July 11, 2013.

Title: Structural Geology of the Mount Polley Cu-Au District, South-Central British Columbia.

Abstract approved:

---

John H. Dilles

Andrew J. Meigs

The Mount Polley copper-gold deposit is one of a series of porphyry copper deposits that occur in a belt of accreted Mesozoic age island arc terranes in the Canadian Cordillera. The deposit comprises three breccia-hosted Cu-Au ore zones that are associated with a series of monzodiorite to monzonite intrusions emplaced into the Nicola Group in the Late Triassic. The Mount Polley deposit has been deformed in a number of structural events and the relative sequence of folding, faulting, and tilting provides insight into the tectonic history of the Quesnel Terrane.

During a period of 8 million years, from 205 Ma to 197 Ma, the Mount Polley deposit was emplaced into the Nicola Group, exhumed to the surface, and buried beneath a sequence of conglomerates, sandstones, and a quartz latite ignimbrite. The oldest faults in the district are the north-northwest-striking reverse faults. These include the Polley Fault and East Cariboo Fault, which displace intrusions, mineralized ore zones, and

plagioclase and K-feldspar porphyry dikes. Reverse faults are coeval with a regional folding event that formed a doubly plunging synform whose fold axis plunges to the northwest in the Mount Polley district. The North Springer Fault is a southwest-striking sinistral fault that cuts the Polley Fault and the East Cariboo Fault. The youngest faults in the district are the Green Giant Fault and the Center Fault, which is inferred from drill hole data. The Green Giant Fault cuts the intrusions, mineralized ore zones, and both porphyry dikes and post-mineral dikes.

A tilting event of unknown age resulted in a 30-35° NW tilt of the sedimentary beds, ore bodies, and dikes in the Mount Polley district. A limited number of apatite fission track data suggest that the district cooled through the apatite partial annealing zone during the Paleocene to Eocene. This study provides insight into the local structural geology of the Mount Polley Cu-Au deposit, and the history of island arc accretion, hinterland development, and post-convergence extensional modification of allochthonous terranes in the Canadian Cordillera.



©Copyright by Stephanie R. Wafforn

July 11, 2013

All Rights Reserved

Structural Geology of the Mount Polley Cu-Au District, South-Central British Columbia

by

Stephanie R. Wafforn

A THESIS

submitted to

Oregon State University

in partial fulfillment of

the requirements for the

degree of

Master of Science

Presented July 11, 2013

Commencement June 2014

Master of Science thesis of Stephanie R. Wafforn presented on July 11, 2013

APPROVED:

---

Major Professor, representing Geology

---

Dean of the College of Earth, Ocean, and Atmospheric Sciences

---

Dean of the Graduate School

I understand that my thesis will become part of the permanent collection of Oregon State University libraries. My signature below authorizes release of my thesis to any reader upon request.

---

Stephanie R. Wafforn, Author

## ACKNOWLEDGEMENTS

First and foremost I'd like to thank my advisors John Dilles and Andrew Meigs for their guidance, support, and help in completing my Master's thesis. I've learned so much working on this project. I'd also like to thank my committee members Dick Tosdal and Nick Piasias for their input, and my field assistants Peter Taylor and Aaron Olson.

Funding for this project and access to the mine site was provided by Imperial Metals. Patrick MacAndless, Steve Robertson, Chris Rees, Lee Ferreira, Melissa Darney and all the geologists at Mount Polley provided great logistical support and numerous insightful conversations into the geology of the Mount Polley district. I received additional funding from NSERC, SEG, and GeoScience BC. A to Z Fission Track provided the apatite fission track data and helpful discussion regarding the methodology and interpreting the data.

I would like to thank my Mum and Dad for their love and support. My friends and I have shared many good times in Corvallis, and Willamette Sport Horses has been a home away from home. Finally I have to thank Nevada, Jury, and Rudy, because no hour of life is wasted that is spent in the saddle.

# TABLE OF CONTENTS

	<u>Page</u>
1: Introduction.....	1
2: Tectonic Setting and Regional Geology .....	3
2.1 Tectonic Setting.....	3
2.2 Geology of the Nicola Group .....	4
2.3 Structural Geology of the Quesnel Terrane.....	5
3: Geology of the Mount Polley Igneous Complex .....	7
3.1 Intrusions in the Mount Polley district.....	7
3.2 Cu-Au Ore Zones .....	9
3.3 Mineralization in the Central Zone .....	9
3.4 Mineralization and Breccia in the Northeast Zone.....	10
3.5 Sedimentary Units .....	11
4: Methods .....	13
4.1 Field Mapping .....	13
4.2 Copper Grade on Cross Sections .....	14
4.3 Structural Analyses .....	15
4.4 Apatite Fission Track Ages .....	16
5: Results.....	19
5.1 Field Relationships and Intrusion Ages in the Mount Polley District.....	19
5.2 Structural Orientations of Planar Features .....	21
5.3 Nature of Faults in the Mount Polley district.....	21
Polley Fault.....	21
East Cariboo Fault .....	22
North Springer Fault.....	23
Green Giant Fault .....	23
Center Fault .....	24
Brown Wall Fault .....	25
5.4 Nature of the Fold and Tilt in the Mount Polley District .....	25

## TABLE OF CONTENTS (Continued)

	<u>Page</u>
5.5 Apatite Fission Track Ages .....	26
6: Discussion .....	27
6.1 Nature of Fault Separation .....	27
Polley Fault .....	27
East Cariboo Fault .....	27
North Springer Fault .....	28
Green Giant Fault .....	28
Center Fault .....	29
6.2 Nature of Tilting .....	30
Magnitude of Tilting .....	30
Restoration of Tilting .....	31
Causes of Tilting .....	33
6.3 Restoration of Post Mineral Deformation .....	35
Central Zone Restoration .....	35
Northeast Zone Restoration .....	36
Mount Polley District Restoration .....	38
6.4 Cooling History of the Mount Polley District .....	40
6.5 Three Structural Events Impacting the Quesnel Terrane .....	42
6.6 Regional Implications of the Structural Events .....	45
7: Conclusion .....	48
References .....	50
Appendices .....	83

## LIST OF FIGURES

<u>Figure</u>	<u>Page</u>
1. Tectonic Setting .....	57
2. Regional Geology Map .....	58
3. Stratigraphic Section .....	60
4. A-A' Cross Section .....	61
5. Geology Map of the Mount Polley district .....	62
6. Bench Map of the Central Zone .....	64
7. Bench Map of the Wight Pit .....	65
8. B-B' Cross Section .....	66
9. Illustration of Copper Grade Simplifications .....	67
10. Stereonets showing Structural Data .....	68
11. Photos of Fault Planes .....	69
12. C-C' Cross Section .....	70
13. D-D' Cross Section .....	71
14. Cu Contour Map across the North Springer Fault .....	72
15. E-E' and F-F' Cross Sections .....	73
16. Structural Contour Map of the Center Fault Plane .....	74
17. Stereonets showing Restoration of Tilt .....	75
18. Restoration of the Central Zone .....	76
19. Restoration of the Northeast Zone .....	77
20. Restoration of the Mount Polley District .....	78
21. Cooling curve of the Mount Polley district .....	79
22. Time line of structural events in the Mount Polley district .....	80

## LIST OF TABLES

<u>Table</u>	<u>Page</u>
1. Summary of geochronology data available for the Mount Polley district .....	81
2. Apatite fission track ages .....	82
3. Depth ranges corresponding to the closure temperatures of the minerals used for thermochronometry .....	82



## LIST OF APPENDICES

<u>Appendix</u>	<u>Page</u>
1. Apatite Fission Track Sample Locations and Descriptions .....	83
2. Apatite Fission Track Age Data .....	84
3. Apatite Fission Track Length Data .....	90

## **1: Introduction**

Porphyry copper deposits are principally associated with subduction-related magmatism on continental and island arcs (Sillitoe, 2010). In the Canadian Cordillera accreted island arc terranes host a belt of porphyry copper deposits that were emplaced between 210 Ma and 195 Ma (McMillan et al., 1996; Mortenson et al., 1995; Lang et al., 1995). One of these island arc complexes is the Quesnel Terrane (Mortimer, 1987; Panteleyev et al., 1996; Logan and Mihalynuk, 2005), which hosts the Cu- Au deposit at Mount Polley. This deposit is considered to be an alkalic porphyry copper deposit (Barr et al., 1976; Lang et al., 1995; Logan et al., 2007). The Mount Polley Cu-Au deposit is characterized by three breccia-hosted Cu-Au ore zones associated with monzonitic intrusions emplaced into the Nicola Group country rock (Figure 1) (Fraser et al., 1995; Gillstrom, 2004; Logan and Mihalynuk, 2005).

Deformation following the Mount Polley district mineralization reflects one or more of the structural events that have impacted the Quesnel Terrane. The earliest of the structural events include potential inter-arc collisions in the Late Triassic (Lang et al., 1995) and Middle Jurassic accretion onto the North American continent (Monger et al., 1982; Dickinson, 2004). The Quesnel Terrane subsequently existed in the hinterland of the Canadian Cordillera until the Eocene, when development of a large scale dextral strike-slip fault system resulted in extension and normal faulting in step-overs between fault strands. In southern British Columbia, Idaho, and Montana subduction of the Kula-Farallon spreading ridge formed a slab window that caused extensive magmatism and formed the Challis-Kamloops magmatic belt (Breitsprecher et al., 2003; Struik, 1993; Lowe et al., 2001).

Geologic mapping studies in the Mount Polley district have largely focused on identification of intrusions and the nature of brecciation (Fraser, 1994; Jackson, 2008; Rees,

2012). Jackson (2008) found mineralized, fluidal clasts of K-feldspar porphyry dike in the Northeast Zone breccia, indicating that the dike was hot and ductile at the time of brecciation and mineralization. Logan et al. (2007) and Mortenson et al. (1995) used the U-Pb zircon and  $^{40}\text{Ar}/^{39}\text{Ar}$  methods to determine the ages of intrusions in the Mount Polley district. Little is known about the relative timing of the post-ore deformation events. Regional structural studies have been completed in the Likely region north of Mount Polley (Bloodgood, 1998), and along the Eureka thrust fault to the east of Mount Polley (Rees, 1981; Fillipone and Ross, 1990). Multiple folding and thrust faulting events are observed in both regions; however, evidence for normal faulting and extension is not well established.

The objectives of this study are to evaluate the structural geology and the nature of post-ore deformation of the Mount Polley deposit. Bench mapping, regional mapping, construction of cross sections, and structural analysis constrain the relative sequence of faulting, folding, and tilting. The geometry of the ore bodies and associated alteration and copper mineralization assemblages are used to understand the nature of the deformation. Using these structural data, the ore bodies in the Mount Polley district are restored. These restorations provide insights for future exploration, as they may indicate where previously unidentified parts of the ore body have been displaced. Furthermore, this study also provides insight into the history of island arc accretion, hinterland development, and post-convergence extensional modification of the Canadian Cordilleran orogenic belt.

## **2: Tectonic Setting and Regional Geology**

### 2.1 Tectonic Setting

The Canadian Cordillera is composed of five morphogeologic belts, which include the ancient North American continental passive margin, accreted pericratonic terranes, and accreted allochthonous terranes (Monger et al., 1972; Monger and Price, 2002; Nelson and Colpron, 2007). The Intermontane Belt makes up much of the interior of British Columbia and includes Devonian to Early Jurassic age plutonic, volcanic, and sedimentary rocks that formed in an island arc setting (Monger et al., 1982; Monger and Price, 2002). One of these island arcs is the Quesnel Terrane, which formed as a product of volcanism above a subduction zone proximal to the North American craton (Figure 1) (Unterschultz, 2002). Accretion of island arcs occurred during the Early-Middle Jurassic, and the geology, including large suture zones between juxtaposed tectonic terranes, suggests severe structural telescoping onto the miogeocline of the Canadian Cordillera (Dickinson, 2004). Mesozoic to Cenozoic retroarc thrusting juxtaposed Quesnel Terrane with the Cache Creek Terrane accretionary complex. Following thrusting, the Quesnel Terrane represented part of the Canadian Cordilleran hinterland, where it remained largely undeforming from the Cretaceous to the Early Eocene (Dickinson, 2004).

Widespread crustal extension affected the Canadian Cordillera in the Eocene. This is evidenced by the presence of normal faults, exposed metamorphic core complexes, and stretching lineations (Lowe et al., 2001). Coeval widespread magmatism initiated at 60 Ma, was at a maximum by 50 Ma, and was sporadic and localized by 40 Ma (Dostal et al., 1998). Initiation of magmatism corresponded with a major plate reorganization in the Pacific basin: subduction of the Kula-Farallon spreading ridge formed a slab window in the Pacific Northwest (Breitspecher et al., 2003), following which the North America and Farallon plates changed from

orthogonal to oblique convergence (Engebretson et al., 1985; Hyndman and Hamilton, 1993). This transition resulted in the formation of dextral strike-slip fault systems that were active during the Tertiary in central British Columbia (Figure 1) (Struik, 1993). Extensional faults connect the en-echelon strands of dextral strike-slip faults, thereby transferring motion from one strike-slip fault to another. The dextral strike-slip faults are mainly northwest- and north-striking, and the normal faults are largely northeast-striking (Wheeler and McFeely, 1987). These faults offset folded thrust sheets in the Cache Creek, Quesnel, Slide Mountain, Cassiar and McGregor terranes (Struik, 1993).

The slab window formed by subduction of the Kula-Farallon spreading ridge resulted in the formation of the Challis-Kamloops volcanic belt. In addition to extension, magmatism also corresponded with an intense period of uplift and granitic plutonism in the Intermontane Belt, the Coast Belt, and the Omineca Belt (Woodsworth et al., 1991). The composition of the volcanic rocks tends to be calc-alkaline, with a predominantly andesite composition (Dostal et al., 1998). Following the period of magmatism and extension, the plate motions along the British Columbia margin changed to essentially strike-slip (Engebretson et al., 1985).

## 2.2 Geology of the Nicola Group

The Nicola Group comprises a diverse range of Late Triassic to Early Jurassic submarine to subaerial rocks that underlies a large portion of the Quesnel Terrane in south-central British Columbia, including the Mount Polley district (Figure 2) (Mortimer, 1987). It is one of the many examples of early Mesozoic volcanism in the North American Cordillera. The oldest, basal assemblage of the Nicola Group comprises volcano-sedimentary rocks that include abundant tuffs, siltstones, limestones, and sandstones (Figure 3) (Panteleyev et al., 1996; Logan and

Mihakynuk, 2005; Bath and Logan, 2006). This assemblage is interpreted to have been deposited in a restricted marginal basin, marking the initiation of island arc volcanic activity (Travers, 1977; Mortimer, 1987). The overlying assemblage is a 5.0 - 6.5 km thick sequence of Carian-Norian submarine, alkali basalts (Figure 3). Norian age limestone lenses, debris-flow breccias, and tuffs fill intervolcanic depressions, and lateral facies changes are locally common (Panteleyev et al., 1996). Norian basalts and limestone lenses make up the basement rocks in the Mount Polley district.

The Mount Polley igneous complex cuts the sequence of basalts, and includes a suite of dioritic to monzonitic plutons. In the case of Mount Polley, these intrusions are associated with Cu-Au mineralization. Unconformably overlying the Mount Polley igneous complex is an Early to Middle Jurassic clastic sequence of conglomerates, poly lithic sedimentary breccias, sandstones and tuffs (Bailey, 1988; Monger et al., 1991). This unit has variably been included as part of the Hazelton Group and the Ashcroft Formation (Gordee, 2006; Travers, 1978). The lithostratigraphic section of the Hazelton Group is very similar to that found in the Mount Polley district, including a greyish-maroon tuff overlain by sandstones and conglomerates. The Hazelton Group, however, has only been identified in the Stikine Terrane (Gordee, 2006). The Ashcroft Formation, on the other hand, is located in the Quesnel Terrane but does not have a similar lithostratigraphic section. It remains unknown to which formation the stratigraphic section overlying the Mount Polley igneous complex belongs.

### 2.3 Structural Geology of the Quesnel Terrane

At the latitude of the Mount Polley district the Quesnel Terrane is faulted on the west against the Late Proterozoic to Middle Mesozoic Cache Creek Terrane (Monger and McMillan,

1989). To the east there is an angular unconformity between the Triassic Nicola Group and the Paleozoic Chapperon Group, and a thrust fault contact between the Quesnel Terrane and the Slide Mountain Terrane (Read and Okulitch, 1977). The Lower Jurassic Ashcroft Formation unconformably overlies the Nicola Group in much of the Quesnel Terrane (Travers, 1978).

There are two phases of folding identified in the Mount Polley region. The  $F_1$  deformation event is represented by northeast-verging isoclinal, overturned, and recumbent folds that occur at a variety of scales (Bloodgood, 1988). The  $F_2$  folds occur as open, buckle, and kink folds that plunge gently to the northwest and southeast, and have axial planes that dip moderately to the northeast and southwest (illustrated in Figure 4). The major thrust fault in the area is the Eureka thrust, which is a low angle, southwest dipping fault that thrusts the Quesnel Terrane over the Paleozoic Crooked Amphibolite. Large thrust faults are also mapped at the base of a metasedimentary package and at the base of a tuff-phyllite unit. Smaller reverse faults oriented north-south are locally common. Thrust faults in the region are believed to be synchronous with the first phase of folding, and are overprinted by the  $F_2$  deformation event.

Numerous steeply dipping, northeast-striking normal faults occur in the area west of the Eureka Fault. These faults clearly post-date the regional folding, however, recognition of major through-going faults is made difficult by the subtlety of the stratigraphic variations (Bloodgood, 1988). Normal faults are believed to be related to Tertiary dextral strike-slip faults that dominate the structure of much of the Quesnel Terrane (Zhang and Hynes, 1994). In the Mount Polley district there are a number of young, northeast-oriented normal faults that were identified by the British Columbia Geological Survey based on both stratigraphic and geophysical data (shown on Figure 2) (Logan et al., 2005).

### **3: Geology of the Mount Polley Igneous Complex**

#### **3.1 Intrusions in the Mount Polley district**

There are three main intrusions in the Mount Polley district, which are gradational between diorite, monzodiorite, and monzonite (Fraser, 1994; Jackson, 2008). These are divided into three map units: Pd1, Pd2 and Pmd (Figure 5). The Pd1 unit is the oldest intrusion which comprises an equigranular augite-biotite diorite. Locally the rock has up to 20 vol. % secondary hydrothermal K-feldspar. Minor amounts of hornblende, magnetite, and disseminated pyrite are also present. The Pd2 unit is a diorite to monzodiorite that intrudes the Pd1 unit in the Bell Pit. The bulk of the Mount Polley igneous complex is the Pmd unit, which is dominated by equigranular augite-bearing monzonite, with lesser K-feldspar bearing diorite and monzodiorite. Where unaltered the rock is creamy gray to pinkish gray, and equigranular to microporphyritic. Compared to the Pd2 unit, the Pmd unit has primary K-feldspar minerals, however, K-feldspar is often less abundant than plagioclase in unaltered rock. Pyrite is commonly found disseminated and in thin veins (<1 mm) in the Pmd unit, generally composing <1% of the rock. Where observed in outcrop, the contact between Pd2 and the Pmd unit is gradational, and distinguishing between Pd2 and Pmd can be complicated by the presence of K-feldspar alteration.

There are three smaller intrusions in the Mount Polley district. The Pmz unit is similar to the Pmd unit, however, Pmz is a more homogenous monzonite that intrudes Pmd. Pmz is grey to pale pink, locally stained red, medium- to coarse-grained, and contains more abundant mafic minerals (>10% augite and minor primary biotite) than the older intrusions (Gillstrom, 2004). A banded dioritic porphyry, the Pdb unit, is pale green to pale gray and fine- to medium-grained. The youngest intrusion in the Mount Polley district is a Jurassic monzodiorite stock found north



of the Junction Zone. The monzodiorite is dark grey, very fine grained, and contains <1 – 2mm K-feldspar and plagioclase crystals.

I divided the dikes in the Mount Polley igneous complex into four map units: two porphyry dikes and two post-mineral dikes. The K-feldspar phyric porphyry dikes, the Pkm unit, comprises irregular to tabular bodies that cut all older intrusions. Rees et al. (2006) identified a coarse-grained K-feldspar porphyry dike that has 1-4 cm long, stubby to blocky K-feldspar phenocrysts that locally show a trachytic texture in a medium-grained groundmass (referred to by Jackson (2008) as megacrystic K-feldspar porphyry dike), and a fine-grained K-feldspar porphyry dike that has 1 mm – 1 cm K-feldspar phenocrysts, which are much more abundant than they are in the coarser dikes. Both the fine- and coarse-grained dikes are almost always strongly altered with K-feldspar constructive alteration. Disseminated hematite is common, giving the rock a strong reddish-orange to pink colour, and disseminated pyrite is also widespread. Disseminated chalcopyrite is locally present, but does not constitute ore grades in most areas (Rees and Ferriera, 2006). Plagioclase feldspar porphyry dikes, the Ppp unit, are irregular to tabular in shape, and vary between <1 m and >10 m width. The Ppp typically contains abundant plagioclase phenocrysts that are up to 5 mm in length in a monzonitic groundmass. The rock is grey to red-pink when altered with K-feldspar constructive alteration and hematite alteration.

The youngest dikes in the Mount Polley igneous complex are widespread augite porphyry dikes and fine-grained monzodiorite dikes of the Pap unit. The augite porphyry dikes are distinguished by 20-30% coarse, euhedral, dark green augite phenocrysts in a fine grained pale-green groundmass. These dikes crosscut the intrusions, the mineralized breccia bodies, and the plagioclase porphyry dikes. They are generally unaffected by hydrothermal alteration (Rees et

al., 2005). The monzodiorite dikes are fine-grained to aphyric, and typically no wider than 2 m. They are thought to be related to the JrMz unit, which is the youngest monzonite intrusion in the Mount Polley igneous complex.

### 3.2 Cu-Au Ore Zones

Mineralization in the Mount Polley district is divided into three zones: the Northeast Zone, Central Zone and Southeast Zone. Each of these zones is further divided into exploration targets, some of which have subsequently been developed into open pits and mined. The Northeast Zone comprises the Wight Pit and the Boundary Zone, Quarry Zone, and Leak Zone, along with other minor exploration targets. The Central Zone comprises the Springer Pit, Cariboo Pit, and Bell Pit and the C2 Zone and WX Zone exploration targets. Future expansion of the Springer Pit is planned in order to mine the C2 mineralization. The Southeast Zone comprises the Southeast Pit and the Pond Zone Pit, both of which have been mined out.

### 3.3 Mineralization in the Central Zone

The Springer, Cariboo, and Bell Open Pits, and the C2 and WX exploration targets are all part of the Central Zone at Mount Polley. Given that the Cariboo and Bell Pits have already been mined out, the focus of this section is mineralization and alteration mapped in the Springer Pit. Mineralized rock in the Springer pit consists of pink, potassically altered poly lithic breccia with angular clasts that range in composition from black, fine-grained volcanic rocks to grey monzodiorite. The matrix comprises abundant fine-grained plagioclase crystals, which can be tabular or broken, and abundant very fine-grained anhedral K-feldspar crystals. Additional lithologies found in the Springer Pit include monzonite in the north and east walls, diorite in the

southeast wall, and a large plagioclase porphyry dike in the south wall. Plagioclase porphyry and augite porphyry dikes, between 1 – 5 m in width, are common throughout the pit (Figure 6).

Copper mineralization is largely composed of chalcopyrite, which occurs disseminated, in veins, and in blebs. Minor amounts of bornite, and trace amounts of supergene mineralization, including covellite, chalcocite, and digenite, are also present. Copper oxides are present in varying amounts throughout the Springer Pit: malachite and azurite occur as fracture fill, and chrysocolla occurs in fractures, veinlets and as blebs. In the strongly mineralized areas veins and veinlets of calcite, epidote, actinolite, and microcline are abundant (Gillstrom, 2004). Magnetite is found within the breccia matrix, and the presence of magnetite correlates to zones of high grade Cu-Au mineralization.

### 3.4 Mineralization and Breccia in the Northeast Zone

The Northeast Zone is the most recent ore body discovered on the Mount Polley property. Mineralization in the Northeast Zone is breccia-hosted, where the hydrothermal breccia consists of a rotated and chaotic facies (often described as a fragmental breccia) and a crackle facies (Figure 7), which reflects a decreasing amount of energy and transport away from the center of brecciation (Jebrak, 1997). Approximately 90% of the clasts are composed of K-feldspar phyric monzonite and the remaining 10% of the clasts are volcanic or strongly potassically altered (Tosdal et al., 2008). Jackson (2008) studied the breccia morphology and mineralogy in the Northeast Zone and found that the breccia body is irregular in shape. The majority of the Cu-Au bearing sulfide minerals form as hydrothermal minerals found in the matrix of the breccia. Chalcopyrite and bornite is most concentrated surrounding a zone of globular-shaped clasts,

implying that the clasts were still ductile at the time of brecciation. This relationship suggests that the fluids responsible for mineralization and brecciation are the same (Jackson, 2008).

There is a clear zonation in the major hydrothermal minerals in the Northeast Zone. Magnetite is present in the deepest part of the ore body. It is commonly replaced by chalcopyrite and, less commonly, pyrite. In the core of the ore body bornite and chalcopyrite co-exist, although cusped textures indicate replacement of bornite by chalcopyrite. In the shallow portions of the ore body the mineralization is dominantly chalcopyrite (Tosdal et al., 2008). In general there is a correlation between high Cu-Au ore grades and (1) breccia that has significant clast transport (fragmental breccia), (2) a matrix composed of hydrothermal minerals as opposed to clastic infill, and (3) a high concentration of fluidal K-feldspar porphyry clasts (Jackson, 2008).

### 3.5 Sedimentary Units

Overlying the monzonite in the Northeast Zone is a pronounced unconformity overlain by a basal conglomerate. The base of the conglomerate section is monomictic, comprising coarse and angular clasts of the underlying monzonite and a rusty colored silty to sandy matrix (Figure 8) (McMillan, 1974). Based on the textural and compositional immaturity of the conglomerate at the base of the section, and the derivation of clasts from the Mount Polley monzonite, the conglomerate is a proximal deposit. This part of the section is exposed immediately north of the Junction Zone. Up section the conglomerate is interbedded with coarse-grained sandstone. Clasts in the conglomerate become subrounded and polymictic, with addition of volcanic clasts that are not sourced from the Mount Polley igneous complex. This part of the section is exposed at surface in the area immediately north and northwest of the Northeast Zone. The polyolithic nature

of the clasts implies an increasingly distal source, possibly due to burial of the Mount Polley district. Tosdal (2008) interpreted the compositional and textural variations in the section to represent fanglomerate deposition on alluvial fans.

Interbedded with the conglomerate is a densely welded quartz-latitude ignimbrite (Figure 8). Crystals include tabular and broken plagioclase laths (<3 mm), hornblende (2-3 mm prisms), quartz eyes, and biotite (2-3 mm booklets). The ignimbrite contains broken lithic fragments, shard-like fragments, and a devitrified glassy matrix. There are also abundant fiamme. The interpreted age of the quartz latitude ignimbrite is  $196.7 \pm 1.3$  Ma, which is based on 4 multigrain zircon fractions of 2-6 grains which were analyzed using TIMS for the U/Pb isotopic compositions and yield a concordant age (Logan et al., 2007). Given that neither the conglomerate nor the quartz latitude ignimbrite are mineralized, this age provides an upper limit for the age of mineralization and a lower limit for the age of the unconformity.

## 4: Methods

### 4.1 Field Mapping

Field mapping was completed during two field seasons at the Mount Polley mine site. Mapping in the Northeast Zone, Quarry Zone, and area north of the Junction Zone was completed at the 1:5000 scale and 1:10,000 scale. Bench mapping in the Wight Pit, Springer Pit, Boundary Pit, uppermost bench of the Cariboo Pit, and the Wishbone Road trench was completed at the 1:500 and 1:200 scale. Structural orientations (strike and dip) were recorded using the right hand rule. For example, a dike striking  $270^{\circ}$  and dipping  $45^{\circ}$  north is recorded as  $270^{\circ}/45^{\circ}$ . Mapping employed a modified Anaconda method (Einaudi, 1997). Particular attention was paid to contacts and changing alteration assemblages, and structural measurements were taken on faults, joints, dikes, and veins. Float mapping at the 1:7,500 scale was completed in the forested area north of the main Polley access road. Due to limited outcrop exposure, this technique was used to establish the approximate location of the contact between the monzonite and the overlying conglomerate. Minor regional mapping at the 1:50,000 scale was completed along the logging roads around Trio Lake, Jacobie Lake, and Gavin Lake Road (Appendix A), however, few structural measurements were obtained.

To complement field mapping observations, core from exploration drill holes around the Mount Polley property was examined. Detailed logging at 1:400 scale was completed for drill holes WB-07-239, WB-07-240, and WB-07-242 that intersect the unconformity between the Pcgl conglomerate and the Pmdu monzonite, and provide insight into the stratigraphy in the overlying sedimentary rocks. In the Wight Pit drill holes were used to evaluate the orientation and nature of the Green Giant fault and Center fault. Changes in the lithology, alteration, and

breccia style were also logged in order to characterize differences between the upper and lower ore bodies, and the host monzonite. In the Central Zone drill holes were used to establish the physical location and orientation of the Polley Fault, East Cariboo Fault, and the North Springer Fault. Lithology and copper grade data from the Mount Polley drill hole database were used to interpret and illustrate the geometry of the ore bodies and estimate separation across faults.

#### 4.2 Copper Grades on Cross Sections

Cross sections were constructed to include the Cu grade data for use in estimating the separation on faults in the Mount Polley district. Lithology was not used because the polyolithic nature of the breccia clasts makes correlation between breccias difficult, even with tightly spaced drill cores. Taking into account this limitation, the cross sections were constructed using copper grade, as it is more consistent and better delineates the extent of the mineralized breccia than the lithologic contacts.

The Central Zone has 64,604,000 tonnes of proven and probable resource, with average grades of 0.310 wt% Cu and 0.259 gram/ton Au, whereas the Northeast Zone has 19,058,806 tonnes of measured resource, with average grades of 0.568 wt% Cu and 0.201 gram/ton Au (Imperial Metals, 2013). As such, the copper grade in both the Central Zone and the Northeast Zone was divided into three categories: >0.5 wt% Cu, 0.1 - 0.5 wt% Cu, and <0.1 wt% Cu. Grade >0.1 wt% Cu is considered to be part of the ore zone, whereas <0.1 wt% Cu is considered to be background. Differences in grade can be attributed to the presence of bornite in the >0.5 wt% Cu category, and the presence of chalcopyrite in the 0.1 - 0.5 wt% Cu category (Jackson, 2008).

In constructing the cross sections a number of assumptions and simplifications were required. Copper assay data is available on 1 to 2.5 m sampling intervals from each drill core and is reported to 0.01 wt% Cu. The detection limits are 1 ppm for Cu and 2 ppb for Au (Imperial Metals, 2012). In order to categorize the copper assays a depth vs. wt% Cu chart was constructed (Figure 9). Depth intervals where the assay values were 0.01 wt% Cu, with no individual interval >0.1 wt Cu were assigned to the <0.1 wt% category. Depth intervals where the assay values were between 0.1 – 0.5 wt% Cu and >0.1 wt% Cu were assigned to those respective categories (Figure 9). Within these intervals, if there was an assay that was lower than the rest of the category (ex. a <5 m interval of 0.01 wt% Cu located inside the >0.5 wt% Cu category) it was ignored and attributed to the presence of a non-mineralized breccia clast or post-mineral dike. The cross sections were constructed by first plotting the drill holes onto the section. The copper grade intervals were then marked next to the drill holes. By correlating between the drill holes on the section the subsurface geometry of the ore body was interpolated.

#### 4.3 Structural Analyses

Structural analyses were completed using stereonet, contouring of copper grade, contouring of structural planes, and 3D visualization software, including Leapfrog Geo and Minesight. Poles to planes were plotted on equal area lower hemisphere projections using Stereosoft 7 software (Allmendinger et al., 2012). Contours of the copper grade were constructed in a similar manner to the cross sections: the drill holes were plotted onto the cross section and the copper grade category was marked at the proper depth intervals next to the drill hole. By contouring between the drill holes, the shape of the >0.1 wt% Cu contour and the >0.5 wt% Cu contour was interpolated. Note that the same simplifications made in constructing the cross sections were also made in constructing the contours in order to eliminate variations caused by



the polyolithic nature of the breccia or the post-mineral dikes. Structural contours on faults in the Northeast Zone were constructed by identifying the depth of the fault in drill core photos, drawing multiple cross sections across the plane, marking the depth of the fault plane on the map, and contouring. The strike and dip of a fault plane is determined from the contour map. Restorations were completed schematically, using all available structural data. Estimates were made as to the magnitude of separation along each fault plane, based on the inferred original geometry of the ore bodies.

#### 4.4 Apatite Fission Track Ages

A pilot apatite fission track (AFT) study was conducted on apatite grains taken from three drill core samples of unaltered monzonite. Sample preparation and analysis was completed by A to Z Fission Track (Viola, Idaho). All samples were taken from 900 m above sea level. Samples were crushed using multiple runs through a jaw-crusher, and sieved using 300  $\mu\text{m}$  sieve cloth. The  $<300 \mu\text{m}$  fraction was separated for apatite using a Frantz Isodynamic magnetic separator, which separates the grains based on magnetic susceptibility, and organic heavy liquid techniques. Using 10 mL of diiodomethane, grains that have a specific gravity greater than  $3.3 \text{ g/m}^3$ , including zircon, sulfides, and tourmaline, will sink to the bottom and apatite grains will float on top. Separated apatite grains were mounted and polished to reveal clear and flat internal grain surfaces across which spontaneous fission tracks have accumulated. The exposed grains are etched using immersion in 5.5  $\text{HNO}_3$  for 20.0 s ( $\pm 0.05$  s) at  $21^\circ\text{C}$  ( $\pm 1^\circ\text{C}$ ) in order to reveal any spontaneous fission tracks that intersect the polished apatite grain surface (Donelick et al., 2005).

Fission tracks densities and lengths were counted and measured at 1562.5x dry magnification using a Nikon Optiphot2 microscope or at 2000x magnification using a Zeiss

Axioplan microscope. All AFT age and AFT length grains were selected to sample the greatest range of observable characteristics, including size, degree of roundness, color, and etch figure size. As the AFT counts are performed by an analyst, there are inherent biases in each of the measurements, however these biases are minimized by calibrating users and setting standards for fission track counting (Donelick et al., 2005).

A to Z Fission Track uses the LA-ICP-MS technique to measure the  $^{238}\text{U}$  content of the apatite grain and subsequently calculate the fission track age. The  $^{238}\text{U}/^{43}\text{Ca}$  ratio for each data scan was calculated using the background-corrected, sum-of-Gaussian-fitted signal values for the two isotopes. The  $^{43}\text{Ca}$  content is measured in each apatite crystal, and is assumed to be directly related to the amount of apatite ablated. Using this assumption, the ratio of  $^{238}\text{U}/^{43}\text{Ca}$  gives a relative measure of the uranium concentration in apatite. Fission track ages are calculated using the scheme presented by Donelick et al. (2005) using a modified zeta calibration approach after Hurford and Green (1983).

$$t_i = \frac{1}{\lambda} \ln(1 + \lambda \zeta_{MS} g \frac{\rho_{s,i}}{P_i})$$

Where subscript  $i$  refers to grain  $i$ ,  $t_i$  = fission-track age of grain  $i$ ,  $\lambda$  = total decay constant of  $^{238}\text{U}$ ,  $\zeta_{MS}$  =  $\zeta$ -calibration factor based on LA-ICP-MS of fission-track age standards adjusted for the sample position during the LA-ICP-MS session,  $g$  = geometry factor for spontaneous fission-tracks,  $\rho_{s,i}$  = spontaneous fission-track density for grain  $i$ , and  $P_i = (^{238}\text{U}/^{43}\text{Ca})$  for apatite grain  $i$ . The error is calculated using the following equation:

$$\sigma_i = \sqrt{\frac{1}{N_{s,i}} + \frac{\sigma_{p_i}^2}{p_i} + \frac{\sigma_{\zeta_{MS}}^2}{\zeta_{MS}}}$$

Where  $\sigma_i$  = the symmetrical error of the AFT single-grain,  $N_{s,i}$  = number of fission tracks counted for grain  $i$ ,  $\sigma_{Pi}$  = one standard deviation error of  $Pi$ ,  $\sigma_{\zeta MS}$  = one standard deviation error of  $\zeta MS$ . During each LA-ICP-MS session involving an unknown sample, at least 50 spots on the DR apatite FT age calibration standard were analyzed for the purpose of calibrating the  $^{238}\text{U}/^{43}\text{Ca}$  ratio (Donelick et al., 2005).

## 5: Results

### 5.1 Field Relationships and Intrusion Ages in the Mount Polley district

Age relationships for the Mount Polley igneous complex are largely established by isotopic dating techniques due to limited surface exposure. A number of ages have been produced for the various intrusions and are summarized in Table 1. Diorite sampled from one of the Mount Polley igneous complex intrusions has a zircon U-Pb isotopic age of  $201.7 \pm 4$  Ma, and a K-feldspar dikes from the Bell Pit has a zircon U-Pb isotopic age of  $205.0 \pm 0.3$  Ma (Mortenson et al., 1995; Logan et al., 2007). The youngest intrusion in the Mount Polley district is the monzodiorite located north of the Junction Zone, which has a hornblende  $^{40}\text{Ar}/^{39}\text{Ar}$  plateau age of  $165.2 \pm 1.8$  Ma (50.9% of the total  $^{39}\text{Ar}$  released). This age may be considered suspect, as there is a complicated hump-shaped release spectra that may indicate excess argon and possible  $^{39}\text{Ar}$  recoil in the hornblende (Logan et al., 2007).

The majority of the potassium feldspar porphyry and plagioclase porphyry dikes are non-brecciated and non-mineralized, as they were intruded after the main brecciation event (Jackson, 2008). One early generation of K-feldspar phyric porphyry dikes with  $>1$  cm K-feldspar phenocrysts occurs as fluidal clasts in the Northeast Zone breccia. These clasts are typically surrounded by the highest concentrations of copper sulfides, including bornite and chalcopyrite. A lack of brecciated clasts found within breccia clasts implies there was likely only one brecciation event that formed the Northeast Zone breccia (Rees et al., 2005; Logan and Bath, 2006; Jackson, 2008). There are no cross-cutting relationships between the breccia in the Northeast Zone and the Central Zone, therefore the relative age of the breccias is unknown.

The conglomerate in the Quarry Zone is younger than the underlying monzonite. Normal graded beds and imbricated conglomerate clasts show that the bedding is upright. The K-feldspar

porphyry and plagioclase porphyry dikes are older than the conglomerate, as they do not cut the unconformity. A U-Pb zircon age of  $205.01 \pm 0.30$  Ma on a K-feldspar porphyry dike provides a constraint on the maximum age of the unconformity. The quartz latite ignimbrite interbedded with the conglomerate approximately 100 m above the unconformity has a U-Pb zircon age of  $196.7 \pm 1.3$  Ma, a minimum age for the unconformity. The augite porphyry dikes are observed intruding the conglomerate in drill core, and the fine-grained monzodiorite dikes are mapped intruding the conglomerate. The later map location is stratigraphically up section from the quartz latite ignimbrite, which provides a maximum age for the fine-grained monzodiorite dikes.

The age relationships between the major faults are difficult to determine based on field relationships. All major faults in the Mount Polley district cut the igneous intrusions, breccia bodies, and mineralized zones. The Polley Fault, East Cariboo Fault, and North Springer Fault cut the plagioclase porphyry and K-feldspar porphyry dikes, but there are no exposures where the augite porphyry dikes are cut by these faults. Field mapping in the Springer Pit revealed one location where a small reverse fault with 1 m slip displaces a plagioclase porphyry dike but does not displace an augite porphyry dike (Figure 6), implying that the reverse faults are younger than the plagioclase porphyry dikes but older than the augite porphyry dikes. The North Springer Fault cuts both the Polley Fault and the East Cariboo Fault. There are no exposed field relationships between the North Springer Fault and the Green Giant fault; however, the latter is mapped displacing the porphyry dikes, the augite porphyry dikes, and the fine-grained monzodiorite dikes and is likely the youngest fault in the district.

## 5.2 Structural Orientations of Planar Features

Systematic measurements of dike, fault, and bedding orientations were taken throughout the Mount Polley district. The small number of exposed K-feldspar porphyry dikes (N=9) and plagioclase porphyry dikes (N=3) did not indicate a preferred orientation (Figure 10). The augite porphyry dikes (N=75) have a north-northeast preferred orientation; all measured dikes dip steeper than 45°. Bedding measurements of conglomerate and sandstone (N=14) in the Quarry Zone were taken at two locations, one close to the unconformity and one up section from the quartz latite ignimbrite. Bedding was very consistent in both locations, averaging 205°/33° NW.

Orientations of major faults in the Mount Polley district were measured where they are exposed in the open pits. The Polley Fault and the East Cariboo Fault strike north-northwest, and dip 69° NE and 78° NE respectively. The Green Giant Fault is oriented 275°/84° N and the inferred Center Fault is oriented 076°/64° S. The North Springer Fault is the only southwest striking fault in the district and dips 80° NW. The minor faults in the district do not show a preferred orientation, however, the majority dip between 60° and 90°. A small number of faults (N=4) dip less than 45°.

## 5.3 Nature of Faults in the Mount Polley district

### *Polley Fault*

The Polley Fault has been well-known at Mount Polley since the initiation of mining, as it marks the limit of ore grade copper mineralization on the east side in the Springer pit. Where exposed in the Springer Pit the attitude of the Polley Fault is 340°/69° ENE. The fault zone is approximately 30cm wide, and consists of gray rock flour that has in places been oxidized to hematite. There are abundant slickenlines on the fault plane, however, they do not have a

consistent orientation, and may be the result of movement during blasting in the pit. The fault juxtaposes a plagioclase porphyry dike in the footwall against diorite in the hanging wall (Figure 11). Proximal to the fault zone both lithologies have been bleached, and the diorite has pervasive post-mineral calcite and chlorite alteration. The plagioclase porphyry contains 2 wt% copper oxides, including malachite and chrysocolla.

Cross section C-C' (Figure 12) shows that the copper mineralization is different in terms of both grade and morphology on either side of the Polley Fault in the east side of the Springer Pit. In the hanging wall the entire length of the drill core intersects grades of 0.1% to >1% Cu. In the footwall the drill core intersects lengths of 0.1% Cu and lengths of barren rock. This pattern could be indicative of patchy mineralization, or of zones of mineralization, that fingers upwards. Fraser (1994) found that the breccia changes across the fault from an albite cemented breccia in the footwall to an actinolite and biotite cemented breccia in the hanging wall. It is not possible to correlate the plagioclase porphyry mapped at surface in the footwall to any other the dikes intercepted in drill cores in the hanging wall of the fault.

#### *East Cariboo Fault*

By the 2012 field season the Cariboo Pit had been largely filled in, and only the top bench was accessible. Where the East Cariboo fault plane is exposed it has an attitude of  $330^{\circ}/78^{\circ}$  NE, and slickenlines in the plane trend and plunge on average  $165^{\circ}\rightarrow 30^{\circ}$  (Figure 11), suggesting components of dip-slip and strike-slip separation. It is unknown whether these slickenlines are related to the main phase of fault separation, to a secondary phase of fault separation with minor slip, or to blasting-related fabric. The fault comprises a 60 cm wide zone

of fault gouge and clay. Patches of the fault gouge have been cemented with calcite. There are no reliable sense of slip indicators on the fault plane other than the slickenlines.

There is a distinct change in lithology across the fault from pink equigranular monzonite in the footwall to dark grey monzodiorite in the hanging wall. Cross section D-D' (Figure 13) shows the lithologies intersected by drill core in the Cariboo Pit. The monzonite in the footwall has chalcopyrite mineralization and  $>0.1$  wt% Cu, whereas the monzodiorite in the hanging wall typically has  $<0.01$  wt% Cu.

#### *North Springer Fault*

The North Springer Fault is exposed in the northwest part of the Springer Pit. The fault plane has an attitude of  $230^{\circ}/80^{\circ}$  NW, with subhorizontal slickenlines. Calcite slickenfibers indicate a sinistral sense of shear. The fault plane juxtaposes a plagioclase porphyry dike in the northwestern side of the fault with diorite in the southeastern side of the fault. Figure 14 shows sinistral separation of the  $>0.1$  wt% and  $>0.5$  wt% Cu contours across the fault plane.

#### *Green Giant Fault*

The Green Giant fault is a prominent feature in the southwest wall of the Wight Pit, in the Northeast Zone. The fault plane has an attitude of  $275^{\circ}/84^{\circ}$  N, and most often consists of fault gouge that is either pink and monzonitic, likely derived from monzonite clasts found in the polyolithic rotational breccia, or green and chlorite-rich, caused by sheared augite porphyry dikes present in the fault plane. The  $<1$  m wide zone of fault gouge is surrounded by a wider zone of fractured rock (Figure 11). Outcrop and drill core observations indicate that the fault cuts through K-feldspar flooded monzonite, fragmental transported breccia, and augite porphyry dikes.



Cross sections drawn across the Green Giant Fault show that north of the fault plane the lithology comprises polyolithic rotational breccia that has zones of  $>0.5$  wt% Cu with both bornite and chalcopyrite and zones of 0.1 wt% Cu with chalcopyrite (Figure 15). South of the fault plane the lithology comprises crackle breccia and monzonite with  $<0.01$  wt% Cu. Jackson (2008) found significant changes in alteration across the fault plane, where south of the Green Giant Fault the alteration assemblage comprises albite and actinolite, and north of the fault plane the alteration assemblage comprises potassium feldspar flooding of the clasts and matrix in the fragmental breccia. A 10 m wide augite porphyry dike is mapped north of the fault plane, however, it was not identified in drill cores south of the fault plane.

#### *Center Fault*

The Center Fault is an inferred fault identified in drill core, but has not been mapped at surface. Core photos show a  $<10$  m wide fracture zone with minor fault gouge that occurs in otherwise coherent monzonite. In cross sections the fault plane juxtaposes monzonite in the hanging wall with rotational breccia in the footwall. There is a distinct change in Cu grade across the fault from  $<0.1$  wt% Cu in the hanging wall to  $>0.1$  wt% Cu in the footwall. Cross section F-F' (Figure 15) shows that the Center Fault marks the boundary of a zone of  $>0.5$  wt% Cu mineralization within the Northeast Zone breccia body. The surface map trace of the Center Fault is inferred on the basis of subsurface drill intercepts. Contouring of the fault plane indicates an orientation of  $076^{\circ}/64^{\circ}$  S (Figure 16). Whereas the fault plane was not mapped or located at surface, the surface trace of the fault projects to the location in the Wight Pit where the benches have become unstable and experienced minor collapse. There is also a lack of continuation of two major ( $>20$  m wide) augite porphyry dikes, which are mapped in the northeast part of the Wight Pit but are not found in the opposite wall; however, it is possible that these dikes were not

continuous when originally emplaced. In summary, there is some evidence that is supportive of the existence of the Center Fault; however, the Center Fault is not required to exist based on the current evidence for the fault.

### *Brown Wall Fault*

The Brown Wall fault was identified by Chris Rees (personal communication, 2011) on the basis of a plane in the southeast part of the Wight Pit that contained apparent slickenlines and sheared fault gouge. This exposure has subsequently been covered by rock fill. Photos and measurements from previous field seasons indicate that the fault plane is oriented  $294^{\circ}/74^{\circ}$  N with slickenlines that trend and plunge on average  $294^{\circ}\rightarrow 15^{\circ}$ . Mapping in the Wight Pit in 2011-2012 did not find any evidence of the Brown Wall Fault in the northwest wall of the Wight Pit, along strike from the previously mapped plane. Other than drill-hole WB-08-250, in which there is a lithology change from weakly mineralized crackle breccia to fine-grained pink monzonite across a narrow zone of fractured rocks, there is a paucity of drill holes in which the fault plane can be identified. Given the lack of continuity of the fault across the Wight Pit, the Brown Wall Fault is interpreted as a minor fault along the edge of the breccia body.

### 5.4 Nature of the Fold and Tilt in the Mount Polley district

Regional mapping done by the British Columbia Geological Survey found that the Mount Polley igneous complex lies near the axial trace of a doubly-plunging open synform. In the Mount Polley district the synform is southeast plunging (See Figure 1) (Bailey, 1988; Bailey et al., 1997; Logan et al., 2005). The timing of the folding event is unknown, although it must have occurred following deposition of the Nicola Group, as sedimentary beds and extrusive rocks in the Nicola Group are folded.

The strongest evidence for tilting in the Mount Polley district is the 30°-35° NW dip of conglomerate bedding in the Quarry Zone. There are few constraints on the timing of the tilt; it must be younger than deposition of the conglomerate beds and the quartz latite ignimbrite, which has an age of  $196.7 \pm 1.3$  Ma. The augite porphyry dikes are also inferred to be tilted, therefore they may be older than the tilting event. Given that the augite porphyry dikes cut the conglomerate beds and the quartz latite ignimbrite, the tilting event must be younger than 196 Ma.

### 5.5 Apatite Fission Track Ages

The apatite fission track ages and track lengths are summarized in Table 2. Fission track ages from samples in the Northeast Zone and the Quarry Zone are  $65.8 +10.2 -12.1$  Ma and  $59.1 +9.45 -11.23$  Ma respectively. The sample from the Southeast Zone has very large uncertainty, and as such the cooling age is considered suspect. The average track length for the Northeast Zone sample is  $13.16 \pm 1.83$   $\mu\text{m}$  and for the Quarry Zone sample is  $13.44 \pm 2.09$   $\mu\text{m}$ . These are shorter than 14  $\mu\text{m}$ , which is the typical track length expected for an apatite crystal that cooled rapidly through the partial annealing zone (Gallagher et al., 1998). Shorter track lengths occur because the apatite crystal spent more time in the apatite partial annealing zone. The shorter track lengths are therefore indicative of slow cooling during the Paleocene to Eocene.

## 6: Discussion

### 6.1 Nature of Fault Separation

#### *Polley Fault*

The sense of separation on the Polley Fault was interpreted based on the morphology of the breccia body. The coherent high grade zone found in the hanging wall likely represents the deep core of the ore zone, whereas the low grade, fingering upward morphology found in the footwall likely represents the shallow levels of the ore zone (Sillitoe, 1973; Seedorff et al., 2005). Based on these interpretations, the hanging wall has been displaced upwards with respect to the footwall, and the Polley Fault is a reverse fault. There are no constraints on lateral offset.

Estimates of the separation on the Polley Fault are based on the distance separating the theoretical coherent high grade zone and low grade upper zone of the ore body which is constrained by drilling data. This separation has been estimated at approximately 500 m, however, the uncertainty is very large, and the separation could be as small as a few hundred meters and as large as a few kilometers. The main factor contributing to the uncertainty is that the depth to the theoretical high grade zone is unconstrained by the drilling data. Similarly, while there could be a component of strike-slip separation on the fault plane there is no mapping or drill core evidence that constrains such separation.

#### *East Cariboo Fault*

It is difficult to evaluate the sense of separation on the East Cariboo Fault based solely on the juxtaposition of lithologies. Given that the East Cariboo Fault and the Polley Fault have very similar orientations, they could both have reverse sense of separation. This is not consistent with the  $165^{\circ} \rightarrow 30^{\circ}$  slickenlines, therefore there could also be a significant component of strike-slip

separation on the fault plane. The very steep nature of the fault plane supports the inference that oblique slip characterizes the separation on the fault plane.

Estimating the amount of separation on the fault is similarly difficult due to the limited drill core data on the eastern side of the fault plane. No dikes can be reliably identified on both sides of the fault. Furthermore, there are zones of 0.1-0.5 wt% Cu and >0.5 wt% Cu in the western side of the fault plane, but the monzonite in the eastern side of the fault has <0.1 wt% Cu. There is no correlation between copper mineralization in either side of the fault. As such, the magnitude of separation on the East Cariboo Fault is unknown.

#### *North Springer Fault*

Sinistral separation on the North Springer Fault is well constrained by separation of a diorite intrusion, a plagioclase porphyry dike, and the >0.1 wt% Cu and >0.5 wt% Cu zones in the Springer Pit (Figure 12). Strike-slip separation is also supported by the presence of sub-horizontal slickenlines, which have an average trend and plunge of  $235^{\circ}\rightarrow 5^{\circ}$ . Based on the separation of the aforementioned features, the magnitude of separation on the fault is  $180\text{ m} \pm 20\text{ m}$ . The uncertainty in the separation is attributed to uncertainties in the location of the diorite and plagioclase porphyry contacts, and to uncertainties in drawing the Cu grade contours from the drill data.

#### *Green Giant Fault*

Offset on the Green Giant Fault juxtaposed a rotational breccia with a jigsaw fit breccia; however, these breccias do not give an indication of the sense of separation on the fault. Jackson (2008) found that an alteration assemblage comprising magnetite, albite, and actinolite occurs at depth in the Wight Pit and at surface in the Leak Zone, which is an area of low grade

mineralization south of the Green Giant Fault. The Wight Pit is located in the hanging wall of the Green Giant Fault and the Leak Zone is located in the footwall. Separation of the magnetite + albite + actinolite alteration zone to depth in the Wight Pit indicates that the Green Giant Fault is a normal fault.

The magnitude of separation on the Green Giant Fault is estimated based on the separation between the alteration assemblages. Jackson (2008) found that the magnetite + albite + actinolite alteration assemblage in the Northeast Zone is found between 650 m and 400 m above sea level. The Leak Zone is currently at 1100 m above sea level, therefore the magnitude of separation on the Green Giant Fault is 450 m - 700 m. There is uncertainty in this separation, as it is unknown whether the alteration assemblage currently exposed in the Leak Zone is the same alteration assemblage as that found in the Wight Pit. Furthermore, it is unknown whether the Leak Zone represents the upper boundary of the alteration assemblage or some intermediate level, in which case the separation would be greater than the estimate.

#### *Center Fault*

The sense of separation on the inferred Center fault is interpreted based on juxtaposition of the upper ore body with the lower ore body in the Northeast Zone. The upper body comprises a bornite core surrounded by chalcopyrite whereas the lower ore zone comprises magnetite, bornite, and chalcopyrite. In porphyry copper deposits magnetite + bornite, and bornite + chalcopyrite are commonly found in the deeper and more central parts of the ore body, whereas chalcopyrite + pyrite is found at shallower depths (Einaudi et al., 2003; Seedorff et al., 2005). Based on the spatial distribution of the sulfides it is assumed that the upper ore zone represents a shallow part of the ore body that has been displaced downwards and adjacent to the deep

mineralization. Therefore the Central Fault has normal separation. While this logic suggests the sense of separation, it is difficult to estimate the magnitude of separation because of the unknown distance the ore zones were originally separated. Furthermore, the Center Fault may have some component of strike-slip separation which is not constrained by the mapping or drilling data.

## 6.2 Nature of Tilting

### *Magnitude of Tilting*

Prior to this study tilting in the Mount Polley district had been evaluated by Logan et al. (2005), who assumed that the plunge of the synform represented the magnitude of tilting in the district. In order to estimate the orientation of the fold axis, structural attitudes were taken on well-bedded sedimentary rocks and waterlain tuffs in the region surrounding Mount Polley. Reliable bedding top indicators show that bedding is upright. Using all reliable bedding measurements, Logan et al. (2005) calculated a Pi girdle with a beta axis of  $353^{\circ} \rightarrow 21^{\circ}$ . In cylindrical folds the beta axis is parallel with the fold axis. Based on this analysis the plunge of the fold is equivalent to the magnitude of the tilt, which is  $21^{\circ}$  north-northwest.

In this study the magnitude of the tilt was evaluated based on the orientation of the bedding in the Quarry Zone. Given that the Mount Polley complex comprises competent igneous plutons, it is unlikely to have experienced significant folding during contraction. As such, the dip of bedding in the Quarry Zone is assumed to be reflective of the magnitude of tilting that has subsequently taken place. The average orientation of bedding in the Quarry Zone is  $205^{\circ}/33^{\circ}$ ; however, the dip of bedding varies between  $30^{\circ}$ - $35^{\circ}$ . As such the magnitude of tilting in the Mount Polley district is  $30^{\circ}$ - $35^{\circ}$  northwest.

### *Restoration of Tilting*

Figure 17 shows restoration of the structural data measured at Mount Polley using the 21° NNW tilt calculated by Logan et al. (2005) and the 30°-35° NW tilt calculated in this study. The first rotation was done about a 173°→353° rotation axis, restoring 21° NNW of tilt, and the second rotation was done about a 25°→205° rotation axis, restoring 33° NW of tilt. The blue poles show restored data using the 21° NNW tilt and the red poles show restored data using the 33° NW tilt.

Bedding measurements (N=14) were taken in the basal conglomerate and sandstones of the Pcgl rock unit overlying the unconformity, on the northwestern flank of the Mount Polley igneous complex. A small number of the beds show normal grading. Restoration of the beds by removal of 21° NNW tilt restores the bedding to a more shallow orientation, but does not restore the beds to horizontal. Restoration of the beds by removal of the 33° NW tilt restores the bedding to horizontal to sub-horizontal (Figure 17, panel A). This is the expected outcome, as the 33° NW tilt was constrained using the bedding measurements.

Restoration of the augite porphyry dikes by removal of 21° NNW tilt restores the majority of the augite porphyry dikes to a dip of 60° - 80°, whereas restoration of the augite porphyry dikes by removal of the 33° NW tilt restores the dip to 70° - 90° (Figure 17, panel B). Given that the 33° NW tilt restores the augite porphyry dikes to near vertical it is assumed that the majority of the augite porphyry dikes were originally emplaced vertically and were subsequently tilted. This is typically the case where the maximum principal stress ( $\sigma_1$ ) is vertical and the minimum principal stress ( $\sigma_3$ ) is horizontal, as dikes adjust during propagation such that  $\sigma_3$  is perpendicular to the dike wall (Rehrig and Heidrick, 1976; Spencer, 1985).



Based on the restoration of the augite porphyry dikes, the 30°-35° NW is considered the preferred value for the magnitude of tilting in the Mount Polley district. This tilt restores the bedding to horizontal to sub-horizontal while also restoring the augite porphyry dikes to near vertical. This evaluation is built on the assumption that only one tilting event has taken place in the Mount Polley district. Cross-cutting relationships mapped in the Mount Polley district show that the augite porphyry dikes are younger than the K-feldspar porphyry and the plagioclase porphyry dikes, therefore these dikes must also be tilted.

When the 33°NW tilt is restored from the K-feldspar porphyry and the plagioclase porphyry dikes the majority of the dikes (N=9) restore to within 10° of vertical. Two of the dikes restore to <30° and one dike restores to 50° (Figure 17, panel C). The dikes that restore to near vertical are interpreted to have been originally intruded as dikes, whereas those that restore close to horizontal are interpreted to have been originally intruded as sills. Field observations indicate that not all of the dikes are planar bodies; some anastomose or change dip, which could explain why not all of the dikes restore to vertical.

The timing of the tilting event is unknown, however, if the augite porphyry dikes are tilted then they must be older than the tilting event. The reverse faults do not cut the augite porphyry dikes, therefore they are older than the augite porphyry dikes and must also be tilted. The Polley Fault restores from its current orientation of 340°/69° NE to 164°/87° SW and the East Cariboo Fault restores from its current orientation of 330°/78° NE to 151°/82° SW (Figure 17, panel D). The relative timing between tilting and faulting that formed the North Springer Fault, the Green Giant Fault, and the inferred Center Fault is unknown. If these faults were tilted the North Springer Fault, which is oriented nearly parallel to the rotation axis and would therefore experience significant rotation, restores from its current orientation of 230°/80° NW to an

orientation of  $238^{\circ}/51^{\circ}$  NW. The Green Giant Fault restores from  $275^{\circ}/84^{\circ}$  N to  $281^{\circ}/74^{\circ}$  N. The inferred Center Fault restores from  $095^{\circ}/64^{\circ}$  S to  $069^{\circ}/87^{\circ}$  S.

Anderson (1951) found that in the shallow crust, where  $\sigma_3$  is vertical, normal and reverse fault displacement is most likely to initiate at an angle of  $60^{\circ}$  and strike-slip fault displacement is most likely to initiate close to  $90^{\circ}$ . The sinistral sense of separation on the North Springer Fault is known with most certainty. Restoration of the North Springer Fault from a dip of  $80^{\circ}$  to a dip of  $51^{\circ}$  would suggest that the North Springer Fault formed after tilting and has not been tilted; however, this is assuming that the Mount Polley district was shallow in the crust and that the  $\sigma_3$  was vertical when the North Springer Fault formed.

### *Cause of Tilting*

There are two structural events that could have potentially caused the  $33^{\circ}$  NW tilt in the Mount Polley district: the Middle Jurassic contraction that resulted in the synform and the thrust and reverse faults in the district, or the Eocene extension that formed a series of normal faults in the district. Evaluation of the regional geology map (Figure 2) shows a number of north-northwest striking approximately located reverse faults and a number of northeast- to east striking approximately located normal faults. In particular, the approximately located thrust fault that projects through the Polley Lake is considered to have significant separation (Figure 4). The magnitude of separation on the normal faults is unknown, however there are a series of fault, which could cumulatively have significant separation.

In a reverse fault system tilting is caused by differential separation on different fault segments. In the Mount Polley district the fault that is buried beneath Polley Lake is inferred to be a large thrust fault with significant separation. This fault could produce a northwest tilt if the

separation on the southern segment of the fault was greater than the separation on the northern segment. If differential separation on a reverse fault was the cause of tilting in the Mount Polley district, the tilting likely occurred during the Middle Jurassic, as this is when the reverse faults and the synform formed in response to contraction during accretion of the island arc onto the North American continent.

On the other hand, tilting could be produced by rotation in the hanging wall block in a normal fault (Proffett, 1977). A series of normal faults would be required to produce a  $33^\circ$  NW tilt, however, to the northwest of the Mount Polley igneous complex are a series of northeast to east striking, approximately located faults that are interpreted as normal faults (Bloodgood, 1988). If normal faulting caused the tilt in the Mount Polley district the tilting event would likely have occurred during the Eocene, as this is the timing of extension and magmatism in the Challis-Kamloops volcanic belt.

The timing of the faulting event has implications for which fault planes have been tilted and which have not. It is known that the sedimentary beds and the quartz latite ignimbrite, and the augite porphyry dikes are tilted. Small reverse faults are older than the augite porphyry dikes, as they do not displace the dikes. Therefore, the reverse faults are likely also tilted. It is unknown whether the younger North Springer Fault, Green Giant Fault and inferred Center Fault are tilted. If the tilting is related to the Middle Jurassic reverse faults the younger faults would not be tilted. On the other hand, if tilting is related to hanging wall block rotation in a series of Eocene normal faults, the youngest faults would be tilted. Given the lack of evidence for tilting of young features, either of these scenarios is possible.

### 6.3 Structural Restoration of Post Mineral Deformation

#### *Central Zone Restoration*

Restoration in the Central Zone was based on restoring tilt and fault separation on the three major faults. The present day orientation of the ore bodies, intrusions, and faults is illustrated in Figure 18, block A. The deep sections of the ore bodies have not been drilled, and are drawn based on extrapolations from the shallow level geometry. As such there is large uncertainty in the nature, depth, and extent of the ore body. Separation on the North Springer Fault and tilting are the first structural events to be restored, as they are thought to be younger than the two reverse faults. The relative timing of tilting and the North Springer Fault is unknown, however, given the robust evidence that the North Springer Fault has sinistral separation, and restoration of tilt causes the North Springer Fault to become significantly shallower, the North Springer Fault is inferred to be younger than tilting. Restoration of slip along the North Springer Fault restores the Junction Zone Cu-Au ore back to the main Springer Pit ore body (Figure 16, block B). When the 33° NW tilt is removed the Polley Fault and East Cariboo Fault restore to 275°/84° N and 282°/64° N respectively (Figure 18, block B).

Separation on the Polley Fault is restored such that the high grade coherent mineralization in the hanging wall restores to be coincident with the inferred high grade zone that occurs at depth in the footwall (Figure 18, block C). This restoration is largely based on the theoretical position of the high grade zone, and is therefore subject to significant uncertainties. Restoration on the East Cariboo Fault results in the monzonite intrusion being restored to a deeper depth. There are no constraints on this restoration.

Once all three of the faults and the tilt have been restored it is possible to interpret the original geometry of the ore bodies and intrusions in the Center Zone. Figure 18, block D shows the shape of the ore bodies, where the C2 and WX zones are deeper than the Springer Pit mineralization. The mineralization exploited by the Bell and Cariboo Pits restores to depth in the hanging wall of the Polley Fault. Based on this restoration the best remaining potential for additional undiscovered Cu-Au ores occurs at great depth in the footwall of the Polley Fault.

#### *Northeast Zone Restoration*

Compared to the restoration in the Central Zone, the relative timing between the tilting and the Green Giant Fault has a larger impact on how to complete the restoration in the Northeast Zone. As such two restorations were constructed: the first with a Middle Jurassic tilt, and the second with an Eocene tilt. The Center Fault was not included in these restorations because, while the fault is suggested by the presently available evidence, it is not strictly required to exist. Should the Center fault be better identified in future, it could easily be added to these reconstructions.

The present day orientation of the ore bodies and spatial distribution of copper minerals are illustrated in Figure 19, panel A. The red shade demarcates the limit of economic grade copper mineralization. Magnetite is largely found at depth in the ore zone, however there are limited occurrences of shallow magnetite mineralization in the breccia. Bornite  $\pm$  chalcopyrite typically occurs at greater depth and centrally compared to chalcopyrite  $\pm$  pyrite. Magnetite identified in the Leak Zone trenches has also been included in the restorations, however the shape and location of this contour is purely schematic.

In Restoration 1 the tilting is assumed to have taken place during the Middle Jurassic. Therefore, the Green Giant Fault is the youngest fault, and is the first to be restored. Restoration of the separation on the Green Giant Fault was completed in order to restore the magnetite + albite + actinolite alteration assemblage found at depth in the Northeast Zone to the same assemblage found at surface in the Leak Zone, and to the magnetite mineralization found at surface in the Skid Zone (Figure 19, Restoration 1, panel B). In this model 500 m of slip on the Green Giant Fault is required to restore the alteration assemblage.

In Restoration 1 the Middle Jurassic tilt is the oldest structural event, and therefore the last to be restored (Figure 17, Restoration 1, panel C). Removal of the 33° NW tilt restores the long axis of the mineralized body to vertical. At this point the ore bodies in the Northeast Zone are restored, and there is no mapped evidence for older events.

The second restoration was completed using the same magnitude of separation on the fault and tilt. The main difference is that with an Eocene tilt the Green Giant Fault could potentially be older than the tilting event. In this case the tilt is restored first, which causes the Green Giant Fault to restore from a dip of 84° to 74°. The long axis of the mineralized ore body also restores to vertical. The Green Giant Fault is then restored as the oldest structural event. Both restorations result in a similar spatial distribution of the original mineralized zones. From an exploration point of view, this restoration of the Northeast Zone implies that the displaced part of the ore body was originally above the Skid and Leak Zones, and has subsequently been eroded away.

*Mount Polley District Restoration*

Based on the restorations in the Central Zone and the Northeast Zone it is possible to complete a schematic restoration of the Mount Polley district (Figure 20). This restoration depends upon mineralogy assemblages, which provide inferences into the structural depth of each ore zone (Rees, 2005; Rees, 2006; Jackson, 2008), and the sense of separation on the various faults. Fault separation on the Green Giant Fault in particular is inferred based solely on the separation of the magnetite + albite + actinolite alteration zone. The tilting event is assumed to be Middle Jurassic in age, as in the Central Zone restoration. Assuming a Middle Jurassic age tilt means that the North Springer Fault and Green Giant Fault are inferred to not be tilted. It is also possible that the tilting is Eocene in age, in which case the restoration would need to be modified to reflect the restored orientation of the North Springer Fault and the Green Giant Fault.

Due to the faulted and tilted nature of the Mount Polley district, it is likely that each of the ore zones represents a different structural level within the mineralizing system (Logan and Mihalynuk, 2007). A 33° NW tilt means that the rocks currently exposed at surface in the Southeast Zone represent a deeper structural level than the rocks currently exposed in the Northeast Zone. This supposition is supported by different Cu:Ag:Mo ratios, alteration assemblages, and brecciation styles in each of the different ore zones. The Northeast Zone, which is stratigraphically closest to the overlying unconformity, is hosted in a polyolithic hydrothermal breccia body (Jackson, 2008). It has the distinctly higher grade than the other deposits, and the mineralization often consists of coarse grained Cu-Fe sulphides. The proximity to the unconformity, the high Ag content, and the lack of Mo suggest a shallow position in the deposit. The Central Zone is hosted in partially hydrothermally brecciated intrusive rocks with veins extending into the surrounding coherent intrusions (Fraser, 1994). It has a Cu-Au rich core

that is surrounded by roughly concentric zones of alteration assemblages, including an inner potassic zone and an outer garnet-epidote zone (Fraser et al., 1995). The Central Zone likely represents a moderate structural depth. The Southeast Zone is hosted in a hydrothermal breccia pipe. It is stratigraphically furthest from the unconformity, and has the highest Au:Cu ratio. It is also the only zone with a significant Mo content. The Southeast Zone likely represents the deepest structural level in the Mount Polley district.

The present day orientation of the various ore zones is represented in Figure 20, panel 1. This simplified schematic diagram generalizes all of the host rocks into the Pmdu unit. The youngest fault to be restored is the Green Giant Fault. Restoration of 500m of normal separation brings the Northeast Zone to a shallower level in the crust (Figure 20, panel 2). Based on the Central Zone restoration, the second fault that must be restored is the North Springer Fault. Restoration on 180 m of sinistral separation on the fault plane brings the Junction Zone back into alignment with the Springer ore zone. This restoration is not shown in a panel.

Given the assumption that the tilting event took place in the Middle Jurassic, the 33°NW tilt is the next structural feature to be restored. This restores the sedimentary beds to horizontal and the long axis of the ore zones to vertical (Figure 20, panel 3). Finally, the oldest faults to be restored are the Polley Fault and the East Cariboo Fault. Restoration of reverse separation on the two fault planes restores the Southeast Zone to a deeper stratigraphic level than the Central Zone. At this point the restoration of the structural features found strictly within the Mount Polley igneous complex is complete.



#### 6.4 Cooling History of the Mount Polley District

Apatite fission track ages and the biotite and hornblende  $^{40}\text{Ar}/^{39}\text{Ar}$  dates presented by Logan et al. (2007) constrain the cooling history of the Mount Polley district. Apatite fission tracks have an annealing temperature of  $60^\circ\text{C}$  -  $110^\circ\text{C}$  (Donelick et al., 2001), whereas biotite has a closure temperature of  $300^\circ\text{C} \pm 20^\circ\text{C}$  (Harrison et al., 1985) and hornblende has a closure temperature of  $450^\circ\text{C} \pm 40^\circ\text{C}$  (Baldwin et al., 1990). The  $^{40}\text{Ar}/^{39}\text{Ar}$  biotite age from monzonite in the Mount Polley district is  $205.2 \pm 1.2$  Ma. Based on the biotite closure temperature, the Mount Polley district has not been warmer than  $300^\circ\text{C} \pm 20^\circ\text{C}$  since the Late Triassic. The small monzodiorite stock has a  $^{40}\text{Ar}/^{39}\text{Ar}$  hornblende age of  $165.2 \pm 1.8$  Ma. Given that the biotite ages were not reset at this time, and that hornblende has a higher closure temperature than biotite, this must represent the cooling age of a young intrusion. The apatite fission track ages are  $65.8 \pm 10.2$  -  $12.1$  Ma and  $59.1 \pm 9.45$  -  $11.23$  Ma, which indicates to Paleocene to Eocene age cooling. The district has not subsequently been above  $110^\circ\text{C}$ .

There are no constraints on the geothermal gradient or surface temperature in the Mount Polley gradient. A normal geothermal gradient of  $25^\circ\text{C}/\text{km}$  and a surface temperature of  $15^\circ\text{C}$  were assumed in order to calculate the depth of the partial annealing zone for apatite and the depth to the closure temperature of biotite and hornblende. Calculations were done using the following equation:

$$\frac{(\text{closure temperature} - 15^\circ\text{C})}{25 \frac{^\circ\text{C}}{\text{km}}} = \text{depth (km)}$$

Depth ranges are summarized in Table 3. The lack of resetting in the biotite ages suggests that the Mount Polley district has been shallower than 12.2 km - 10.6 km since the Late Triassic.

The unconformity and sedimentary rocks overlying the Mount Polley complex are indicative that at least once during this period the Mount Polley district was at surface. There is no evidence of Jurassic age erosional features or widespread regional metamorphism in the Mount Polley district, which also supports the inference that following accretion the Quesnel Terrane remained fairly shallow within the hinterland of the Canadian Cordillera. Immediately prior to the Paleocene-Eocene the Mount Polley district must have been at a depth greater than 3.8 km – 1.8 km in order for the apatite fission tracks to have been partially annealed. Following the Eocene the Mount Polley district remained above the apatite partial annealing zone, and at some point was exhumed to surface.

The shaded region in Figure 21 shows a potential history of burial and exhumation. The depth of emplacement of the Mount Polley Cu-Au zones is estimated based on the work by Burnham (1985), who found that the mechanical energy released from hydrous magmas in subvolcanic environments is sufficient to form a hydrothermal breccia in even the strongest wall rocks to depths of 4 to 5 km. This depth range is supported by Seedorff et al. (2005) whose compilation of the depths of porphyry copper deposits shows that they form from <1.5 to 9 km, with the majority in the range from 1.5 to 5 km. The presence of an unconformity overlying the Northeast zone indicates that the deposit was at surface prior to the deposition of the quartz latite ignimbrite. Finally, the apatite fission track data is used as a third constraint for the potential timing of exhumation.

## 6.5 Three major structural events impacting the Quesnel Terrane

### 1. Late Triassic intrusion of the Mount Polley Igneous Complex

The Mount Polley igneous complex was emplaced into the Nicola Group in the Late Triassic. Brecciated monzonite in the Northeast Zone has a biotite  $^{40}\text{Ar}/^{39}\text{Ar}$  age of  $205.2 \pm 1.2$  Ma and the K-feldspar porphyry dikes have a zircon U-Pb age of  $205.01 \pm 0.3$  Ma (Logan et al., 2007). These ages suggest that the host rock and the mineralization associated with the fluidal K-feldspar porphyry dikes are coeval. Following ore deposition the Mount Polley district was rapidly exhumed to the surface, as indicated by the presence of an unconformity and a basal conglomerate containing clasts of the underlying monzonite. A quartz latite ignimbrite interbedded with the conglomerate has a zircon U-Pb age of  $196.7 \pm 1.3$  Ma (Logan et al., 2007). The age of the interbedded quartz latite ignimbrite provides a constraint on the timing of the of the unconformity, which had to have formed after 205 Ma (in order to contain clasts of the monzonite) and before 197 Ma. Therefore, in a period of approximately 8 Ma the Mount Polley intrusions were emplaced into the upper crust, uplifted and exhumed via erosion to reach the surface, and partially eroded to form a conglomerate (Figure 21).

Lang et al. (1995) suggest that during the Late Triassic the Quesnel Terrane experienced either a collisional event between island arcs or a cessation of active subduction. No structural features have been identified in the Quesnel Terrane that can conclusively be related to collision in the island arc; however the discrete pulse of alkalic magmatism that occurred between 210 and 200 Ma, and an overall decline in active magmatism could be indicative of a changing structural setting within the island arc (Lang et al., 1995). Collision in the island arc, or extension related to the cessation of subduction, could both provide an explanation for the uplift and erosion that

occurred immediately following the Mount Polley mineralization event. On the other hand, the topographic relief generated by active island arc magmatism could lead to an increase in erosion, in which case the erosion could be the cause of the significant exhumation evidenced in the Mount Polley district.

## 2. Middle Jurassic Island Arc Accretion

The Quesnel terrane was accreted onto the margin of the North American continent in the Middle to Late Jurassic (Figure 22) (Anderson, 1976; Monger et al., 1982; Mortimer, 1986). Contraction related to orogenesis resulted in the formation of a fold and thrust belt in the Canadian Cordilleran foreland (Monger and Price, 2002). It is possible that this contraction resulted in the formation of the reverse Polley Fault and East Cariboo Fault, and folding of the Nicola Group. Alternatively, these features could have formed once the Quesnel Terrane was accreted onto North American and was located in the hinterland of the Canadian Cordilleran fold and thrust belt. The thrust faults and folds are likely contemporaneous; a similar age relationship between thrust faults and folds was found by Bloodgood (1988) in the Likely area, just north of the Mount Polley district.

A monzodiorite stock with a hornblende  $^{40}\text{Ar}/^{39}\text{Ar}$  age of  $165.2 \pm 1.8$  Ma was intruded into the Mount Polley igneous complex in the Middle Jurassic. This is contemporaneous with accretion of the Quesnel island arc onto the North American continent. There are no age dates on the augite porphyry dikes or the fine-grained monzodiorite dikes, however, the compositional similarity between the Jurassic monzodiorite stock and the fine-grained monzodiorite dikes suggests that they are genetically related and likely intruded at approximately the same time.

Tilting in the Mount Polley district impacts the Late Triassic intrusions, the dikes, and all of the bedded rocks. It is unknown whether the North Springer Fault, the Green Giant Fault, and the inferred Center Fault are tilted. If tilting in the Mount Polley district is caused by different magnitudes of separation on a reverse fault, the tilting is likely Middle Jurassic in age.

### 3. Paleocene to Eocene Extension

Apatite fission track ages indicate that the Mount Polley district was most recently exhumed through the apatite partial annealing zone during the Paleocene to Eocene. There are a number of structural events that are known to cause uplift and exhumation, including isostatic uplift, extension and thinning, and compression. During the Tertiary the margin between the North American continent and the Farallon plate shifted from orthogonal to oblique subduction, and transtension resulted in the formation of dextral strike-slip fault systems along the length of the North American Cordillera (Struik, 1993). In the Intermontane Belt these strike-slip faults are named, from north to south, the Teslin Fault, Finlay Fault, Pinchi Fault, Fraser Fault, and Yalakom Fault (Umhoefer and Schiarizza, 1996). In British Columbia normal faulting is often related to extension between two en echelon strike-slip fault segments in the dextral strike-slip fault zone. This is the case for normal faulting and uplift in the Endako mining district, north of Mount Polley (Lowe et al., 2001). Additionally, Eocene extension is widespread in the Northwest USA. Houston and Dilles (2013) document the transition from Laramide-related compression, which lasted from approximately 75 to 55 Ma, to extension around 53 Ma. The Laramide orogeny is characterized by thick-skinned tectonics and overthickening of continental crust. Lui (2001) proposes that a thickened crust in isostatic equilibrium is dynamically unstable and will collapse given a sufficiently weakened lithosphere; therefore extension could also be attributed to gravitational collapse of the North American Cordillera.

In the Intermontane Belt dextral strike-slip faults are oriented approximately north-south, and there are a number of potential conjugate and complimentary fault orientations. The southwest-striking sinistral North Springer Fault could potentially be an example of an R' fault conjugate to the main dextral strike-slip fault zone. The Green Giant Fault is a young normal fault and is interpreted as forming at this time.

It is unknown whether the tilting event impacts these younger fault planes. If the North Springer Fault and the Green Giant Fault are tilted, the tilting event must have occurred during or following Eocene extension. A young tilting event would likely be related to block rotation in the hanging wall of a series of normal faults that occur to the northwest of the Mount Polley district.

#### 6.6 Regional Implications of the structural events

The structural events that have taken place in the Mount Polley district can be used to corroborate some of the current thinking regarding the tectonic history of the Quesnel Terrane. Lang et al. (1995) proposed that a deformation event occurred in the island arc that resulted in a decline in active magmatism in the Late Triassic. The unconformity and conglomerate overlying the Northeast Zone is evidence for significant exhumation and erosion of at least 1.5 to 3 km in the Quesnel Terrane. This is indicative of the island arc becoming emergent and experiencing erosion.

The Quesnel Terrane accreted onto the North American continent during the Middle Jurassic, which likely resulted in the formation of the doubly plunging synform and the reverse faults in the Mount Polley district. With the exception of the North Springer Fault, Green Giant Fault, and Center Fault, there was been little structural deformation following the initial folding and reverse faulting. This can be attributed to occurrence of the Quesnel Terrane in the hinterland of the

North American orogenic belt following accretion (Price and Monger, 2002). Assuming that the fold and thrust belt had already attained a critical taper by the time the Quesnel Terrane was accreted, it would have experienced little deformation in the hinterland; thus explaining the lack of structural activity and metamorphism in the Quesnel Terrane during the late Mesozoic and early Cenozoic (Logan et al., 2005).

Throughout British Columbia and the Northwest USA the Eocene is associated with widespread extension and magmatism. At the continental scale the suggested driving factor of extension is gravitational collapse, which could have been caused by overthickening of the crust during the Laramide orogeny (Lui and Furlong, 1993; Liu and Shen, 1998; Lui, 2001). At the local scale, Struik (1993) identified normal faults related to step-overs between fault strands in three major strike-slip fault zones in British Columbia. Isotopic ages of flows displaced by the dextral strike-slip faults found at least two distinct phases of dextral faulting: one in the Early to Middle Eocene and another in the Late Eocene to Early Oligocene. The apatite fission track dates from the Mount Polley district supports that exhumation was taking place during the Paleocene to Eocene.

Although there are no large scale normal faults that break the surface in the Quesnel terrane, evidence of large scale crustal extension is provided by the occurrence of metamorphic core complexes, including the Wolverine core complex in north central British Columbia, the occurrence of normal faulting and tilting in the Endako district, and multiple crustal scale dextral strike-slip fault zones (Struik, 1993; Lowe et al., 2001). Given the paucity of fault exposure or bedded rocks in the Mount Polley region, there had been little evidence for extension in central

British Columbia (Struik, 1993). Therefore, evidence for exhumation and extension in the Mount Polley district supports the hypothesis that extension occurs well into the central Intermontane Belt.



## **7: Conclusions**

The Mount Polley Cu-Au deposit was emplaced in the Quesnel Terrane during the Late Triassic. Fluidal clasts of strongly mineralized K-Feldspar porphyry dikes are found in hydrothermal breccias and suggest that the early porphyry dikes, mineralization, and brecciation are coeval. Overlying mineralized hydrothermal breccia in the Northeast Zone is a prominent unconformity overlain by a basal conglomerate, quartz latite ignimbrite, and intercalated sandstone and conglomerate. The isotopic age of the Mount Polley monzonite is 205 Ma, and the isotopic age of the quartz latite ignimbrite is 197 Ma. Based on these age constraints, the Mount Polley igneous complex was emplaced into the Late Triassic volcanic and sedimentary rocks of the Nicola Group, exhumed to surface, and partially eroded within a time span of 8 million years. These magmatic and erosional features are indicative of uplift and exhumation in an active island arc.

The Quesnel Terrane was accreted onto the North American continent during the Middle Jurassic. Regional mapping in the Likely region surrounding the Mount Polley district shows that the folding event and northwest-striking reverse faults formed at this time. The oldest faults in the Mount Polley district are the northwest-striking reverse Polley Fault and East Cariboo Fault, which displace intrusions and Cu-Au ore zones. These faults are interpreted as forming coeval with a doubly plunging synform, in which the Mount Polley district lies exposed near the fold hinge. The sinistral North Springer Fault is younger than the two major reverse faults; however there is no constraint on its minimum age.

The Mount Polley district experience a tilting event of unknown age that tilted intrusions, ore bodies, sedimentary beds, and dikes 30-35°NW. The cause of this tilting event is also unknown,

however it could be related to either contraction or extension that have taken place in the Mount Polley district. Contraction took place in the Middle Jurassic, and tilting could have resulted from different magnitudes of separation on sections of a large-scale reverse fault, such as the one that is interpreted to be buried beneath Polley Lake. On the other hand, tilting could be related to Eocene extension, where hanging wall block rotation in a series of normal faults resulted in a tilt. There are a series of interpreted normal faults to the northwest of the Mount Polley district.

The Green Giant Fault and the inferred Center Fault are interpreted as the youngest faults in the district and have a normal sense of separation. Preliminary apatite fission track ages indicate that the Mount Polley district was uplifted through the apatite partial annealing zone during the Paleocene to Eocene. This timing corresponds to the formation of three large-scale dextral strike-slip fault systems in British Columbia, and to widespread extension and magmatism in both the Canadian Cordillera and the NW United States. Extension and associated uplift may have caused the exhumation in the Mount Polley district.

For the purposes of exploration, restoring the structural deformation in the Mount Polley district provides insight into the original geometry of the ore zones. Identifying parts of the ore zones that have yet to be discovered, and understanding how and where they have been displaced, may lead to additional discoveries at Mount Polley. In addition to the local implications of the restorations, each of the structural events identified in the Mount Polley district can be used to establish the tectonic history of the Quesnel Terrane and the other porphyry copper deposits that it hosts.

## References

- Allmendinger, R.W., Cardozo, N. and Fisher, D.M. 2012. *Structural Geology Algorithms: Vectors and Tensors*. Cambridge University Press, Cambridge, UK.
- Anderson, E.M. 1951. *The Dynamics of Faulting and Dyke Formation*. Oliver and Boyd, Edinburgh.
- Anderson, P. 1976. Oceanic crust and arc-trench gap tectonics in southwestern British Columbia. *Geology*, **4**: 443-446.
- Bailey, D.G. 1988. Geology of the Hydraulic map area, NTS 093A/12 [map]. 1:50,000. British Columbia Ministry of Energy, Mines, and Petroleum Resources, Vancouver, BC.
- Bailey, D.G. and Archibald, D.A. 1990. Age of the Bootjack Stock, Quesnel Terrane, south-central British Columbia. *In Geological fieldwork 2005*. British Columbia Ministry of Energy, Mines, and Petroleum Resources, Paper 1990-1, pp. 79-82.
- Bailey, D.G., Bloodgood, M.A., Campbell, R.B., Panteleyev, A., Hancock, K.D. and Struik, L.C. 1997. Geology of the Central Quesnel Belt British Columbia [map]. 1:100,000. British Columbia Ministry of Employment and Investment, Vancouver, BC.
- Baldwin, S.L., Harrison, T.M., and FitzGerald, J.D. 1990. Diffusion of  $^{40}\text{Ar}$  in metamorphic hornblende. *Contributions to Mineralogy and Petrology*, **105**: 691–703.
- Barr, D.A., Fox, P.E., Northcote, K.E., and Preto, V.A. 1976. The alkaline suite porphyry deposits – a summary. *In Porphyry Copper Deposits of the Canadian Cordillera. Edited by A. Sutherland-Brown*. CIM Special Volume No 15, pp. 359-367.
- Bath, A.B., and Logan, J.M. 2006. Geochemistry of the Late Triassic Boothack Stock (NTS 093A/12), South-Central British Columbia. *In Geological fieldwork 2005*. British Columbia Ministry of Energy, Mines, and Petroleum Resources, Paper 2006-1, pp. 5-20.
- Breitsprecher, K., Thorkelson, D.J., Groome, W.G. and Dostal, J. 2003. Geochemical confirmation of the Kula-Farallon slab window beneath the Pacific Northwest in Eocene time. *Geology*, **31**: 351-354.
- Breitsprecher, K., Scoates, J.S., Anderson, R.G., and Weis, D. 2007. Geochemistry of Mesozoic Intrusions, Quesnel and Stikine Terranes (NTS 082; 092; 093), South-Central British Columbia: Preliminary Characterization of Sampled Suites. *In Geological fieldwork 2006*. British Columbia Ministry of Energy, Mines, and Petroleum Resources, Paper 2007-1, pp. 247-257.

- Bloodgood, M.A. 1988. Geology of the Quesnel Terrane in the Spanish Lake Area, Central British Columbia. *In Geological fieldwork 1987*. British Columbia Ministry of Energy, Mines, and Petroleum Resources, Paper 1988-1, pp. 139-145.
- Burnham, C.W. 1985. Energy Release in Subvolcanic Environments: Implications for Breccia Formation. *Economic Geology*, **80**: 1515-1522.
- Davis, D., Suppe, J. and Dahlen, F.A. 1983. Mechanics of Fold-and-Thrust Belts and Accretionary Wedges. *Journal of Geophysical Research*, **88**: 1153-1172.
- Dewey, J. F. 1988. Extensional collapse of orogens. *Tectonics*, **7**: 1123–1139.
- Dickinson, W.R. 2004. Evolution of the North American Cordillera. *Annual Review of Earth and Planetary Science*, **34**: 13-45.
- Donelick, R.A., O’Sullivan, P.B. and Ketcham, R.A. 2005. Apatite Fission Track Analysis. *Reviews in Mineralogy & Geochemistry*, **58**: 49-94.
- Dostal, J., Robichaud, D.A., Church, B.N. and Reynolds, P.H. 1998. Eocene Challis-Kamloops volcanism in central British Columbia: an example for the Buck Creek basin: *Canadian Journal of Earth Science*, **35**: 951-963.
- Einaudi, M.T. 1997. Mapping altered and mineralized rocks: An introduction to the Anaconda method: Unpublished report, Stanford, California, Department of Geological and Environmental Sciences, Stanford University.
- Einaudi, M.T., Hedenquist, J.W. and Inan, E.E. 2003. Sulphidation state of fluids in active and extinct hydrothermal systems: Transitions from porphyry to epithermal environments. *Society of Economic Geologists Special Publication*, **10**: 285-313.
- Engelbreton, D.C., Cox, A. and Gordon, R.G. 1985. Relative motions between oceanic and continental plates in the Pacific basin. *Geological Society of America, Special Paper* 206.
- Fillipone, J.A. and Ross, J.V. 1990. Deformation of the western margin of the Omineca Belt near Crooked, Lake, east-central British Columbia. *Canadian Journal of Earth Sciences*, **27**: 414-425.
- Fraser, T.M. 1994. Hydrothermal breccias and associated alteration of the Mount Polley copper gold deposit (93A/12). *In Geological fieldwork 1993*. British Columbia Ministry of Energy, Mines, and Petroleum Resources, Paper 1994-1, pp. 259-267.
- Fraser, T.M., Stanley, C.R., Nikic, Z.T., Pesali, R. and Gorc, D. 1995. The Mount Polley alkalic porphyry copper gold deposit, south-central British Columbia. *In Porphyry Deposits of the Northwestern Cordillera of North America. Edited by T.G. Schroeter*. Canadian Institute of Mining and Metallurgy, Special Volume 46, pp. 609-622.

Gallagher, K., Brown, R. and Johnson, C. 1998. Fission Track Analysis and its Applications to Geological Problems. *Annual Review of Earth and Planetary Sciences*, **26**: 519-572.

Gillstrom, G. 2004. Mount Polley Mine 2004 Feasibility Study; 43-101 Technical Report. Available from Imperial Metals Corporation, Vancouver.

Gordee, S.M. 2006. Volcanostratigraphy, age and geologic setting of the Lower-Middle Jurassic Upper Hazelton Group, west-central British Columbia. M.Sc. thesis, Department of Geological Sciences, The University of British Columbia, Vancouver, B.C.

Harrison, T.M., Duncan, I. and McDougall, I. 1985. Diffusion of  $^{40}\text{Ar}$  in biotite: temperature, pressure and compositional effects. *Geochimica et Cosmochimica Acta*: **55**: 1435–1448.

Houston, R.A. and Dilles, J.H. 2013. Structural Geologic Evolution of the Butte District, Montana. *Economic Geology*, **108**: 1397-1424.

Hurford, A.J. and Green, P.F. 1983. The zeta age calibration of fission track dating. *Isotope Geoscience*, **1**: 285-317.

Hyndman, R.D. and Hamilton, T.S. 1993. Queen Charlotte area Cenozoic tectonics and volcanism and their association with relative plate motions along the Northeastern Pacific margin. *Canadian Journal of Earth Science*, **98**: 257-277.

Imperial Metals, 2012. 2012 Annual Information Form. Imperial Metals Corporation, Vancouver, BC.

Imperial Metals, 2013. Our Operations and Projects – Mount Polley Mine [online]. Available from <http://www.imperialmetals.com/s/MountPolleyMine.asp?ReportID=562601> [cited 24 June 2013].

Jackson, M.L. 2008. Evolution of the Northeast Zone Breccia Body, Mount Polley Mine, British Columbia. M.Sc. thesis, Department of Geological Sciences, The University of British Columbia, Vancouver, B.C.

Jebrak, 1997. Hydrothermal breccias in vein-type ore deposits: A review of mechanisms, morphology and size distribution. *Ore Geology Reviews*, **12**: 111-134.

Lang, J.R., Lueck, B., Mortenson, J.K., Russell, J.K., Stanley, C.R. and Thompson, J.F.H. 1995. Triassic-Jurassic silica-undersaturated and silica-saturated alkalic intrusions in the Cordillera of British Columbia: Implications for arc magmatism. *Geology*, **23**: 451-454.

Li, W., Wang, L., Lang, M., Trautmann, C. and Ewing, R.C. 2011. Thermal annealing mechanisms of latent fission tracks: Apatite vs. zircon. *Earth and Planetary Science Letters*. **302**: 227-235.

Liu, M. and Shen, Y. 1998. Crustal collapse, mantle upwelling, and Cenozoic extension in the North American Cordillera. *Tectonics*, **17**: 311-321.

Lui, M. 2001. Cenozoic extension and magmatism in the North American Cordillera: the role of gravitational collapse. *Tectonophysics*, **342**: 407-433.

Lui, M. and Furlong, K.P. 1993. Crustal shortening and Eocene extension in the Southeastern Canadian Cordillera: some thermal and rheological considerations. *Tectonics*, **12**: 776-786.

Logan, J.M. and Mihalynuk, M.G. 2005. Regional geology and setting of the Cariboo, Bell, Springer, and Northeast porphyry Cu-Au zones at Mount Polley, south-central British Columbia. *In Geological fieldwork 2004*. British Columbia Ministry of Energy, Mines, and Petroleum Resources, Paper 2005-1, pp. 249-270.

Logan, J.M., Mihalynuk, M.G., Ullrich, T. and Friedman, R.M. 2007. U-Pb Ages of Intrusive Rocks and  $^{40}\text{Ar}/^{39}\text{Ar}$  Plateau Ages of Copper-Gold-Silver Mineralization Associated with Alkaline Intrusive Centers at Mount Polley and the Iron Mask Batholith, Southern and Central British Columbia. *In Geological fieldwork 2006*. British Columbia Ministry of Energy, Mines, and Petroleum Resources, Paper 2007-1, pp. 93-116.

Lowe, C., Enkin, R.J. and Struik, L.C. 2001. Tertiary extension in the central British Columbia Intermontane Belt: magmatic and paleomagnetic evidence from the Endako region. *Canadian Journal of Earth Science*, **38**: 657-678.

McMillan, W.J. 1974. Stratigraphic section from the Jurassic Ashcroft Formation and Triassic Nicola Group contiguous to the Guichon Creek batholith. *In Geological fieldwork 1974*. British Columbia Ministry of Energy, Mines and Petroleum Resources, Paper 1975-1, pp. 27-34.

McMillan, W.J., Thompson, J.F.H., Hart, C.J.R. and Johnston, S.T. 1995. Regional geological and tectonic setting of porphyry deposits in British Columbia and Yukon Territory. *In Porphyry Deposits of the Northwestern Cordillera of North America. Edited by T.G. Schroeter*. Canadian Institute of Mining and Metallurgy, Special Volume 46, pp. 40-57.

McMillan, W.J., Thompson, J.F.H., Hart, C.J.R. and Johnston, S.T. 1996. Porphyry Deposits of the Canadian Cordillera. *Journal of the Geological Association of Canada*, **23**: 125-134.

Monger, J.W.H., Souther, J.G. and Gabrielse, H. 1972. Evolution of the Canadian Cordillera: A plate-tectonic model. *American Journal of Science*, **272**: 577-602.

Monger, J.W.H., Price, R.A. and Tempelman-Kluit, D.J. 1982. Tectonic accretion and origin of the two major metamorphic and plutonic belts in the Canadian Cordillera. *Geology*, **10**: 70-75.

Monger, J.W.H., Wheeler, J.O., Tipper, H.W., Gabrielse, H., Harms, T., Struik, L.C., Campbell, R.B., Dodds, R.B., Gehrels, G.E. and O'Brien, J. 1991. Cordilleran terranes: Upper Devonian to Middle Jurassic assemblages. *In Geology of the Cordilleran Orogen in Canada. Edited by H.*

Gabrielse, and C.J. Yorath. Chapter 8; Geological Survey of Canada, Geology of Canada, No. 4, pp. 281-327.

Monger, J. and Price, R. 2002. The Canadian Cordillera: Geology and Tectonic Evolution. CSEG Recorder, **27**: 17-36.

Mortenson, J.K., Ghosh, D.K. and Ferri, F. 1995. U-Pb geochronology of intrusive rocks associated with copper-gold porphyry deposits in the Canadian Cordillera. *In* Porphyry deposits of the northwestern Cordillera of North America. *Edited by* T.G. Schroeter. CIM Special Volume No. 46, pp. 142-158.

Mortimer, N. 1986. Late Triassic, arc-related, potassic igneous rocks in the North American Cordillera. *Geology*, **14**: 1035-1038.

Mortimer, N. 1987. The Nicola Group: Late Triassic and Early Jurassic subduction-related volcanism in British Columbia. *Canadian Journal of Earth Sciences*, **24**: 2521-2536.

Nelson, J., and Colpron, M. 2007. Tectonics and metallogeny of the British Columbia, Yukon and Alaskan Cordillera, 1.8 Ga to the present. *In* Mineral Deposits of Canada: A Synthesis of Major Deposit-Types, District Metallogeny, the Evolution of Geological Provinces, and Exploration Methods. *Edited by* W.D. Goodfellow. Geological Association of Canada, Mineral Deposits Division, Special Publication No. 5, pp. 755-791.

Panteleyev, A., Bailey, D.G., Bloodgood, M.A. and Hancock, K.D. 1996. Geology and mineral deposits of the Quesnel River-Horsefly map area, Central Quesnel Trough, British Columbia. *In* Bulletin 97. British Columbia Ministry of Employment and Investment, pp. 156.

Price, R.A. 1995. Cordilleran Tectonics and the Evolution of the Western Canada Sedimentary Basin. *In* Geological Atlas of the Western Canada Sedimentary Basin. *Edited by* G.D. Mossop and I. Shetsen. Canadian Society of Petroleum Geologists and Alberta Research Council, URL <[http://www.ag.gov.ab.ca/publications/wcsb\\_atlas/atlas.html](http://www.ag.gov.ab.ca/publications/wcsb_atlas/atlas.html)>, [May 27, 2013].

Proffett, J.M. 1977. Cenozoic geology of the Yerington district, Nevada, and implications for the nature and origin of Basin and Range faulting. *Geological Society of America Bulletin*, **88**. 247-266.

Rees, C.J. 1981. Western Margin of the Omineca Belt at Quesnel Lake, British Columbia. *In* Current Research, Part A, Geological Survey of Canada, Paper 8-A, pp. 223-226.

Rees, C., Bjornson, L., Blackwell, J., Ferreira, L., McAndless, P., Robertson, S., Roste, G., Stubley, T., and Taylor, C. 2005. Geological Report on the Mount Polley Property and Summary of Exploration in 2003-2004. Imperial Metals Corporation, internal report. .

- Rees, C., Ferreira, L., Bjornson, L., Blackwell, J., Roste, G., Stubley, T. and Taylor, C. 2006. Geological report on the Mount Polley property and summary of 2005 exploration. Imperial Metals Corporation, internal report.
- Rees, C. 2012. Geology of the Mount Polley Complex (Pre-mining, except Cariboo-Bell zones) [map]. 1:8,000. Imperial Metals Corporation, Vancouver, BC.
- Rehrig, W.A. and Heidrick, T.L. 1976. Regional tectonic stress during the Laramide and late Tertiary intrusive periods, Basin and Range province, Arizona. *Arizona Geological Society Digest*, **10**: 205-228.
- Seedorff, E., Dilles, J.H., Proffett, J.M., Einaudi, M.T., Zurcher, L., Stavast, W.J.A., Johnson, D.A. and Barton, M.D. 2005. Porphyry Deposits: Characteristics and Origin of Hypogene Features. *Society of Economic Geologists*, **100**: 251-298.
- Sillitoe, R.H. 1973. The Tops and Bottoms of Porphyry Copper Deposits. *Economic Geology*, **68**: 799-815.
- Sillitoe, R.H. 2010. Porphyry Copper Systems. *Economic Geology*, **105**: 3-41.
- Spencer, J.E. 1985. Miocene low-angle normal faulting and dike emplacement, Homer Mountain and surrounding areas, southeastern California and southernmost Nevada. *Geological Society of America Bulletin*, **96**: 1140-1155.
- Struik, L.C. 1986. Imbricated terranes of the Cariboo gold belt with correlations and implications for tectonics in southeastern British Columbia. *Canadian Journal of Earth Sciences*, **23**: 1047-1061.
- Struik, L.C. 1988. Regional imbrication within Quesnel terrane, central British Columbia, as suggested by conodont ages. *Canadian Journal of Earth Sciences*, **25**: 1608-1617.
- Struik, L.C. 1993. Intersecting intracontinental Tertiary transform fault systems in the North American Cordillera. *Canadian Journal of Earth Science*, **30**: 1262-1274.
- Tosdal, R.M., Jackson, M., Pass, H.E., Rees, C., Simpson, K.A., Cooke, D.R., Chamberlain, C.M. and Ferreira, L. 2008. Hydrothermal breccia in the Mount Polley alkalic porphyry copper-gold deposit, British Columbia. *In* *Geoscience BC Summary of Activities 2007*. Geoscience BC, Report 2008-1, pp. 105-114.
- Travers, W.B. 1977. Overtuned Nicola and Ashcroft strata and their relation to the Cache Creek Group, Southwestern Intermontane Belt, British Columbia. *Canadian Journal of Earth Science*, **15**: 99-116.



Umhoefer, P. and Schiarizza, P. 1996. Latest Cretaceous to early Tertiary dextral strike-slip faulting on the southeastern Yalakom fault system, southeastern Coast Belt, British Columbia. *Geological Society of America Bulletin*, **108**: 768-785.

Unterschutz, J., Creaser, R.A., Erdmer, P., Thompson, R.I., and Daughtry, K.L. 2002. North American margin origin of Quesnel terrane strata in the southern Canadian Cordillera: inferences from geochemical and Nd isotopic characteristics of Triassic metasedimentary rocks. *Geological Society of America Bulletin*, **114**: 462-475.

Wells, M.L., Hoisch, T.D., Cruz-Urbe, A.M. and Vervoort, J.D. 2012. Geodynamics of synconvergent extension and tectonic mode switching: Constraints from the Sevier-Laramide orogeny. *Tectonics*, **31**: 1-20.

Wheeler, J.O. and McFeely, P. 1987. Tectonic assemblage map of the Canadian Cordillera and adjacent parts of the United States of America. Geological Survey of Canada, Open File 1565.

Woodsworth, G.J., Anderson, R.G. and Armstrong, R.L. 1991. Plutonic regimes. *In* *Geology of the Cordilleran Orogen in Canada*. Edited by H. Gabrielse and C.J. Yorath. Geological Survey of Canada, *Geology of Canada*, No. 4, Chap. 15, pp. 491-531.

Zhang, G. and Hynes, A. (1994): Fabrics and kinematic indicators associated with the local structures along Finlay-Ingenika Fault, McConnell Creek area, north-central British Columbia. *Canadian Journal of Earth Sciences*, **31**: 1687-1699.

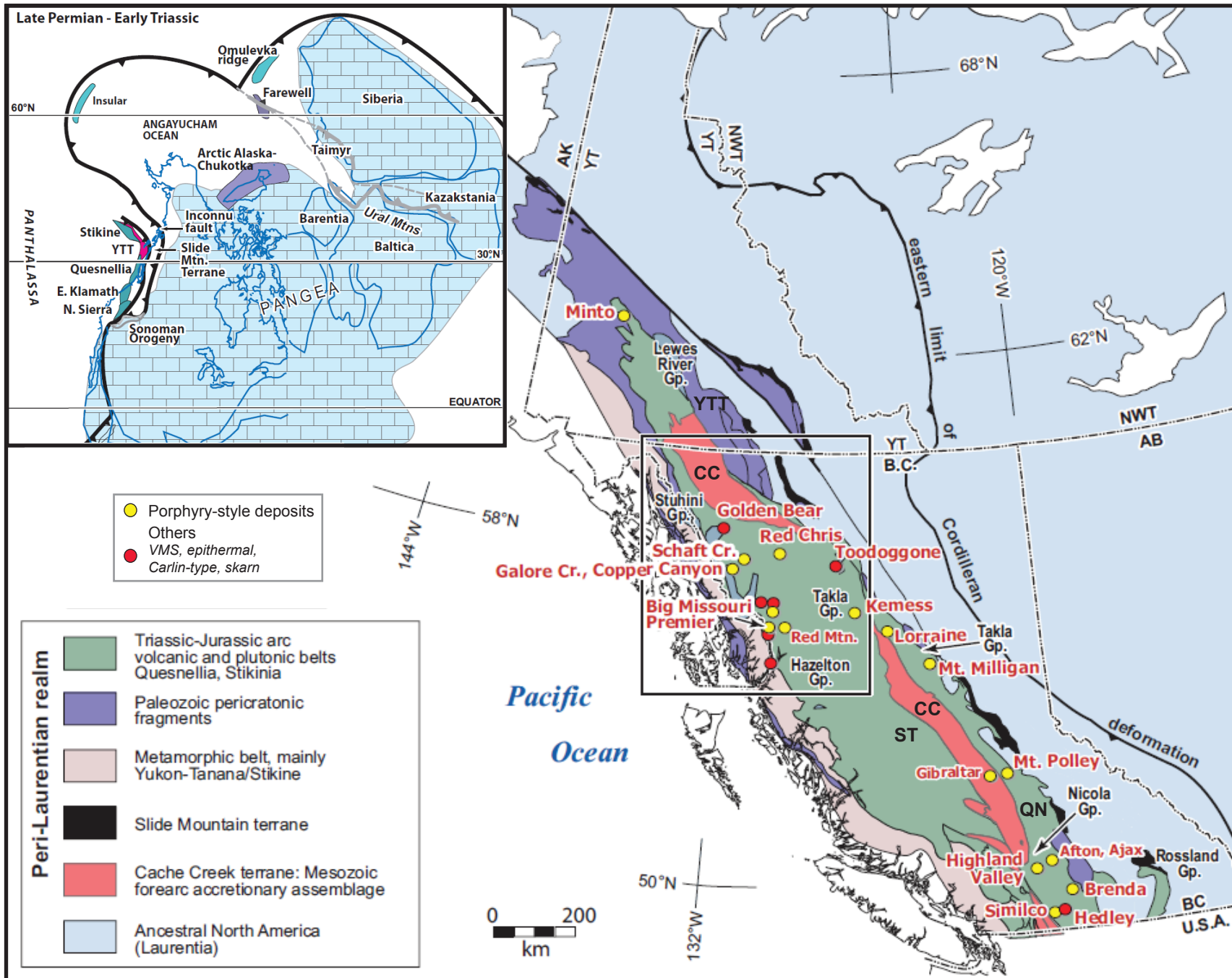


Figure 1: Triassic to Middle Jurassic magmatic belts and associated deposits of the Intermontane terranes. Deposit locations are from McMillan et al. (1995). Inset shows End Paleozoic (Late Permian – Early Triassic) schematic reconstruction. QN - Quesnel Terrane, ST - Stikine Terrane, CC - Cache Creek Terrane, YTT – Yukon-Tanana Terrane. Modified from Nelson and Colpron (2007).

## Legend

Quaternary Alluvium and Glacial Till: Qal

### Unnamed Cretaceous Conglomerate

K cg Polymictic clast-supported cobble conglomerate, includes gneiss, marble, chert, granitoid and volcanic clasts

### Unnamed Sinemurian to Pleinsbackian Sediments

EJ sn Red, brown-grey siltstone, sandstone, and conglomerate

### Sinemurian (196 Ma)

EJ t Quartz phyrlic latite tuff

### Late Triassic to Early Jurassic

TJ vcg Well-bedded and sorted, polymictic volcanic conglomerate pink, monzonite to K-spar megacrystic syenite clasts

TJ mz Pyroxene-hornblende monzodiorite, hornblende-biotite monzonite and potassium feldspar megacrystic syenite

### Late Triassic (205-200 Ma)

MPic Hydrothermal altered intrusive: holocrystalline dioritic to monzonitic intrusions

LT BJ Melanocratic pseudoleucite syenite

### Late Triassic Nicola Group

LT Nvl Red-brown, massive, polymictic breccia, feldspar and hornblende crystal tuff

LT Nhv Hornblende phyrlic andesite basalt flows and breccias

LT Npt Plagioclase phyrlic, pyroxene lapilli tuff, breccia and minor flows

LT Nlm Limestone, ash and crystal-rich sandstone and maroon siltstone

LT Nav Pink-white analcime pyroxene ± olivine basalt breccia, flows and tuffs

LT Npv Green and maroon pyroxene porphyry breccias, pyroxene-olivine basalt flows and crystal-rich sediments

LT Nvb Massive, coarse polymictic volcanic breccias, graded sandstones, siltstone and rare limestone breccia horizons

LT Ns Graphitic and quartzose phyllite, shale, siltstone and sandstone

### Middle to Late Triassic

MLT Ns Grey siltstone, normal graded sandstone and cherty shale with pyroxene and plagioclase-rich crystal sandstones

## Symbols

- Contact - well defined (<10 m)
- - - Contact - moderately defined (<50 m)
- Contact - poorly defined (<100 m)
- Fault - slip unknown
- ▲ Thrust Fault
- - - Fault - approximate
- ... Buried/ concealed fault
- ... Unconformity
- 50 Bedding
- Qal Contact

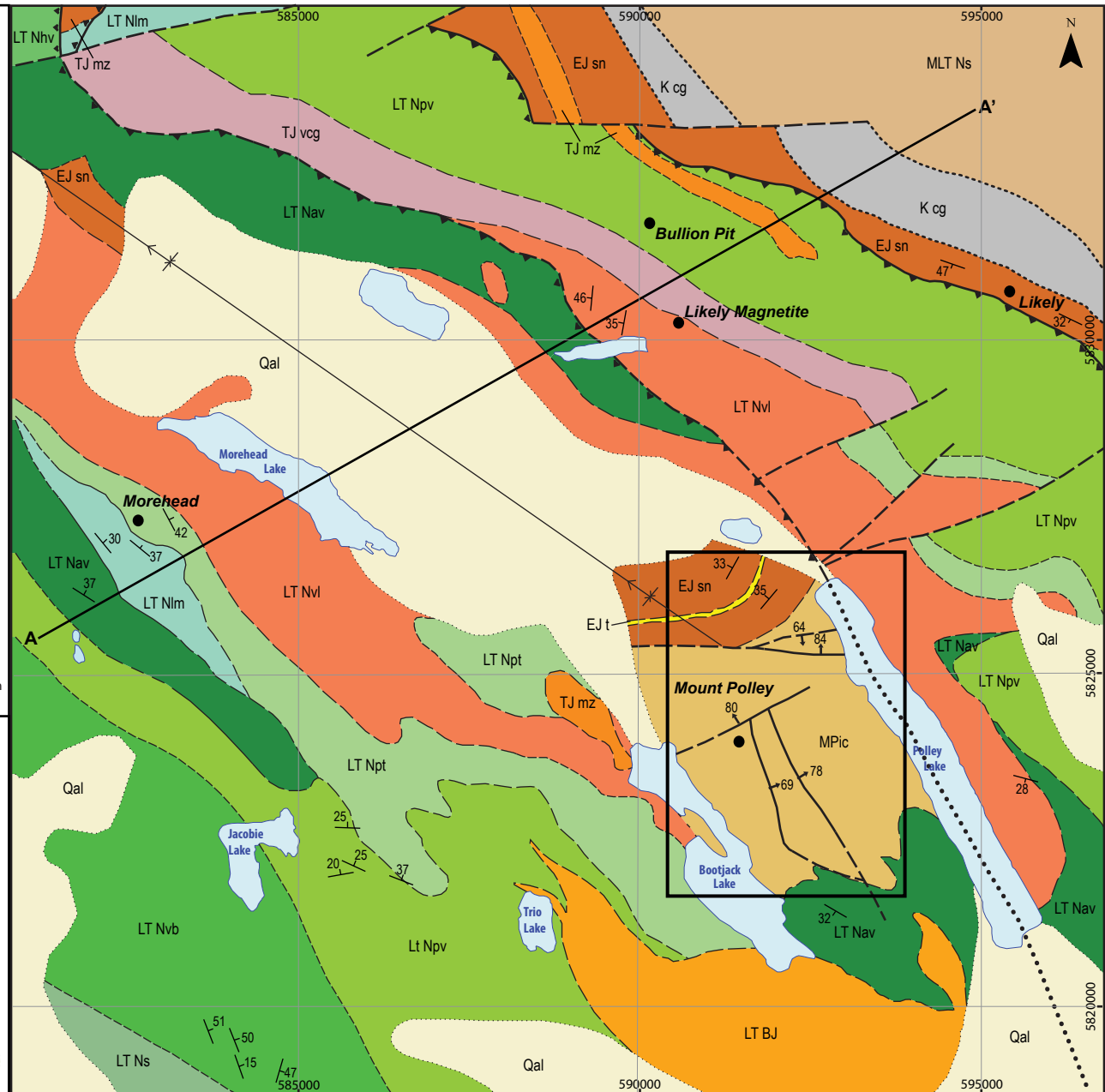
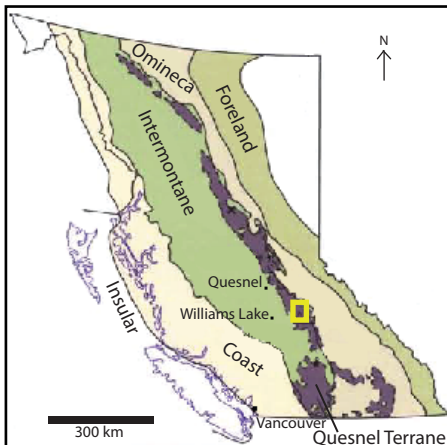


Figure 2: Regional geologic map of the Mount Polley mine and surrounding district. Inset map shows the location of the five morphogeologic belts of the Canadian Cordillera, with the Quesnel Terrane shaded purple. Black box shows the location of the Geology of the Mount Polley District map. Modified from Geoscience Map 2007-1, 1:50,000.

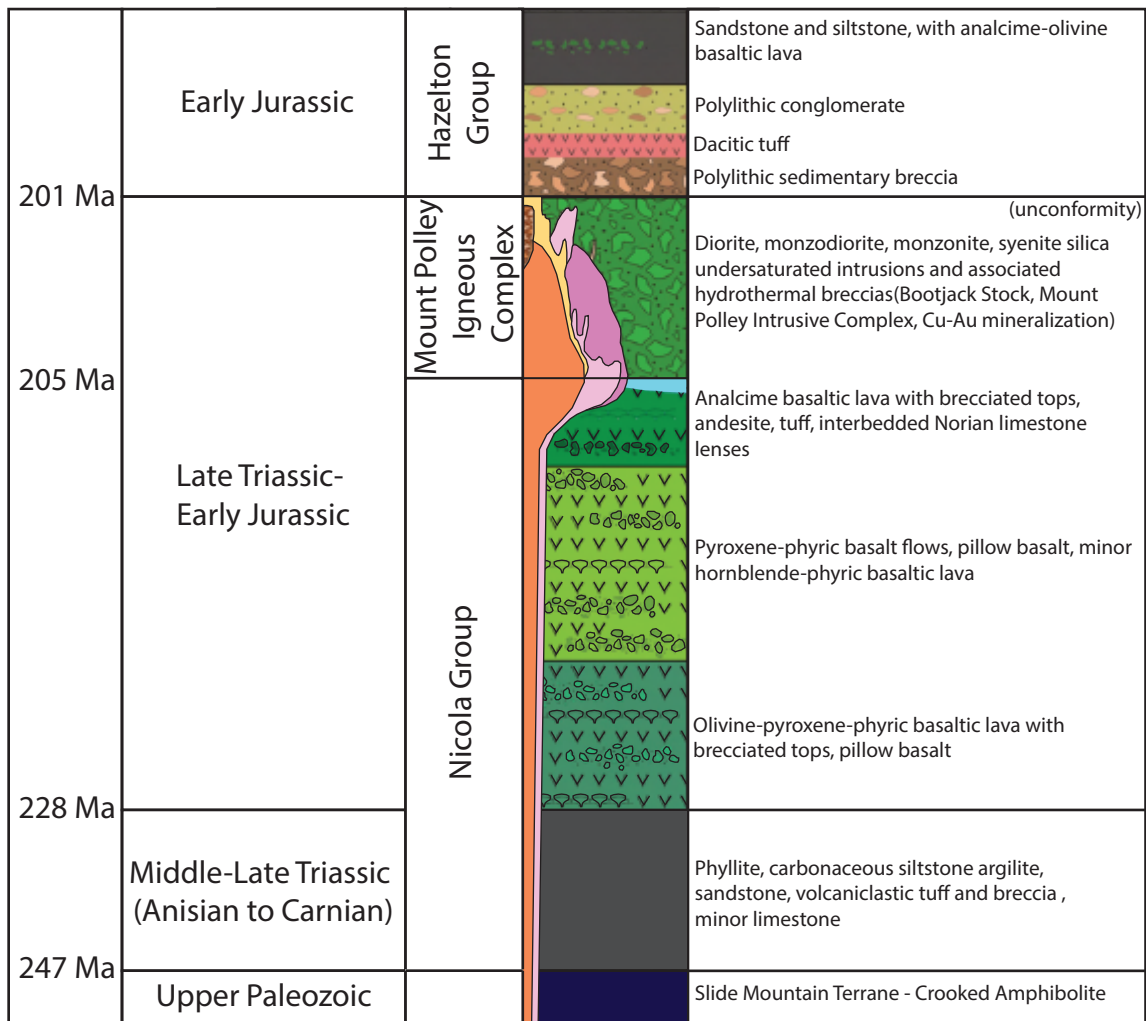


Figure 3: Simplified stratigraphic column of the lithologies in the Mount Polley district from Jackson (2008; after Bailey, 1978; Panteleyev et al., 1996; Logan and Mihalynuk, 2004; Logan and Bath, 2006; Logan et al., 2007).

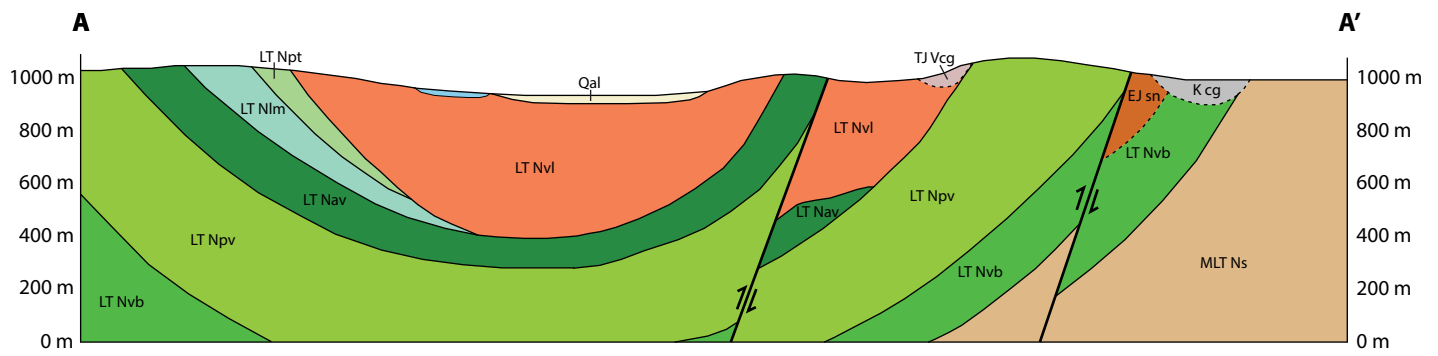
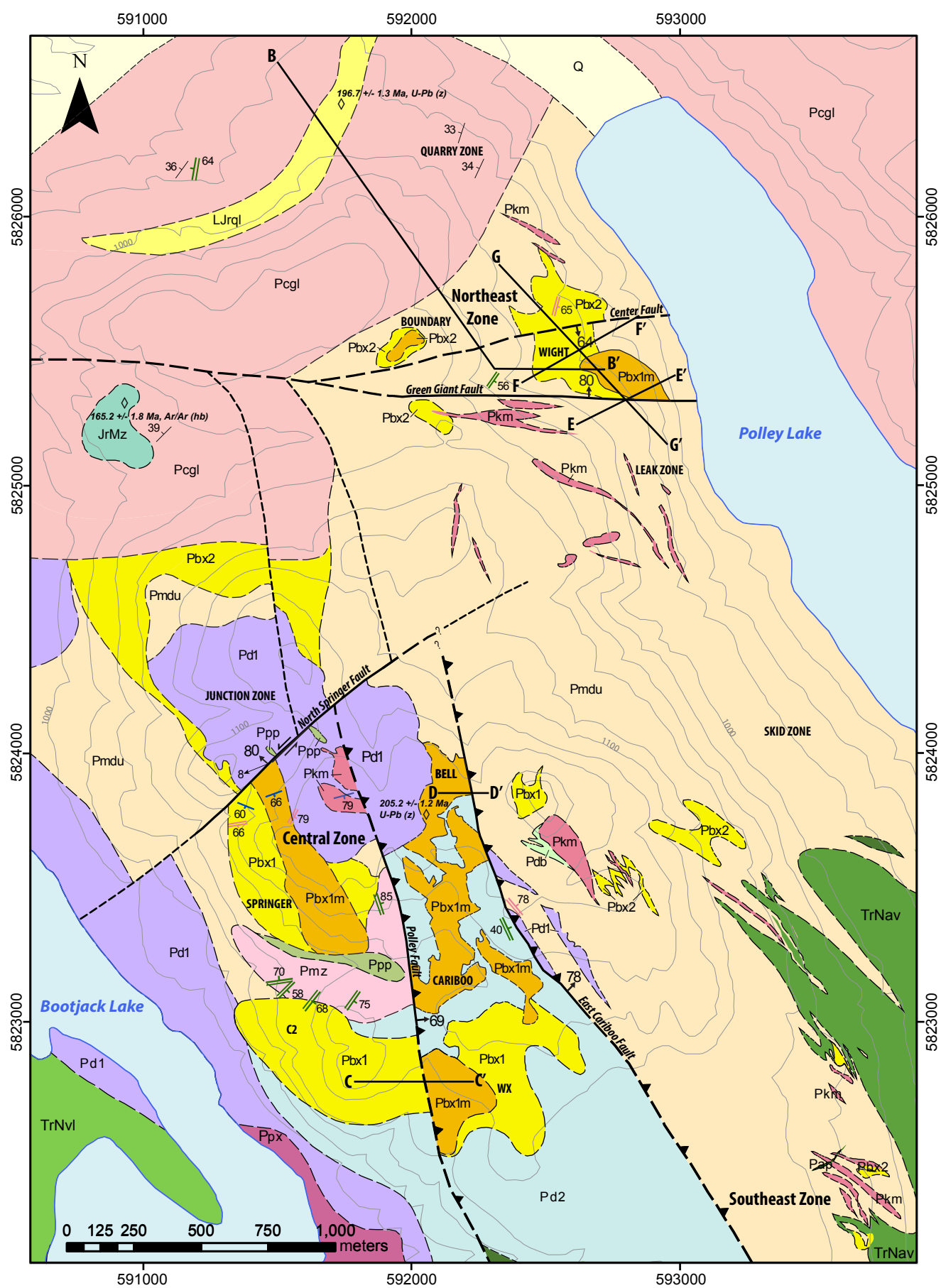


Figure 4: Cross Section A-A', located on Figure 1. Modified from Geoscience Map 2007-1, 1:50,000.





## Legend

### QUATERNARY

**Q** Till, glaciofluvial, glaciolacustrine deposits.

### LATE TRIASSIC - JURASSIC

**Pap** Augite porphyry dike. Green-grey, very fine grained basaltic-andesitic dikes with subequant clinopyroxene phenocrysts; map includes similar but aphyric basaltic-andesite dikes.

**JrMz** Monzodiorite intrusion (165.2 +/- 1.8 Ma, Ar/Ar hb). Dark grey, very fine grained, containing <1-2 mm K-feldspar and plagioclase phenocrysts.

**LJrqI** Quartz Latite (196.7 +/- 1.3 Ma, U-Pb zircon). Plagioclase-hornblende-biotite- and minor quartz phenocrysts in aphanitic mauve-grey matrix.

**Pcgl** Sedimentary breccia and conglomerate. Massive, coarse, matrix-supported polymictic breccia and minor cobble conglomerate, with clasts of intermediate intrusives, various volcanics, and microporphyries, in a grey to maroon crystal-lithic matrix; minor graded bedding. Interbedded graded sandstones. Up section breccia clasts become increasingly porphyritic, derived from the Mount Polley igneous complex. Strong hematite cement locally.

### LATE TRIASSIC

#### Mount Polley Igneous Complex

**Pbx1** Hydrothermal fragmental breccia (polymictic to oligomictic) comprising subangular to subrounded diorite to monzonite porphyry clasts in a igneous cement or matrix of fine to coarse porphyritic rock flour. Gradational contact to monomictic jigsaw-fit breccia to coherent diorite to monzonite intrusions. Pbx1 - characteristic texture-destructive alteration due to moderate to strong secondary K-feldspar/biotite +/- albite +/- magnetite +/- actinolite/diopside replacing groundmass or breccia matrix. Pbx1m - mineralized to ore or near ore-grade with chalcopyrite +/- bornite or pyrite.

**Pbx2** Pbx2 - same as Pbx1 but occurs outside the central MPIC and is characterized by less texture-destructive alteration.

**Pbx2m** Pbx2m - mineralized to ore or near ore-grade.

**Pkm** Potassium feldspar-(plagioclase) phyric monzonite. Very pale to deep pink, fine- to medium-grained groundmass, mm to megacrystic (2-3cm) phenocrysts, trachytoid alignment in some dikes or larger intrusions.

**Ppp** Plagioclase feldspar porphyry (monzodiorite). Grey, to red-pink where altered, typically crowded with phenocrysts up to 5mm, locally aligned, in fine-grained groundmass

**Pmz** Monzonite to monzodiorite. Pale pink, medium grained, even textures, interstitial K-feldspar, probably primary. More homogenous than units Pd2, Pmd, and lacking inclusions.

**Pdb** Dioritic porphyry, banded. Pale green and pale grey, fine to medium grained, wispy laminated (possible flow banding) leucodiorite. Gradational unit with Pmd.

**Pmd** Monzodiorite to monzonite, some diorite, undivided. Heterogeneous unit of intermediate intrusions with ill-defined internal contacts. Pink to grey, fine to medium grained, equigranular to plagioclase phyric; mafic lithic and other inclusions common. Includes small dikes and isolated hydrothermal breccias, not differentiated on map.

**Pd2** Uneven textured diorite to monzodiorite, leucodiorite, and minor monzonite. Grey to green-grey, cream-grey (pink where more altered), medium grained, usually inequigranular to subporphyritic (plagioclase, locally augite). Variable textures and numerous small inclusions characteristic.

**Pd1** Even textured augite (biotite) diorite to monzodiorite. Speckled medium-grey, medium to coarse grained, mostly equigranular.

**Ppx** Pyroxenite, minor melagabbro. Dark green to black, medium to coarse grained.

### NORIAN (-RHAETIAN?)

#### Nicola Group

**TrNvl** Red-brown, massive, polymictic volcanic breccia, feldspar and hornblende crystal tuff

**TrNav** Pink-white analcime pyroxene and olivine basalt breccia, lava flows, and tuffs

#### Key to Symbols

—	Contact - well defined (<10m)	↗	Small fault, unknown slip
- - -	Contact - moderately defined (<50m)	↘	Bedding
- - - -	Contact - poorly defined (<100m)	↗↘	Augite porphyry dike and monzodiorite dikes (<10m)
— / —	Fault, location well-defined	↗↘	Plagioclase porphyry and K-feldspar porphyry dike (<10m)
- - / - -	Fault, location moderately defined	↗↘	Lineation
- - - / - - -	Fault, location poorly defined	◇	Geochronology Sample
— / — / —	Sinistral fault, location well-defined		
- - / - - / - -	Reverse fault, location well-defined		
- - - / - - - / - - -	Reverse fault, location moderately defined		

Figure 5: Geologic map of the Mount Polley igneous complex, modified from Rees (unpublished map, 1:8,000). Isotopic age dates from Logan et al. (2007).



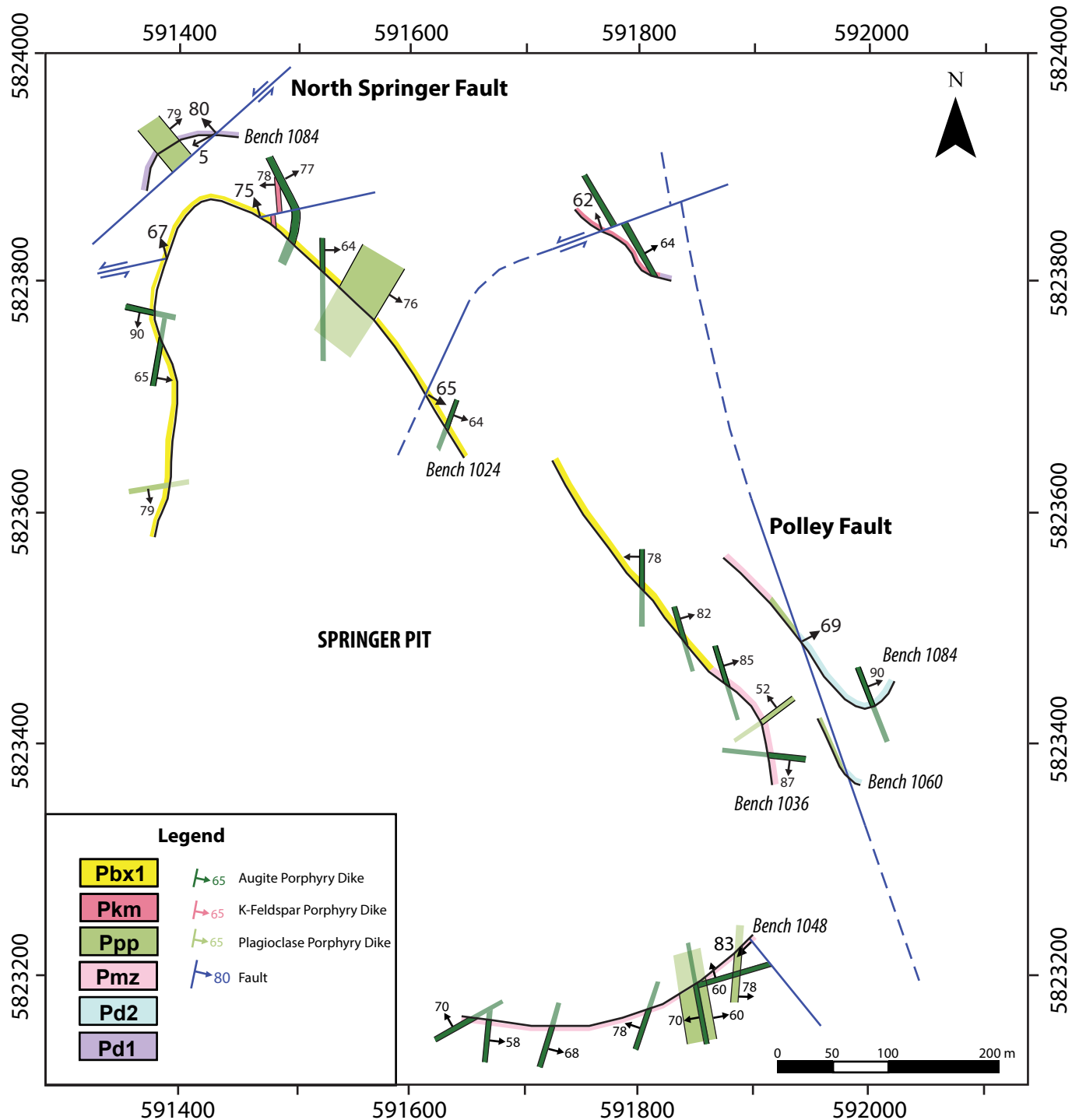


Figure 6: Compilation geologic map of bench mapping in the Springer Pit. Dark colors of dikes and continuous lithology colors are shown on rock side of the bench face line. Surface represents mining level during the 2012 field season. Bench elevations are in meters. Mapped at 1:5,000 scale.

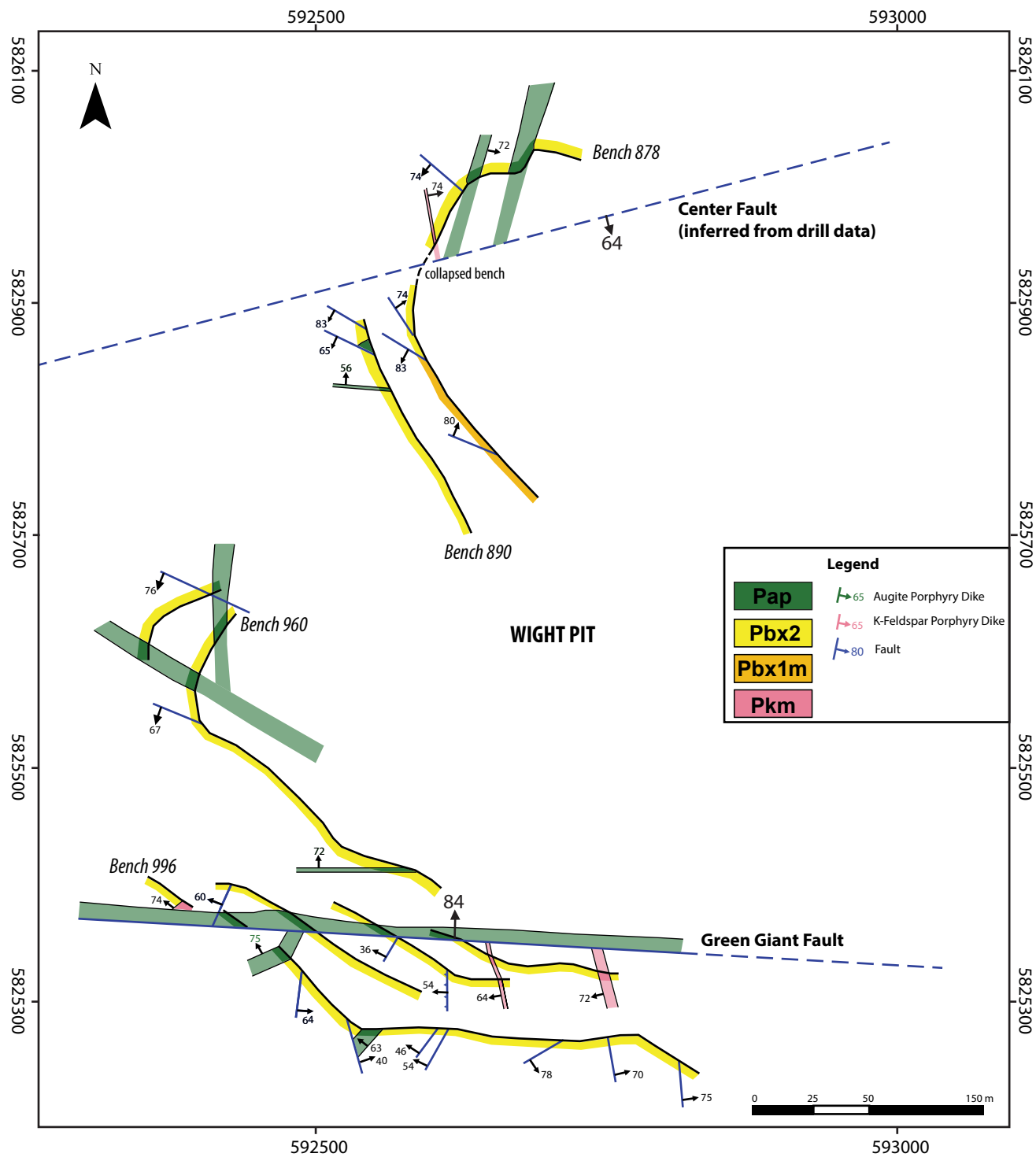


Figure 7: Compilation geologic map of bench mapping in the Wight Pit. Dark colors of dikes and continuous lithology colors are shown on rock side of the bench face line. Surface represents open pit benches exposed during the 2012 field season. Mapped at 1:7500 scale.

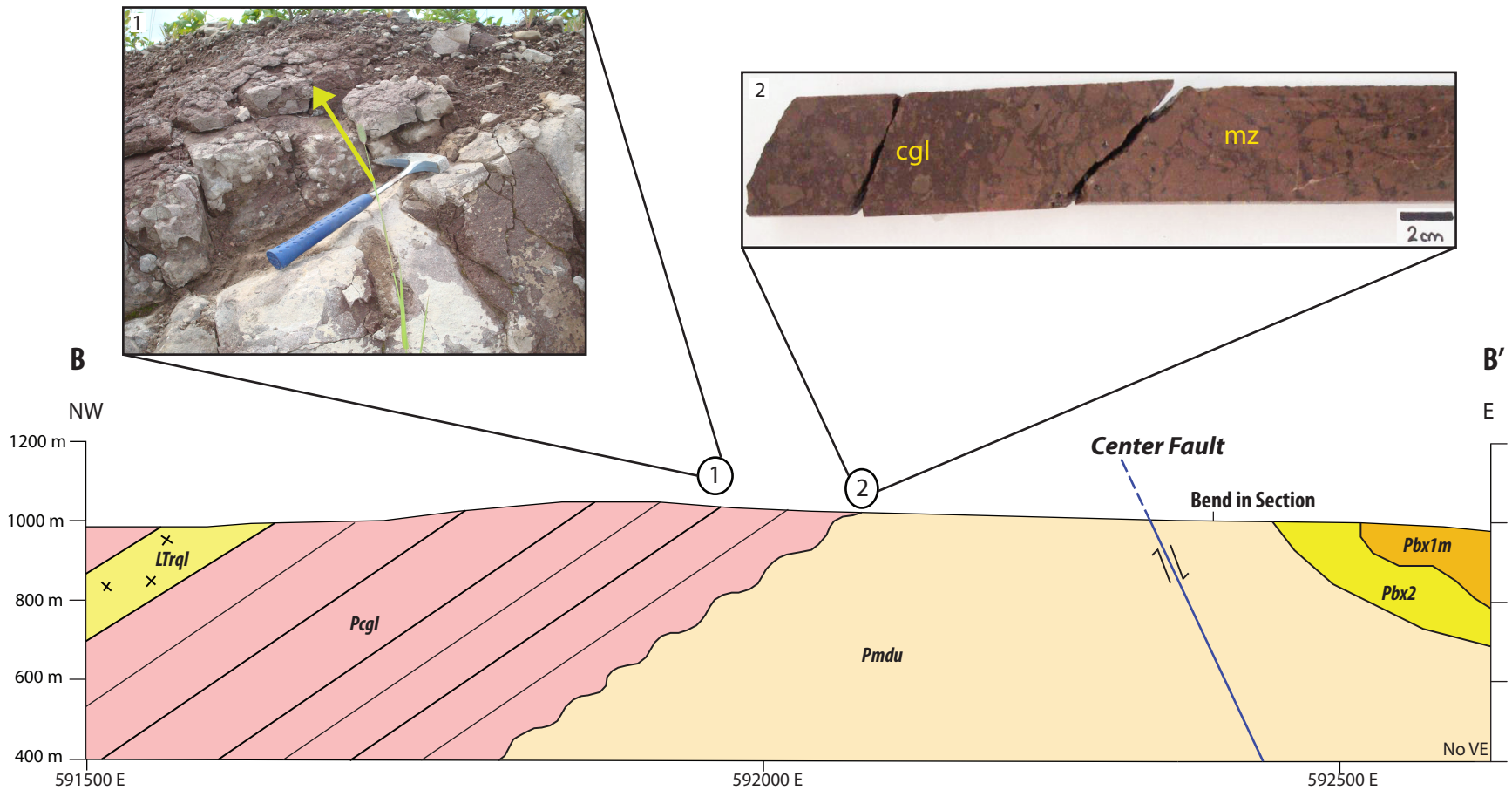


Figure 8: Cross section B-B', location shown on Figure 5. Section shows the Northeast Zone mineralization, overlying unconformity, basal conglomerate, tilted bedding, and quartz latite ignimbrite. See Figure 5 for key and unit descriptions. Bedding in Pcgl unit shown for illustration. Photo 1 shows bedding in the conglomerate, where the yellow arrow indicates stratigraphic tops. Photo 2 shows the unconformity in drill core hole WB-08-253 from 91.40 m to 91.75 m. mz - monzonite, cgl - conglomerate.

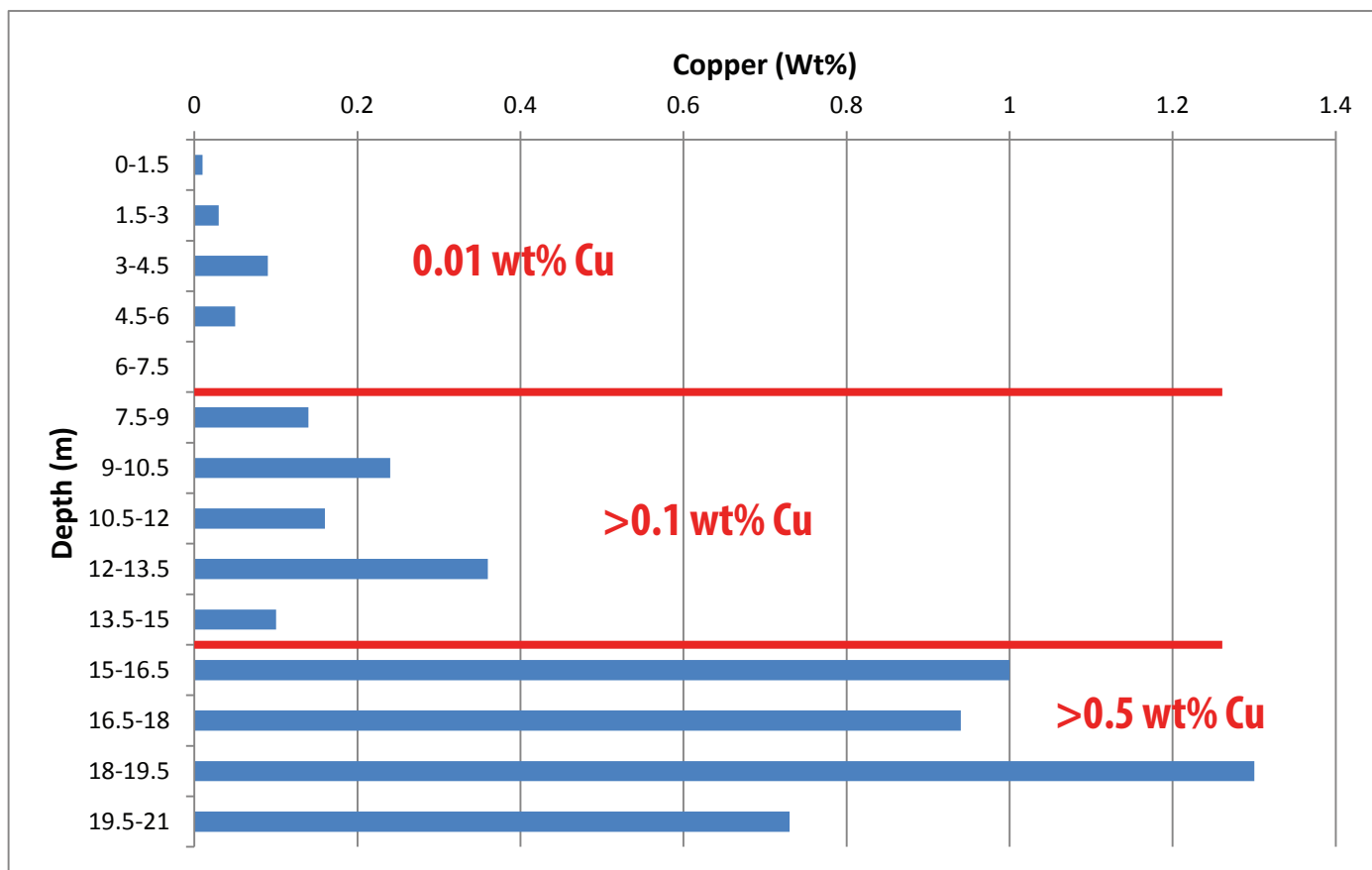


Figure 9: Copper grade vs. depth chart showing how simplifications were made in order to group the copper assays into three categories: <0.1 wt% Cu, 0.1 - 0.5 wt% Cu and >0.5 wt% Cu.

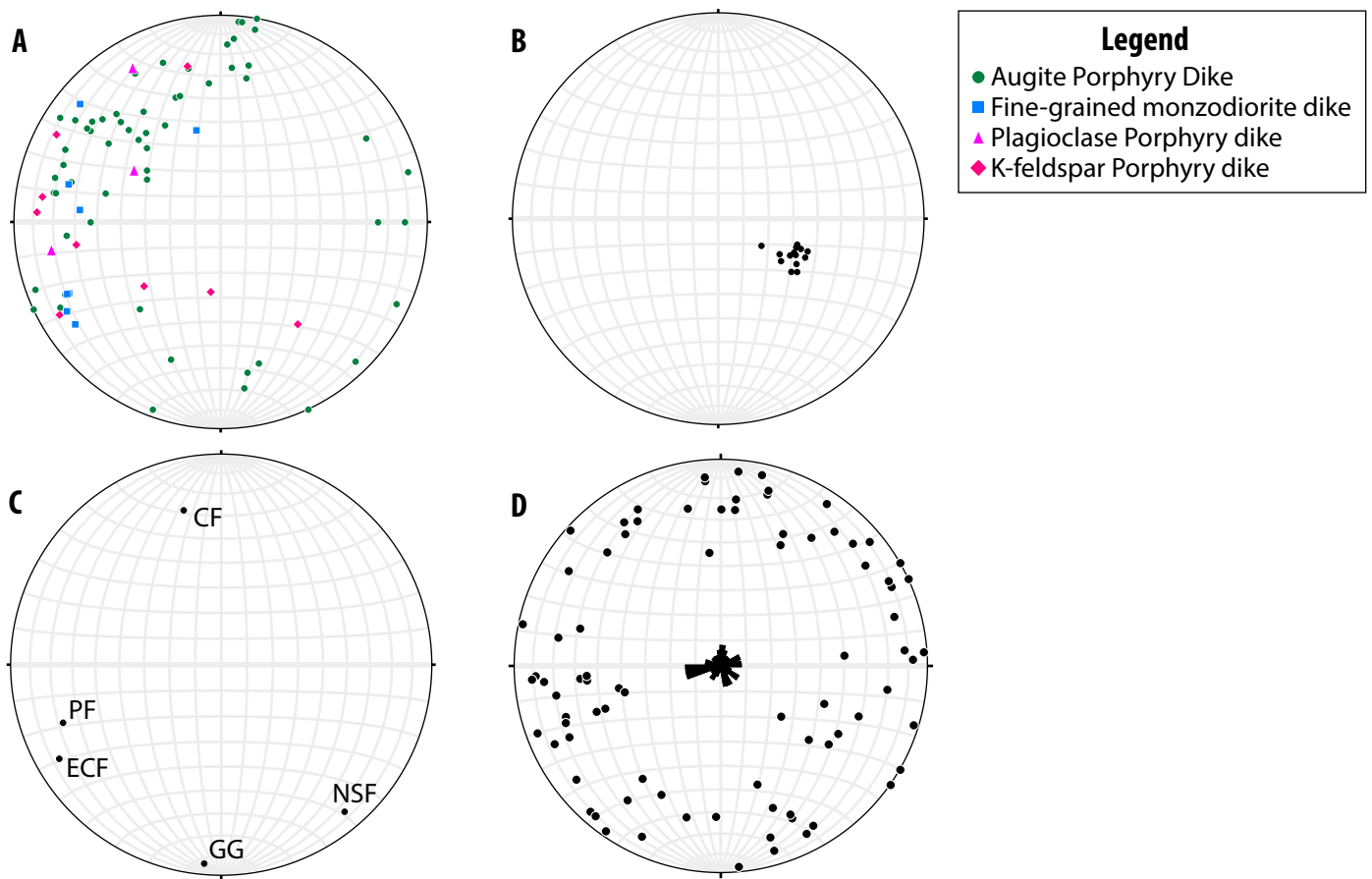


Figure 10: Lower hemisphere stereonet showing poles to planes of structural data from the Mount Polley district. (A) orientations of K-feldspar porphyry, plagioclase porphyry, augite porphyry, and fine-grained monzodiorite dikes. Symbols explained in the legend. (B) orientation of bedding in rock unit Pcgl (C) Orientations of the major faults. PF - Polley Fault, ECF- East Cariboo Fault, NSF - North Springer Fault, GG- Green Giant Fault, CF - Center Fault. (D) Orientations of the minor faults in the district. Rose diagram shows a weak east-west preferred orientation.



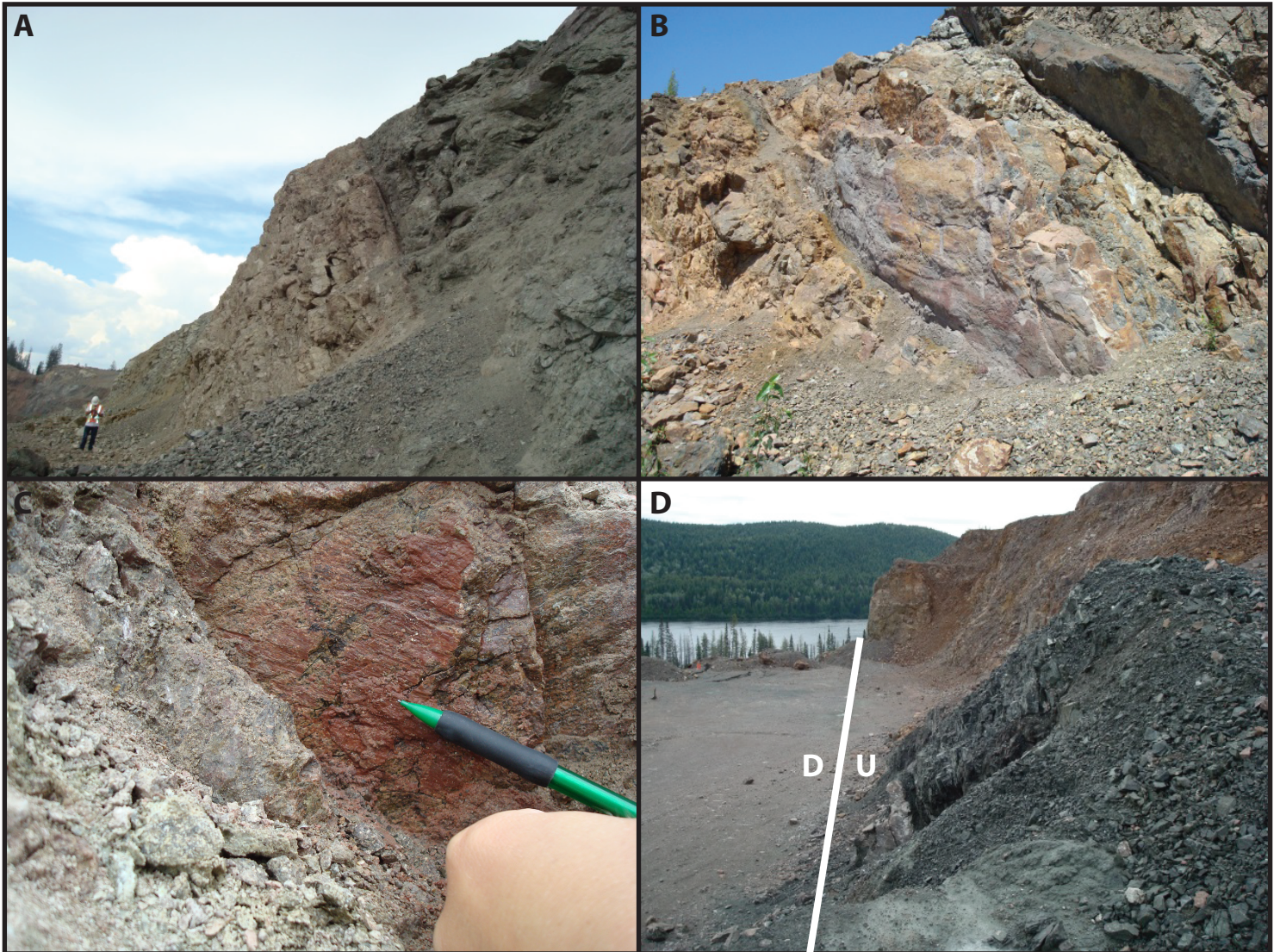


Figure 11: (A) Photo of the Polley Fault looking northwest from the southeastern part of the Springer Plt. Fault juxtaposes plagioclase porphyry dike (left) and diorite (right). (B) Photo of the East Cariboo Fault looking north from the uppermost bench in the Cariboo Pit. Slickenlines on the fault plane plunge  $30^\circ$  (C) Photo of slickenlines shallowly plunging to the southwest on the North Springer Fault. Photo was taken on the 1084 bench in the Springer Pit. (D) Photo looking east from the top bench of the Wight Pit showing the fault trace of the Green Giant Fault. At surface the fault is hosted by a green augite porphyry dike. White line indicates the location of the fault trace.

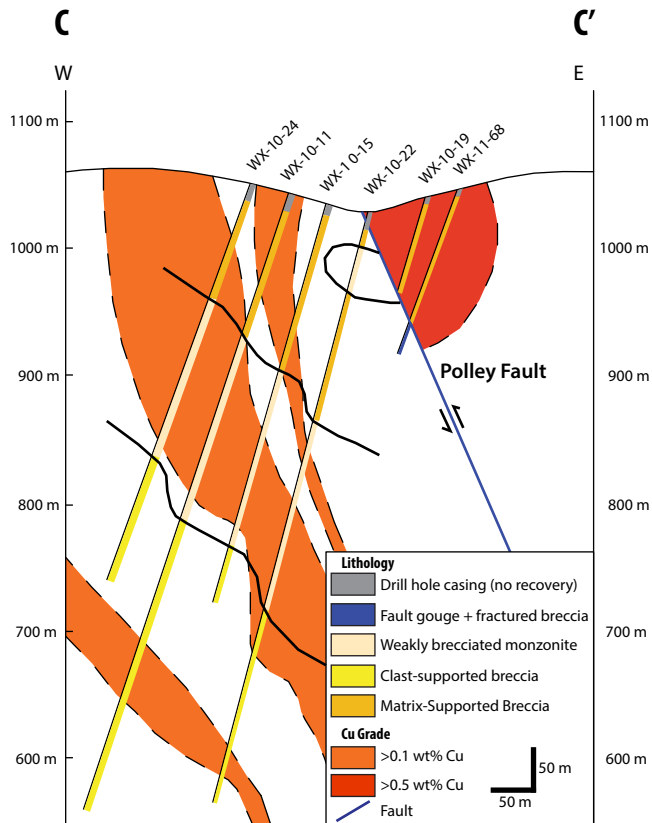


Figure 12: Cross section C-C', location shown on Figure 5. Lithology is indicated adjacent to the drill hole. Black lines indicate contacts. Greater than 1 wt% Cu occurs in the hanging wall of the Polley Fault and zones of disseminated low grade (>0.1 wt% Cu) is found in the footwall.

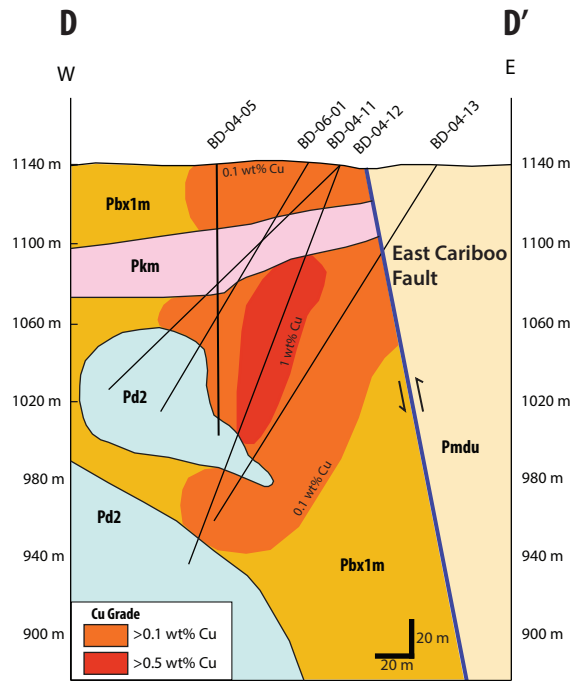


Figure 13: Cross section D-D', location shown on Figure 5. Lithology labels same as in Figure 5. Where indicated >0.1 wt% Cu is located within the Pbx1m lithology. Monzonite in the hanging wall and the plagioclase porphyry dike (Pkm) in the footwall of the East Cariboo Fault have no copper mineralization.





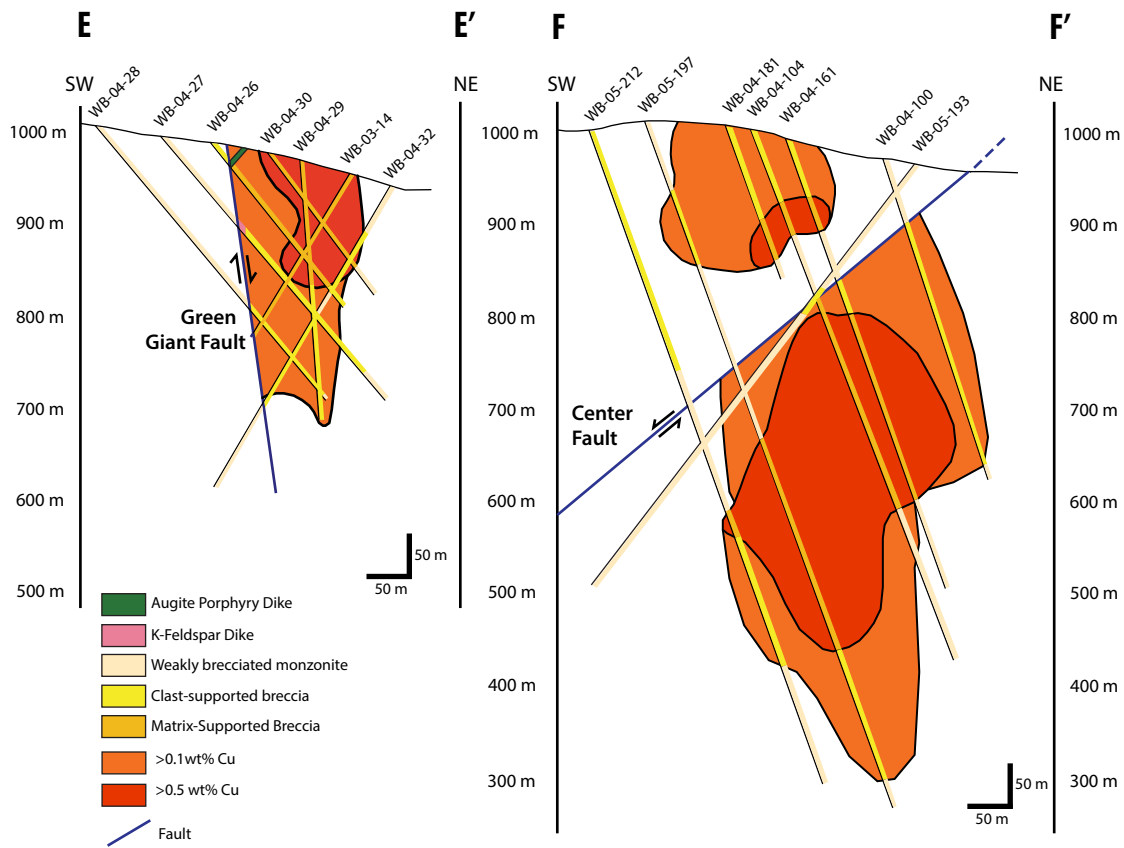


Figure 15: Cross section E-E' and F-F', locations shown on Figure 5. Both cross sections constructed using the copper grade in each drill hole. Lithology is indicated adjacent to each drill hole. Both the upper and lower ore zones are shown, where the Center Fault is inferred to cut the lower ore body, and the Green Giant Fault cuts the upper ore zone. The shallow dip of the Center Fault reflects the oblique angle of the cross-section relative to the fault.

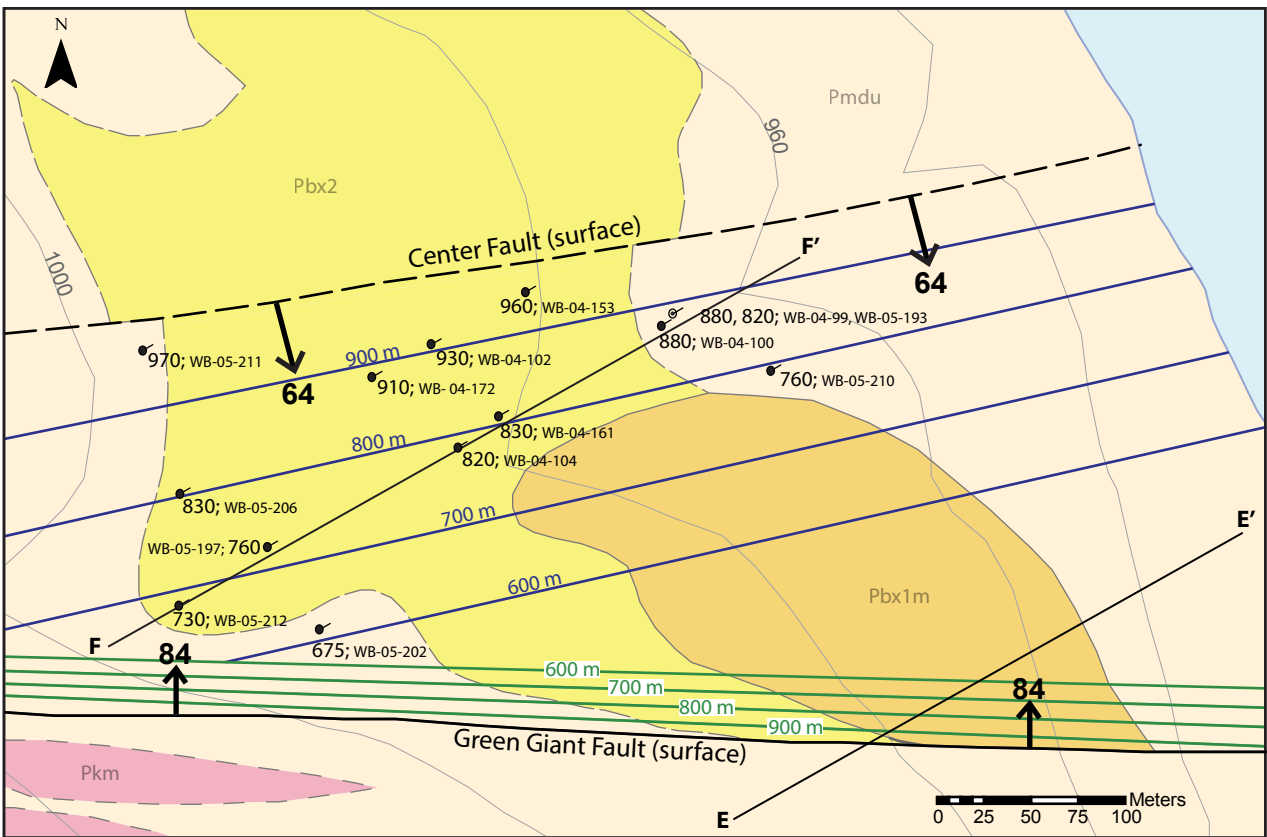
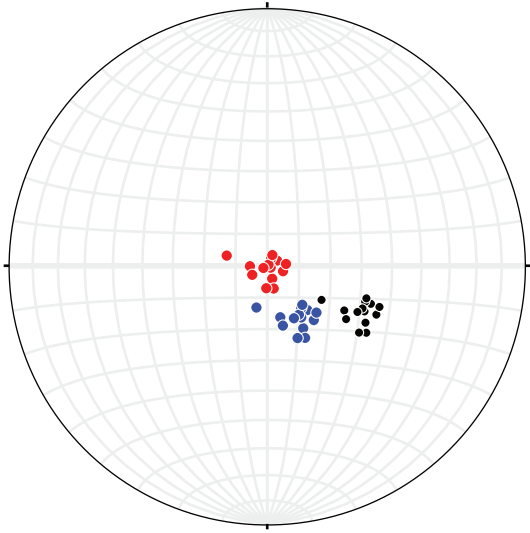
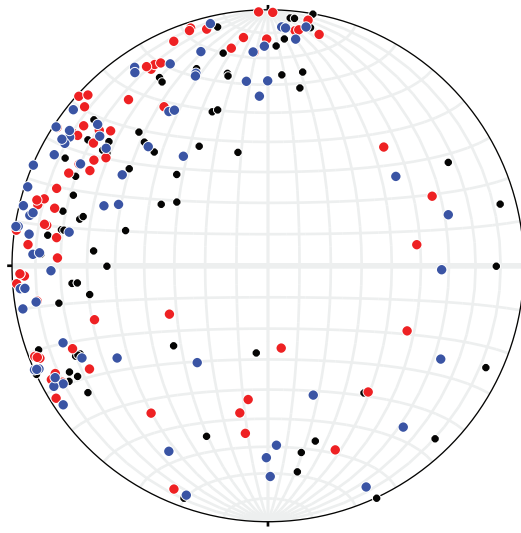


Figure 16: Structural contour map of the Green Giant Fault and the Center Fault, showing the inferred surface trace of the latter. Blue lines show contours on the Center Fault fault plane, and green lines show contours on the the Green Giant Fault fault plane. Lithology descriptions same as Figure 5. Ex: ●675; WB-05-202: ● indicates location of the drill hole collar and the dip direction of the drill hole, 675 - depth at which the drill hole crosses the fault plane. WB-05-202 - hole i.d. ○ indicates a collar with two drill holes of different dip.

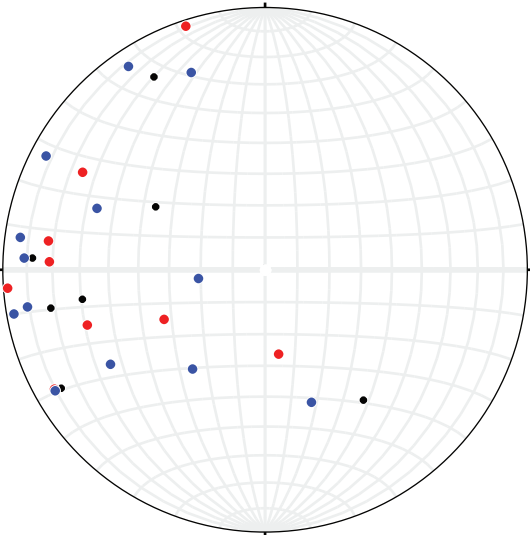
## A. Bedding



## B. Augite Porphyry Dikes



## C. K-Feldspar porphyry and Plagioclase porphyry Dikes



## D. Major Faults

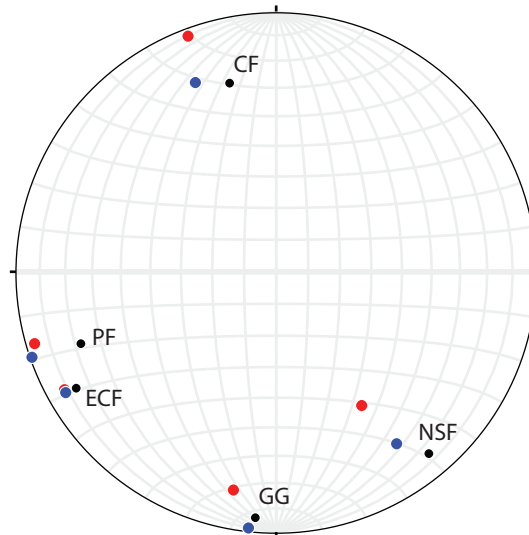
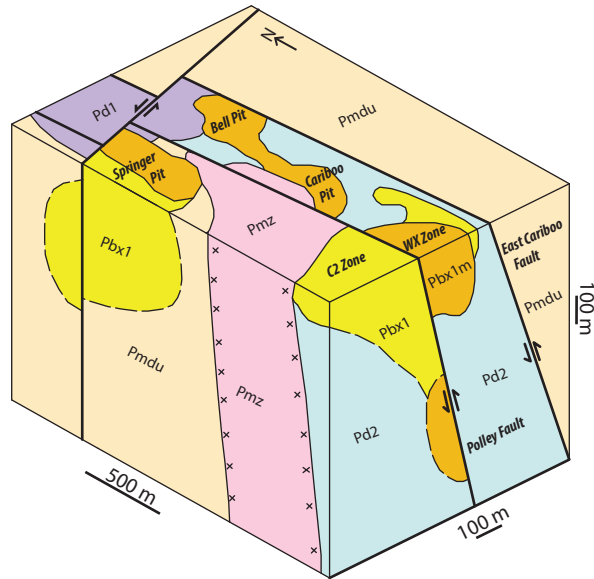
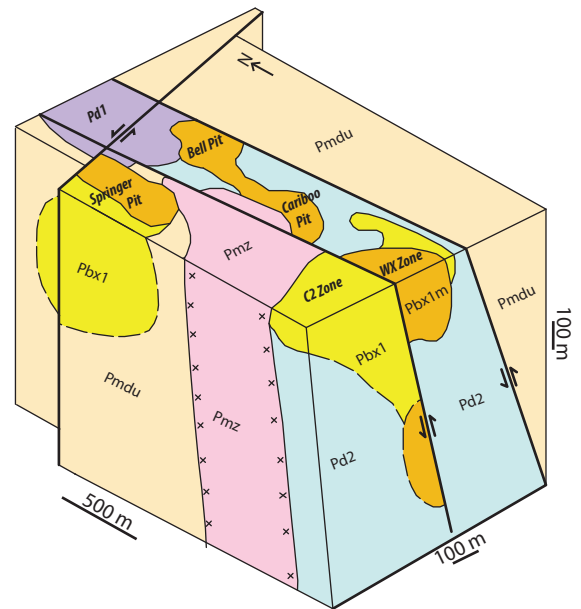


Figure 17: Stereonets showing poles to planes of restored structural data. The black poles show the present day orientation. The blue poles show restored data using the 21° NNW tilt and the red poles show restored data using the 33° NW tilt. The first rotation (BLUE) was done about a 173° - 353° rotation axis, restoring 21° NNW of tilt. The second rotation (RED) was done about a 25° - 205° rotation axis, restoring 33° NW of tilt. (A) Bedding. (B) Augite porphyry dikes. (C) K-feldspar porphyry and plagioclase porphyry dikes. (D) Major faults in the Mount Polley district. PF - Polley Fault, ECF - East Cariboo Fault, NSF - North Springer Fault, GG - Green Giant Fault, CF - inferred Center Fault.

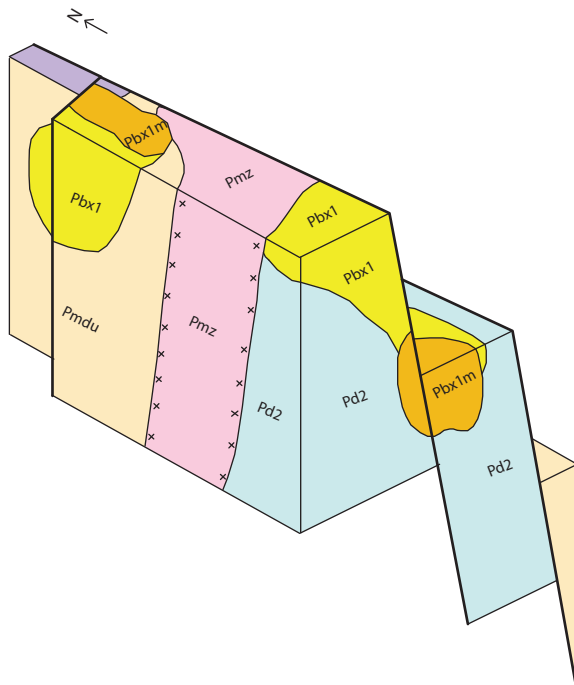
A. Present



B. Restored North Springer Fault



C. Restored 33° NW Tilt, Polley Fault, and East Cariboo Fault



D. Original Geometry

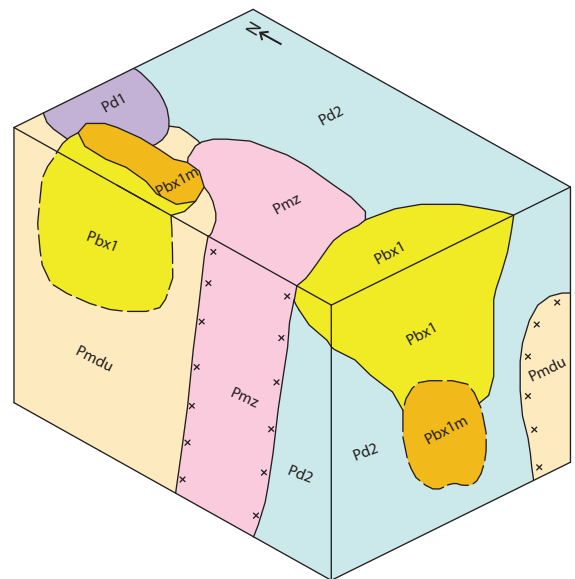


Figure 18: Proposed restoration of the Central Zone. Lithologies correspond to map units in Figure 5. (A) Present orientation of the major faults and ore bodies in the Central Zone. (B) Restoration of sinistral slip on the North Springer Fault. (C) Restoration of 33° NW tilt, and reverse slip on the Polley Fault and East Cariboo Fault. (D) Model of the original shape of the ore bodies immediately following porphyry emplacement. Location of open pits and exploration zones indicated in block A.

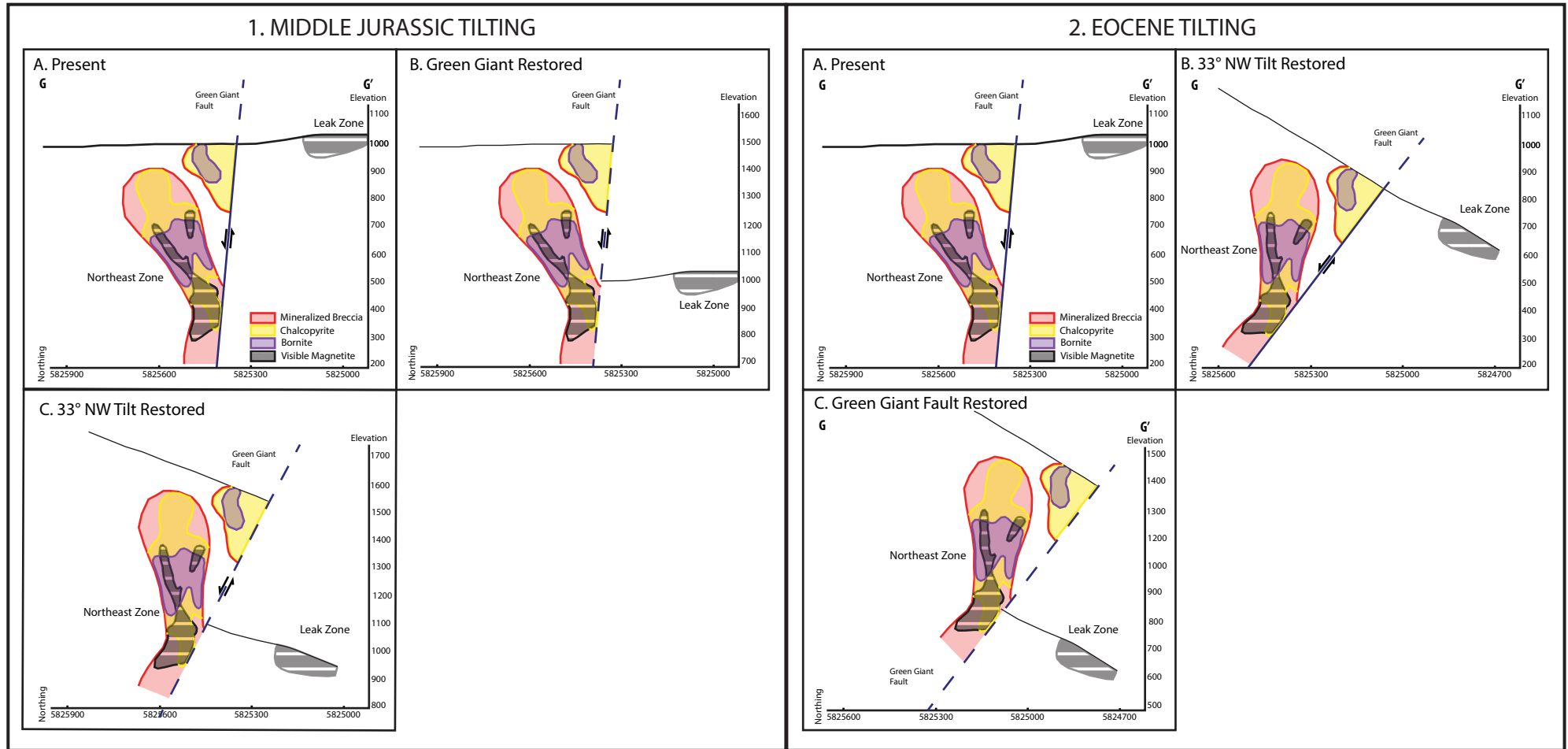
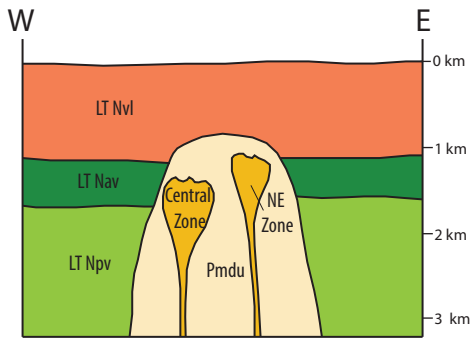
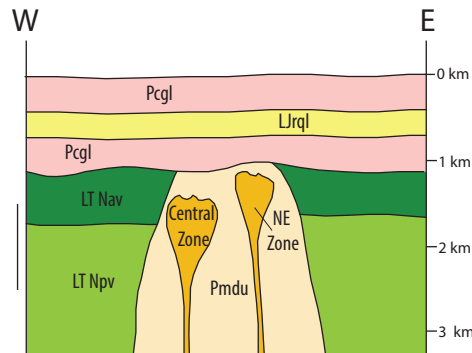


Figure 19: Two potential reconstructions of the Northeast Zone. Section G-G' looks NE. (Left) Restoration assuming that the tilting event occurred in the Middle Jurassic. (Right) Restoration assuming that the tilting event occurred during the Eocene. The red outline illustrates the boundary of the Cu-Au breccia mineralization. Interior coloured lines are contours showing the location of minerals within the breccia body, including chalcopyrite, bornite, and magnetite.

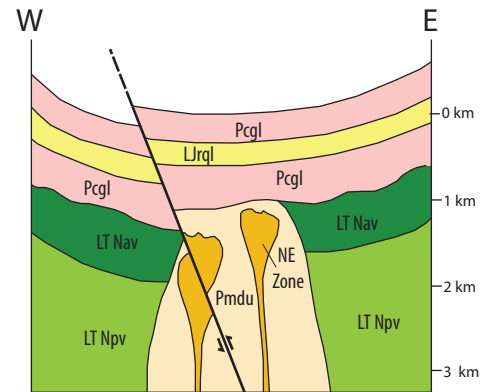
## 1. Intrusion of the MPIC



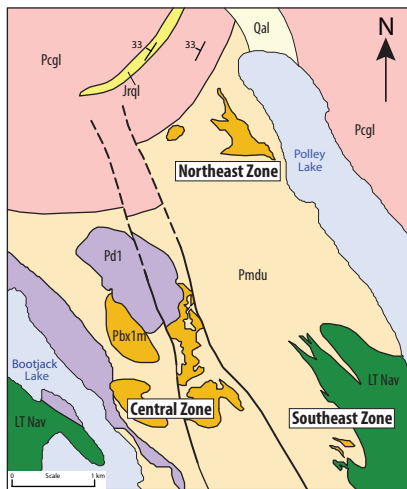
## 2. Erosion and Burial



## 3. Folding and Reverse Faulting



## 4. 33° NW Tilting



## 5. Normal &amp; Strike-Slip Faulting

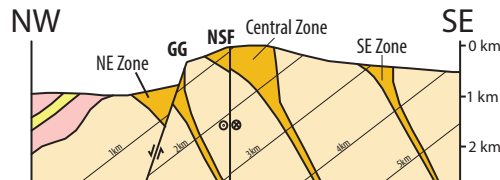
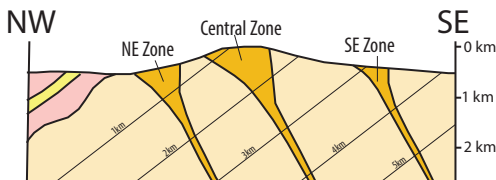
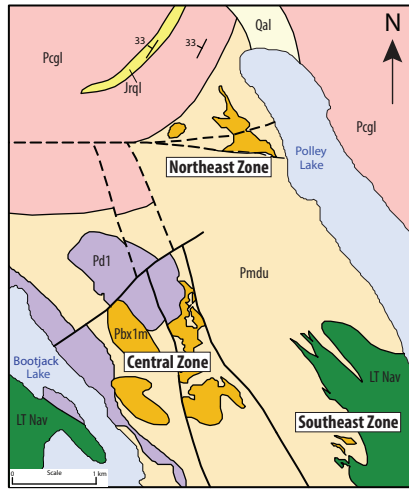


Figure 20: Schematic restoration of the ore zones in the Mount Polley district. Host rock is simplified into the Pmdu unit, and mineralized rock is simplified into the Pbx1m unit. (1) Emplacement of the Mount Polley igneous complex (MPIC) into the Nicola Group. The Northeast Zone is relatively shallower than the Central Zone. The Southeast Zone (not shown in this section) is the deepest ore zone. (2) Erosion and burial of the Mount Polley district results in the unconformity and the deposition of conglomerates, sandstones, and a quartz latite ignimbrite. (3) Reverse faults are the oldest structural event to impact the Mount Polley district. Approximately coeval is a regional folding event. (4) The Mount Polley district is tilted 33° NW. (5) Normal and strike-slip faults are the youngest structural events in the district, although their relative timing is unknown. In panels 4 and 5 the erosion level represents the present day exposure. Contours represent the paleodepth beneath the unconformity.

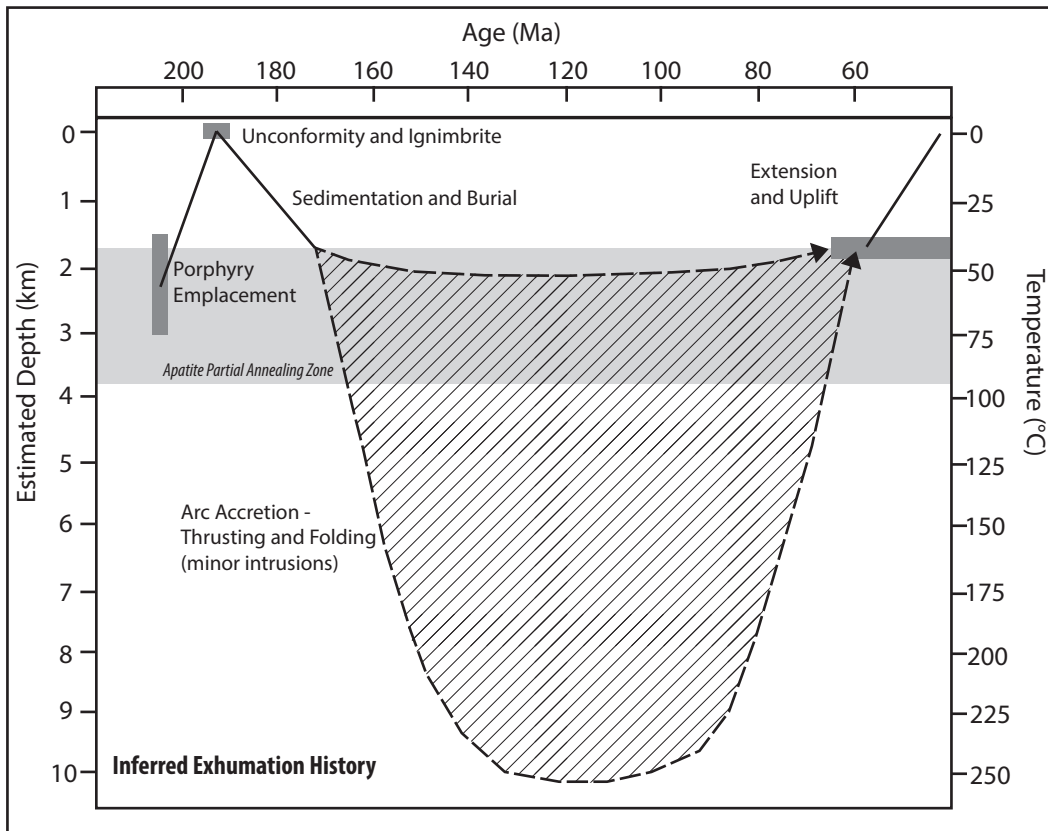


Figure 21: Inferred exhumation history of the Mount Polley district. Dark grey boxes show the measured and inferred depth and time constraints on each of the constrained structural events. Shaded zone shows the location of all possible cooling paths during the unconstrained time period. The light grey box demarcate the approximate depth of the apatite partial annealing zone, constructed assuming a normal geothermal gradient of 25 °C/km.



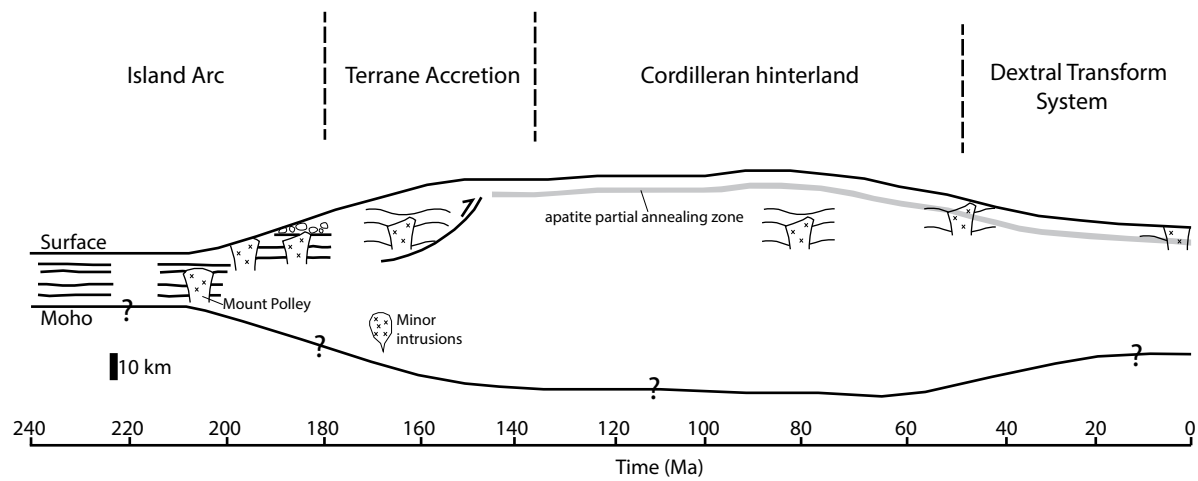


Figure 22 Schematic timeline showing the thickness of the crust in the Mount Polley porphyry copper district, and the relative depth of the Mount Polley igneous complex in the crust. Mount Polley has remained relatively shallow in the crust - deeper than 1.8 - 3.8 km and shallower than approximately 10.6 - 12.2 km, as indicated by apatite fission track and biotite  $^{40}\text{Ar}/^{39}\text{Ar}$  thermochronometry.

Location	Rock Type	Mineral	Method	Age (Ma)	Reference
Bootjack Stock	Coarse grained syenite	Hornblende	40Ar/39Ar	203.1 $\pm$ 2.0	Bailey and Archibald (1990)
Bootjack Stock	Orbicular syenite	Zircon	U-Pb	202.7 $\pm$ 7.1	Mortenson et al. (1995)
Bootjack Stock	Pseudoleucite syenite	Titanite	Pb-Pb	200.7 $\pm$ 2.8	Mortenson et al. (1995)
MPIC	Diorite	Zircon	U-Pb	201.7 $\pm$ 4	Mortenson et al. (1995)
MPIC	Plagioclase porphyry	Zircon	U-Pb	204.7 $\pm$ 3	Mortenson et al. (1995)
MPIC	Monzonite	Zircon	U-Pb	203.1 $\pm$ 1.6 - 12.7	Logan et al. (2007)
Polley Road	Monzonite	Hornblende	<sup>40</sup> Ar/ <sup>39</sup> Ar	165.2 $\pm$ 1.8	Logan et al. (2007)
Bell Pit	K-feldspar porphyry dikes	Zircon	U-Pb	205.01 $\pm$ 0.3	Logan et al. (2007)
Cariboo Pit	Monzonite	Biotite	<sup>40</sup> Ar/ <sup>39</sup> Ar	220.8 $\pm$ 1.3	Logan et al. (2007)
Northeast Zone	Crackle Breccia	Biotite	<sup>40</sup> Ar/ <sup>39</sup> Ar	205.2 $\pm$ 1.2	Logan et al. (2007)
Quarry Zone	Quartz Latite Ignimbrite	Zircon	U-Pb	196.7 $\pm$ 1.3	Logan et al. (2007)

Table 1: Summary of geochronology data available for the Mount Polley district. All ages reported with 2 sigma error.

Sample	Location	Easting	Northing	Sample Elevation (m)	FT Age (Ma $\pm$ 1 $\sigma$ )	Mean Track Length ( $\mu$ m $\pm$ 1 $\sigma$ )
WB-07-240	Quarry Zone	592240	5826217	896.5 - 898.9	65.8 +10.2 -12.1	13.16 $\pm$ 1.83
WB-05-212	Wight Pit	592448	5825389	895.5 - 898	59.1 +9.45 -11.23	13.44 $\pm$ 2.09
SE-09-81	Southeast Zone	593489	582113	897.7 - 900	45.9 +21.5 -40.3	14.38 $\pm$ 1.49

Table 2: Apatite Fission Track Ages. Easting and Northing are recorded using the UTM coordinate system, Zone 10N. Datum: NAD83.

Mineral	Closure Temperature ( $^{\circ}$ C)	Depth Range (km)
Apatite (FT)	60-110	1.8-3.8
Biotite (Ar-Ar)	300 $\pm$ 20	10.6-12.2
Hornblende (Ar-Ar)	450 $\pm$ 50	15.4-19.4

Table 3: Depth ranges corresponding to the closure temperatures of the minerals used for thermochronometry. Depth range is calculated using

$$\frac{(\text{closure temperature} - 15^{\circ}\text{C})}{25 \frac{^{\circ}\text{C}}{\text{km}}} = \text{depth (km)}$$

assuming a normal geothermal gradient of  $25 \frac{^{\circ}\text{C}}{\text{km}}$  and a surface temperature of  $15^{\circ}\text{C}$ .

### Appendix 1: Apatite Fission Track Sample Locations and Descriptions

Sample Number	Location	Hole ID	Easting	Northing	Elevation (m)	Azimuth	Dip (°C)	From (m)	To (m)	Sample Elevation (m)
258259	Wight Pit	WB-05-212	592448	5825390	1014	60	70	122.5	125	896.5 - 898.9
478048	Quarry Zone	WB-07-240	592240	5826217	988	290	88.3	90	92.5	895.5 - 898
625589	Southeast Zone	SE-09-81	593490	5832113	1088	90	70	200	202.5	897.7 - 900

Table 1: Location and Drill hole information for the three apatite fission track samples. The sample elevation is calculated using the following formulas (repeated using from the From and To distances).

$$\text{sample distance from surface} = \sin(\text{dip}) * \text{From}$$

$$\text{sample elevation} = \text{drill collar elevation} - \text{sample distance from surface}$$

Sample Number	Lithology
258259	Weakly altered monzonite - minor K-feldspar flooding, and strong red colour in K-feldspar phenocrysts. Widely spaced <5 mm wide calcite veins present.
478048	Weakly altered monzonite underlying the unconformity - minor red staining of Kfeldspar crystals. Minor hematite in the matrix.
625589	Weakly altered monzonite - fresh with no fractures or alteration. Pale pink color, fine-grained.

Table 2: Lithology description of the apatite fission track samples.

## Appendix 2: Apatite Fission Track Age Data

**Sample:**

**258259**

**Grain**

<b>Number</b>	<b>Area cm<sup>2</sup></b>	<b>FT Age (Ma)</b>	<b>95%-CI(Ma)</b>	<b>95%+CI(Ma)</b>	<b>Etch Figs.</b>	<b>Dpar (um)</b>	<b>Dper (um)</b>
1	1.6987E-05	51.14	33.41	95.68	3	2.55	0.41
2	1.3590E-05	355.31	171.62	323.74	4	2.55	0.36
3	3.8828E-05	98.96	42.68	74.63	4	2.56	0.83
4	3.1062E-05	27.31	17.66	49.79	4	1.82	0.31
5	1.3590E-05	148.01	102.76	327.63	3	2.67	0.47
6	1.2134E-05	69.16	52.79	219.28	2	2.09	0.37
7	1.2134E-05	71.61	62.11	452.10	1	2.53	0.68
8	1.4561E-05	0.00	0.00	0.00	2	2.48	0.52
9	1.7473E-05	70.98	39.36	87.76	4	2.04	0.35
10	1.4561E-05	107.56	93.29	667.44	1	1.95	0.42
11	3.1062E-05	1.92	1.66	12.53	1	2.26	0.49
12	3.1062E-05	45.36	34.65	145.05	2	2.44	0.55
13	1.4561E-05	30.40	26.37	195.77	1	2.58	0.46
14	2.3782E-05	37.87	32.84	242.92	2	2.40	0.40
15	2.9121E-05	140.77	75.04	158.74	4	2.25	0.45
16	1.2134E-05	0.00	0.00	0.00	1	2.25	0.40
17	2.4268E-05	121.45	92.77	381.38	2	2.45	0.42
18	1.7473E-05	145.20	80.44	177.87	4	2.82	0.43
19	4.3682E-05	129.63	66.89	136.76	3	2.31	0.50
20	2.9121E-05	62.56	36.29	85.83	4	2.76	0.41
21	1.7473E-05	33.97	25.95	109.04	2	1.96	0.37
22	3.3975E-05	51.78	26.73	55.01	2	2.13	0.30
23	2.9121E-05	100.52	53.56	113.67	3	2.89	0.50
24	2.9121E-05	17.65	15.32	114.96	1	2.17	0.30
25	2.9121E-05	147.96	90.06	226.14	3	2.31	0.36
26	2.9121E-05	97.37	84.43	606.04	1	2.44	0.51
27	1.2134E-05	82.40	62.88	260.06	2	2.40	0.36
28	1.4561E-05	27.25	23.64	175.81	1	2.60	0.68
29	1.4561E-05	73.29	55.94	232.17	2	1.99	0.40
30	1.7473E-05	69.22	33.73	65.45	4	2.24	0.33
31	2.4268E-05	84.28	73.06	526.91	1	2.29	0.43
32	2.4268E-05	21.31	16.28	68.54	1	1.98	0.45
33	1.4561E-05	69.24	36.90	78.53	2	2.37	0.50
34	4.8535E-05	41.98	29.21	95.37	2	2.54	0.36
35	1.4561E-05	117.78	71.61	180.16	2	3.04	0.51
36	2.9121E-05	39.31	21.79	48.71	4	2.53	0.51
37	1.2134E-05	205.73	118.71	274.71	4	3.21	0.56
38	3.1062E-05	52.64	30.49	72.04	4	2.26	0.33

Pooled age (Ma)	59.06
95%-CI (Ma)	9.45
95%+CI (Ma)	11.23
Primary Zeta	8.2727
+/- 1 sigma	0.1407
Number of Spots	36
Number of Tracks	167
Rho	0.000023284
+/- 1 sigma	8.6428E-07
Cation Isotope	43Ca
chi-squared	89.6052
Q(chi-squared)	0
Mean Dpar (um)	2.4
Mean Dper (um)	0.45
Mean [U] (ppm)	3.06
Mean [Th] (ppm)	23.21
Mean [Sm] (ppm)	66.59
Analyst Initials	Pos

**Sample:****478048****Grain**

<b>Grain Number</b>	<b>Area cm^2</b>	<b>FT Age (Ma)</b>	<b>95%-CI(Ma)</b>	<b>95%+CI(Ma)</b>	<b>Etch Figs.</b>	<b>Dpar (um)</b>	<b>Dper (um)</b>
1	1.0192E-05	95.72	49.34	101.01	4	2.43	0.45
2	1.7473E-05	67.05	43.36	121.58	3	2.19	0.40
3	1.1648E-05	61.86	47.20	196.25	3	2.13	0.35
4	9.7070E-06	119.49	58.16	112.35	4	2.14	0.39
5	1.7473E-05	142.95	67.77	127.59	4	2.00	0.37
6	2.9121E-05	31.78	16.96	36.27	4	2.25	0.45
7	3.8828E-05	72.97	34.64	65.60	4	2.02	0.25
8	2.9121E-05	64.10	41.43	116.11	2	1.82	0.42
9	1.7473E-05	66.12	29.46	52.91	4	2.16	0.32
10	1.7473E-05	97.75	50.34	102.98	4	2.18	0.30
11	2.4268E-05	61.63	32.90	70.20	3	1.90	0.25
12	1.9414E-05	84.75	49.06	115.46	3	2.07	0.41
13	1.2134E-05	212.06	136.49	372.08	3	2.27	0.36
14	1.7473E-05	65.75	31.99	62.00	3	2.16	0.49
15	1.7473E-05	54.18	35.03	98.32	3	2.03	0.46
16	2.0385E-05	40.52	24.68	62.83	4	2.02	0.37
17	2.4268E-05	35.67	19.81	44.38	4	2.18	0.42
18	9.7070E-06	131.13	75.69	176.59	2	2.31	0.42
19	2.0385E-05	35.61	15.91	28.68	4	2.10	0.35
20	9.7070E-06	121.51	60.76	120.40	4	1.95	0.33

21	1.3590E-05	32.37	24.74	104.04	2	1.90	0.36
22	1.7473E-05	84.88	43.72	89.54	4	2.21	0.36
23	2.9121E-05	84.01	44.77	95.15	3	2.25	0.37

Pooled age (Ma) 65.77  
 95%-CI (Ma) 10.23  
 95%+CI (Ma) 12.1  
 Primary Zeta 8.2727  
 +/- 1 sigma 0.1407  
 Number of Spots 23  
 Number of Tracks 181  
 Rho 0.000022651  
 +/- 1 sigma 8.4705E-07  
 Cation Isotope 43Ca  
 chi-squared 35.9997  
 Q(chi-squared) 0.0304  
 Mean Dpar (um) 2.11  
 Mean Dper (um) 0.38  
 Mean [U] (ppm) 7.09  
 Mean [Th] (ppm) 44.33  
 Mean [Sm] (ppm) 90.4  
 Analyst Initials pos

**Sample:**  
**6259909**

Grain Number	Area cm^2	FT Age (Ma)	95%-CI(Ma)	95%+CI(Ma)	Etch Figs.	Dpar (um)	Dper (um)
1	2.4268E-05	9.20	8.02	62.64	1	2.19	0.51
2	1.7473E-05	128.49	83.08	230.92	3	2.03	0.46
3	2.9121E-05	88.57	67.58	278.99	3	1.97	0.42
4	2.9121E-05	52.05	39.78	166.63	2	2.11	0.33
5	1.4561E-05	62.27	58.63	931.26	1	2.11	0.42
6	1.4561E-05	62.86	54.51	397.88	1	2.28	0.53
7	1.4561E-05	35.23	30.56	226.63	1	2.61	0.65

Pooled age (Ma) 45.94  
 95%-CI (Ma) 21.49  
 95%+CI (Ma) 40.26  
 Primary Zeta 8.2727  
 +/- 1 sigma 0.1407  
 Number of Spots 7  
 Number of Tracks 12  
 Rho 2.1534E-06

+/- 1 sigma	2.758E-07
Cation Isotope	43Ca
chi-squared	7.4312
Q(chi-squared)	0.2828
Mean Dpar (um)	2.18
Mean Dper (um)	0.48
Mean [U] (ppm)	1.92
Mean [Th] (ppm)	17.46
Mean [Sm] (ppm)	68.77
Analyst Initials	pos



Appendix 2: Apatite fission track ages are calculated using the following formulas

$$t_i = \frac{1}{\lambda} \ln(1 + \lambda \zeta_{MS} g \frac{\rho_{s,i}}{P_i})$$

Where subscript  $i$  refers to grain  $i$ ,  $t_i$  = fission-track age of grain  $i$ ,  $\lambda$  = total decay constant of  $^{238}\text{U}$ ,  $\zeta_{MS}$  =  $\zeta$ -calibration factor based on LA-ICP-MS of fission-track age standards adjusted for the sample position during the LA-ICP-MS session,  $g$  = geometry factor for spontaneous fission-tracks,  $\rho_{s,i}$  = spontaneous fission-track density for grain  $i$ , and  $P_i = (^{238}\text{U}/^{43}\text{Ca})$  for apatite grain  $i$ . The  $(^{238}\text{U}/^{43}\text{Ca})$  ratio for each data scan was calculated using the background-corrected, sum-of-Gaussian-fitted signal values for each isotope (Donelick et al., 2005).

The error is calculated using the following equation:

$$\sigma_i = \sqrt{\frac{1}{N_{s,i}} + \frac{\sigma_{p_i}^2}{p_i} + \frac{\sigma_{\zeta_{MS}}^2}{\zeta_{MS}}}$$

Where  $\sigma_i$  = the symmetrical error of the AFT single-grain,  $N_{s,i}$  = number of fission tracks counted for grain  $i$ ,  $\sigma_{p_i}$  = one standard deviation error of  $P_i$ ,  $\sigma_{\zeta_{MS}}$  = one standard deviation error of  $\zeta_{MS}$ . During each LA-ICP-MS session involving an unknown sample, at least 50 spots on the DR apatite FT age calibration standard were analyzed for the purpose of calibrating the  $^{238}\text{U}/^{43}\text{Ca}$  ratio (Donelick et al., 2005). The error of the weighted mean  $^{238}\text{U}/^{43}\text{Ca}$  ratio was calculated as follows:

$$\left( \frac{^{238}\text{U}}{^{43}\text{Ca}} \right)_{\sigma} = \left( N \left( \frac{\sigma_{\text{isotope-}^{43}\text{Ca}}}{\sum ^{43}\text{Ca}} \right)^2 + N \left( \frac{\sigma_{\text{isotope-}^{238}\text{U}}}{\sum ^{238}\text{U}} \right)^2 \right)^{1/2}$$

Where  $\Sigma^{43}\text{Ca}$  = sum of  $S_{scan}$  values for  $^{43}\text{Ca}$  above a depth of  $l_0/2$ ,  $\Sigma^{238}\text{U}$  = sum of  $S_{scan}$  values for  $^{238}\text{U}$  above a depth of  $l_0/2$ , and  $N$  = number of scans above a depth of  $l_0/2$ .

$D_{per}$  and  $D_{par}$  are the number of fission tracks measured perpendicular and parallel to the c-axis.

### Appendix 3: Apatite Fission Track Length Data

**Sample:**  
**258259**

Track Number	Length	Etch Figs.	Dpar (um)	Dper (um)	Angle to c
1	13.60	4	2.01	0.34	38.79
2	12.26	4	2.01	0.34	28.01
3	15.08	4	2.01	0.34	23.61
4	14.64	4	2.01	0.34	65.59
5	12.72	4	2.01	0.34	64.41
6	11.34	4	2.01	0.34	42.83
7	15.05	4	2.19	0.48	60.58
8	15.40	4	2.52	0.59	20.81
9	15.96	4	2.52	0.59	38.69
10	16.30	4	2.52	0.59	72.65
11	14.15	4	2.18	0.52	71.67
12	15.49	4	2.18	0.52	71.78
13	14.76	4	2.97	0.64	41.23
14	13.30	4	2.97	0.64	72.30
15	15.69	4	2.97	0.64	16.58
16	14.99	4	2.97	0.64	33.62
17	16.53	4	2.97	0.64	34.29
18	15.67	4	2.97	0.64	40.58
19	13.64	4	2.97	0.64	61.43
20	9.92	2	2.74	0.55	76.83
21	13.96	3	2.48	0.46	38.45
22	14.25	3	2.48	0.46	21.08
23	11.71	3	2.48	0.46	81.75
24	14.68	3	2.48	0.46	55.26
25	12.64	3	2.48	0.46	74.90
26	9.79	3	2.48	0.46	42.11
27	9.99	4	2.14	0.50	73.50
28	8.61	4	2.94	0.53	58.35
29	10.77	4	2.94	0.53	43.45
30	15.27	4	2.94	0.53	52.07
31	12.36	4	2.94	0.53	41.87
32	15.12	4	2.94	0.53	47.46
33	18.19	4	2.94	0.53	17.20
34	15.41	4	2.89	0.50	63.85
35	16.14	4	2.89	0.50	24.67
36	12.56	4	2.89	0.50	44.07
37	12.29	4	2.30	0.58	36.25
38	13.46	4	2.30	0.58	87.67

39	15.87	4	2.30	0.58	23.99
40	8.66	4	2.30	0.58	71.59
41	15.46	4	2.30	0.58	56.81
42	13.48	4	2.30	0.58	46.99
43	12.96	4	2.30	0.58	29.09
44	12.52	4	2.30	0.58	69.34
45	13.59	4	2.30	0.58	41.47
46	13.95	4	2.30	0.58	87.32
47	10.00	4	2.30	0.58	56.74
48	10.86	4	2.30	0.58	89.17
49	12.65	4	2.30	0.58	67.24
50	14.73	4	2.30	0.58	36.41
51	13.25	4	2.57	0.35	17.71
52	13.92	4	2.57	0.35	19.35
53	12.58	4	2.57	0.35	24.63
54	14.25	4	2.34	0.35	82.17
55	14.16	2	1.95	0.39	63.01
56	11.86	2	1.95	0.39	42.87
57	12.97	2	1.95	0.39	41.46
58	10.36	2	1.95	0.39	49.75
59	14.78	2	1.95	0.39	38.62
60	13.84	2	1.95	0.39	66.62
61	15.03	2	1.95	0.39	26.67
62	12.95	4	2.74	0.43	35.94
63	7.68	4	2.74	0.43	88.94
64	13.00	4	2.74	0.43	58.37
65	10.27	4	2.74	0.43	76.51
66	9.84	4	2.74	0.43	62.31
67	6.86	4	2.74	0.43	28.14
68	12.01	4	2.74	0.43	73.00
69	13.06	4	2.74	0.43	59.63
70	15.45	4	3.28	0.46	25.82
71	14.75	4	3.28	0.46	33.68
72	15.18	4	3.28	0.46	52.61
73	12.41	4	3.28	0.46	45.75
74	13.03	4	3.28	0.46	61.64
75	10.46	4	3.28	0.46	70.62
76	15.99	4	2.72	0.51	71.25
77	13.95	4	2.72	0.51	64.36
78	14.34	4	2.53	0.46	50.53
79	11.08	4	2.53	0.46	54.00
80	13.56	4	2.53	0.46	43.25
81	15.65	4	2.53	0.46	34.74

82	9.90	4	2.90	0.73	73.92
83	9.51	4	2.66	0.58	56.28
84	14.84	4	2.66	0.58	72.02
85	15.58	4	2.03	0.41	54.22
86	13.09	4	2.03	0.41	63.97
87	13.76	4	2.03	0.41	33.85
88	12.07	4	2.03	0.41	69.08
89	16.28	4	2.03	0.41	30.83
90	13.43	4	2.03	0.41	46.49
91	14.78	4	2.03	0.41	66.32
92	14.38	3	2.31	0.42	88.56
93	15.10	4	2.54	0.43	43.48
94	13.37	4	2.54	0.43	49.73
95	13.95	4	2.54	0.43	38.88
96	10.93	4	2.54	0.43	61.98
97	14.30	4	2.54	0.43	33.70
98	10.28	4	2.54	0.43	70.04
99	10.92	4	2.54	0.43	81.11
100	14.07	4	2.54	0.43	33.45
101	11.22	4	2.54	0.43	63.29
102	12.58	4	2.54	0.43	66.24
103	14.87	4	2.54	0.43	39.71
104	15.13	4	2.54	0.43	53.13
105	15.90	4	2.54	0.43	37.82
106	14.95	4	2.63	0.68	56.87
107	15.42	4	2.63	0.68	5.87
108	14.48	4	2.63	0.68	71.65
109	13.79	4	2.35	0.56	63.65
110	14.61	4	2.35	0.56	61.12
111	7.46	4	2.35	0.56	78.25
112	14.96	4	2.35	0.56	37.54
113	14.23	4	2.77	0.50	52.21
114	11.99	4	3.14	0.46	52.85
115	16.57	4	3.14	0.46	42.47
116	13.49	4	3.14	0.46	51.23
117	15.18	4	3.14	0.46	48.04
118	14.79	4	2.56	0.59	56.41
119	11.64	4	2.56	0.59	86.39
120	15.13	4	2.70	0.63	65.72
121	10.89	4	2.70	0.63	72.99
122	14.33	4	2.66	0.39	54.73
123	13.08	4	2.66	0.39	81.85
124	15.74	4	2.03	0.34	57.40

125	15.13	4	2.03	0.34	64.99
126	10.89	4	2.47	0.44	56.91
127	13.83	4	2.47	0.44	44.44
128	13.83	4	2.47	0.44	35.82
129	12.56	4	2.47	0.44	52.88
130	11.84	4	2.72	0.52	51.82
131	12.95	4	2.72	0.52	66.26
132	10.08	4	2.72	0.52	51.45
133	13.05	3	2.60	0.46	75.79
134	15.25	3	2.60	0.46	7.60
135	13.56	4	2.43	0.41	74.10
136	16.14	4	2.68	0.46	52.76
137	15.11	4	2.68	0.46	28.79
138	11.80	4	2.33	0.46	49.61
139	15.92	4	2.33	0.46	48.32
140	15.09	4	2.33	0.46	65.55
141	14.61	4	2.33	0.46	52.47
142	16.05	4	2.33	0.46	40.43
143	12.66	4	2.33	0.46	55.68
144	15.96	4	2.33	0.46	42.13
145	12.81	4	2.64	0.49	41.73
146	14.19	4	2.64	0.49	52.49
147	17.67	4	2.64	0.49	42.49
148	14.83	4	2.64	0.49	70.73
149	8.87	2	2.27	0.53	55.39
150	12.45	2	2.27	0.53	60.25
151	13.80	2	2.27	0.53	80.23
152	15.39	4	2.58	0.46	28.73
153	14.98	4	2.58	0.46	33.64
154	15.01	4	2.58	0.46	48.83
155	12.55	4	2.58	0.46	47.86
156	15.98	2	2.75	0.49	37.61
157	11.39	2	2.75	0.49	59.91
158	15.43	4	2.66	0.41	41.90
159	15.31	4	2.66	0.41	76.05
160	11.10	4	3.28	0.84	42.87
161	12.84	4	3.28	0.84	55.68
162	14.69	4	3.28	0.84	85.71
163	11.41	4	3.28	0.84	57.56
164	14.43	4	3.28	0.84	51.79
165	16.73	4	3.28	0.84	60.36
166	16.45	4	3.28	0.84	72.94
167	11.47	4	3.28	0.84	62.33

168	11.01	4	2.96	0.80	57.57
169	15.90	4	2.96	0.80	40.62
170	14.77	4	2.96	0.80	57.10
171	15.54	3	3.50	1.05	23.67
172	12.44	4	2.71	0.71	53.33
173	11.46	4	2.71	0.71	50.61
174	14.97	4	2.71	0.71	61.72
175	11.45	4	2.35	0.42	78.01
176	10.97	4	2.35	0.42	66.61
177	15.77	3	2.13	0.46	33.38
178	10.11	3	2.13	0.46	52.78
179	12.54	3	2.13	0.46	63.91
180	12.27	3	2.13	0.46	59.28
181	12.35	4	2.63	0.46	36.55
182	10.12	4	2.63	0.46	56.90
183	13.51	4	2.63	0.46	65.27
184	10.41	4	2.35	0.54	80.87
185	13.17	4	2.35	0.54	43.20
186	8.32	4	2.35	0.54	84.24
187	14.26	4	2.35	0.54	56.77
188	13.13	4	2.35	0.54	39.25
189	15.85	4	2.35	0.54	34.08
190	12.09	4	2.35	0.54	74.19
191	12.80	4	2.59	0.48	62.94
192	15.76	4	2.59	0.48	22.99
193	16.52	4	2.59	0.48	45.31
194	12.87	4	2.59	0.48	56.55
195	13.87	4	2.59	0.48	48.47
196	14.26	4	2.59	0.48	80.37
197	13.24	4	2.59	0.48	66.60
198	15.19	4	2.59	0.48	31.30
199	13.40	4	2.59	0.48	65.98
200	11.47	2	2.29	0.36	60.96

Mean (um)	13.44
Std. error (um)	0.15
Std. dev (um)	2.09
Skewness	-0.6168
Kurtosis	0.0237
Number tracks	200
Mean Dpar (um)	2.56
Mean Dper (um)	0.51
Mean [U] (ppm)	14.73

Mean [Th] (ppm) 65.12  
Mean [Sm]  
(ppm) 69.34  
Analyst Initials pos

**Sample: 478048**

Track Number	Length	Etch Figs.	Dpar (um)	Dper (um)	Angle to c
1	11.80	4	2.31	0.43	55.09
2	12.52	4	2.31	0.43	55.84
3	13.50	4	2.23	0.49	44.06
4	7.25	4	2.23	0.49	88.19
5	14.08	4	2.23	0.49	53.43
6	12.31	4	2.23	0.49	44.35
7	13.14	4	2.23	0.49	39.91
8	15.05	4	2.23	0.49	41.49
9	13.17	4	2.22	0.35	41.29
10	14.74	4	2.22	0.35	56.09
11	15.91	4	2.22	0.35	20.39
12	13.69	3	2.18	0.42	53.35
13	14.00	3	2.18	0.42	36.82
14	5.25	3	2.18	0.42	64.54
15	14.87	4	2.10	0.46	56.43
16	10.76	4	2.10	0.46	24.87
17	11.48	4	2.10	0.46	55.44
18	11.71	4	2.10	0.46	34.96
19	12.00	4	2.10	0.46	79.72
20	13.70	4	2.10	0.46	59.39
21	12.77	4	2.13	0.50	53.18
22	13.84	4	2.13	0.50	51.90
23	13.95	4	2.13	0.50	71.81
24	14.70	3	2.28	0.33	48.00
25	13.90	3	2.28	0.33	62.22
26	13.61	3	2.28	0.33	36.36
27	13.52	3	2.28	0.33	69.39
28	14.31	3	2.28	0.33	44.00
29	13.54	3	2.28	0.33	67.45
30	8.49	3	2.28	0.33	82.49
31	8.61	4	2.51	0.41	67.75
32	13.36	4	2.51	0.41	30.28
33	13.41	4	2.51	0.41	58.32
34	15.30	2	2.02	0.38	61.89
35	14.50	4	1.75	0.30	84.94



36	11.48	4	1.75	0.30	84.82
37	12.02	4	1.75	0.30	57.22
38	15.09	4	1.75	0.30	33.65
39	13.44	3	2.01	0.40	61.21
40	15.21	3	2.01	0.40	70.71
41	12.08	4	2.05	0.39	38.50
42	11.97	4	2.05	0.39	56.57
43	11.28	4	2.05	0.39	56.30
44	15.53	4	2.05	0.39	26.59
45	11.40	4	2.20	0.40	85.49
46	14.75	4	2.20	0.40	50.12
47	14.48	4	2.20	0.40	51.33
48	14.59	4	2.20	0.40	74.18
49	12.92	4	2.20	0.40	54.57
50	13.09	4	2.20	0.40	83.12
51	14.93	4	2.20	0.40	72.20
52	12.93	4	2.46	0.41	35.64
53	15.53	4	2.46	0.41	47.37
54	14.28	4	2.46	0.41	32.62
55	12.54	4	2.46	0.41	39.11
56	15.51	3	2.04	0.45	31.22
57	14.37	3	2.04	0.45	23.40
58	14.06	4	1.85	0.35	62.87
59	11.01	4	1.85	0.35	79.33
60	11.90	4	1.85	0.35	62.52
61	10.90	4	1.85	0.35	59.21
62	14.26	4	1.85	0.35	57.74
63	9.84	4	1.85	0.35	43.70
64	10.60	4	1.85	0.35	84.72
65	14.21	4	1.85	0.35	47.46
66	14.19	4	2.30	0.37	75.59
67	14.68	3	2.03	0.36	41.46
68	15.65	4	2.00	0.39	59.00
69	13.71	4	2.00	0.39	83.61
70	13.90	4	2.00	0.39	39.42
71	11.66	2	2.23	0.40	48.93
72	14.17	2	2.23	0.40	34.29
73	12.40	2	2.23	0.40	68.97
74	12.82	2	2.23	0.40	25.61
75	12.71	4	2.10	0.42	44.29
76	13.87	4	2.07	0.35	58.08
77	11.60	4	2.07	0.35	70.77
78	10.29	4	2.20	0.32	60.62

79	15.29	4	2.20	0.32	36.06
80	12.11	4	1.91	0.36	27.84
81	12.16	4	1.91	0.36	67.61
82	9.51	3	2.14	0.38	50.70
83	11.28	3	2.14	0.38	67.06
84	11.59	3	2.14	0.38	78.22
85	14.97	4	2.03	0.40	31.54
86	14.78	4	2.03	0.40	74.63
87	14.48	4	2.03	0.40	28.65
88	8.68	4	2.03	0.40	78.23
89	12.24	3	2.31	0.49	66.44
90	10.71	3	2.31	0.49	70.08
91	12.78	3	2.31	0.49	66.78
92	14.88	3	2.31	0.49	51.42
93	12.31	3	2.31	0.49	76.16
94	14.55	4	2.42	0.46	63.41
95	11.92	4	2.42	0.46	65.42
96	10.27	4	2.42	0.46	54.20
97	13.26	4	2.42	0.46	70.42
98	15.41	4	2.42	0.46	59.10
99	12.54	4	2.11	0.38	72.83
100	14.09	4	2.11	0.38	37.91
101	14.89	4	2.11	0.38	51.01
102	14.27	4	2.11	0.38	33.33
103	14.92	4	2.44	0.32	53.00
104	13.87	4	2.44	0.32	43.61
105	13.06	2	1.97	0.35	62.79
106	13.43	2	1.97	0.35	81.39
107	11.44	2	1.97	0.35	87.43
108	13.59	2	1.97	0.35	56.85
109	11.90	2	1.97	0.35	44.49
110	9.37	2	1.97	0.35	64.62
111	13.75	2	1.97	0.35	62.84
112	15.23	2	1.97	0.35	39.74
113	14.34	2	1.97	0.35	77.43
114	15.26	2	1.97	0.35	30.69
115	15.26	4	2.61	0.41	82.38
116	16.61	4	2.61	0.41	28.42
117	11.85	4	2.16	0.35	82.68
118	13.58	4	2.16	0.35	32.17
119	12.76	4	2.16	0.35	35.12
120	10.38	4	1.81	0.33	65.99
121	13.83	3	2.36	0.46	36.57

122	13.28	4	2.56	0.37	76.83
123	12.80	4	2.56	0.37	68.22
124	12.82	4	2.56	0.37	46.74
125	11.48	4	2.56	0.37	63.64
126	13.17	4	2.56	0.37	69.88
127	12.45	4	2.56	0.37	32.75
128	12.32	4	2.56	0.37	53.95
129	14.22	4	2.56	0.37	26.54
130	14.88	4	2.56	0.37	59.24
131	15.53	4	2.56	0.37	54.29
132	13.84	4	2.56	0.37	60.46
133	14.41	4	2.56	0.37	28.96
134	15.23	4	2.56	0.37	66.87
135	15.54	4	2.05	0.35	71.91
136	14.51	4	2.05	0.35	27.11
137	12.58	4	2.05	0.35	77.55
138	10.74	4	2.15	0.56	54.53
139	13.07	4	2.15	0.56	79.68
140	10.55	4	2.15	0.56	54.04
141	13.81	4	2.15	0.56	70.28
142	13.94	4	2.15	0.56	62.90
143	10.26	4	1.94	0.38	63.86
144	13.29	4	1.94	0.38	35.75
145	10.19	4	1.94	0.38	81.40
146	10.22	4	1.94	0.38	43.30
147	11.79	4	1.94	0.38	55.46
148	14.45	4	1.96	0.34	73.46
149	10.47	4	1.96	0.34	41.60
150	12.80	4	2.20	0.33	65.08
151	15.52	4	1.90	0.35	51.64
152	12.49	4	1.90	0.35	59.17
153	14.24	4	1.90	0.35	26.18
154	14.60	4	1.90	0.35	43.40
155	13.72	4	1.90	0.35	71.44
156	12.94	4	1.90	0.35	41.80
157	14.30	4	1.90	0.35	74.79
158	12.59	4	1.90	0.35	43.30
159	14.07	4	1.90	0.35	69.46
160	14.22	4	2.37	0.35	33.69
161	14.70	4	2.15	0.31	54.12
162	15.24	4	2.38	0.35	42.70
163	14.25	4	2.38	0.35	57.42
164	10.58	4	2.23	0.36	88.37

165	14.50	4	1.92	0.34	64.83
166	13.92	4	1.92	0.34	45.37
167	13.91	4	1.92	0.34	60.11
168	12.95	4	1.92	0.34	47.58
169	13.82	4	1.92	0.34	51.49
170	16.00	3	2.11	0.48	48.59
171	13.30	3	2.11	0.48	71.73
172	16.08	4	2.47	0.48	46.54
173	12.88	4	2.47	0.48	52.96
174	18.09	4	2.47	0.48	12.74
175	13.51	4	2.25	0.31	57.71
176	12.69	4	2.25	0.31	76.88
177	13.90	4	2.25	0.31	62.02
178	12.11	4	2.25	0.31	49.85
179	13.32	4	2.25	0.31	39.39
180	12.15	4	2.25	0.31	54.96
181	10.60	4	2.25	0.31	56.19

Mean (um) 13.16  
 Std. error (um) 0.14  
 Std. dev (um) 1.83  
 Skewness -0.8744  
 Kurtosis 1.6431  
 Number tracks 181  
 Mean Dpar (um) 2.16  
 Mean Dper (um) 0.39  
 Mean [U] (ppm) 8.17  
 Mean [Th] (ppm) 34.39  
 Mean [Sm] (ppm) 102.22  
 Analyst Initials pos

**Sample:**  
**6255909**

Track Number	Length	Etch Figs.	Dpar (um)	Dper (um)	Angle to c
1	15.98	4	2.10	0.34	53.23
2	14.47	4	2.10	0.34	76.01
3	13.27	4	2.30	0.44	48.18
4	14.90	4	2.59	0.35	87.35
5	14.53	4	2.59	0.35	24.33
6	11.18	4	2.25	0.50	49.39
7	15.08	4	2.39	0.35	47.84
8	13.81	4	2.39	0.35	67.62

9	10.56	4	2.39	0.35	75.32
10	14.13	4	2.35	0.40	40.35
11	12.66	4	2.50	0.47	51.68
12	12.85	4	2.50	0.47	49.22
13	13.91	4	2.01	0.30	89.21
14	14.74	4	2.22	0.35	50.64
15	14.08	4	2.22	0.35	36.58
16	13.52	4	3.04	0.41	58.54
17	11.29	4	2.54	0.41	54.86
18	12.83	4	2.54	0.41	45.95
19	13.16	4	2.21	0.51	51.51
20	15.40	4	2.39	0.35	35.52
21	14.80	4	2.39	0.35	35.56
22	15.17	4	2.30	0.36	42.24
23	14.19	4	2.30	0.36	52.42
24	15.65	4	2.30	0.36	41.39
25	11.20	4	2.30	0.36	85.25
26	16.36	4	2.30	0.36	50.30
27	14.59	4	2.15	0.39	50.81
28	13.27	4	2.15	0.39	50.42
29	16.10	4	1.91	0.32	49.87
30	15.45	4	1.91	0.32	74.66
31	14.58	4	2.20	0.41	68.89
32	15.56	4	2.47	0.47	74.63
33	15.12	4	2.47	0.47	24.33
34	14.91	2	2.37	0.40	38.76
35	11.02	3	2.05	0.45	54.26
36	13.52	3	2.05	0.45	53.72
37	13.85	4	2.53	0.36	63.64
38	16.23	4	2.61	0.44	32.46
39	15.60	4	2.61	0.44	39.91
40	15.91	4	2.17	0.41	83.78
41	13.87	4	2.48	0.46	25.37
42	13.13	3	2.25	0.44	62.91
43	12.44	3	2.25	0.44	55.21
44	14.37	4	2.38	0.50	70.63
45	14.90	4	2.25	0.44	44.98
46	13.78	4	2.25	0.44	62.63
47	15.92	4	2.79	0.46	51.34
48	15.56	4	2.79	0.46	61.67
49	16.73	4	2.79	0.46	68.80
50	15.31	4	2.18	0.38	26.70
51	16.04	4	2.65	0.50	52.70

52	14.94	4	2.65	0.50	47.75
53	15.80	4	2.57	0.45	42.14
54	16.17	4	2.41	0.36	60.20
55	15.86	4	2.41	0.36	26.62
56	14.85	3	2.49	0.57	54.02

Mean (um)	14.38
Std. error (um)	0.2
Std. dev (um)	1.49
Skewness	-0.7776
Kurtosis	-0.0582
Number tracks	56
Mean Dpar (um)	2.37
Mean Dper (um)	0.41
Mean [U] (ppm)	2.68
Mean [Th] (ppm)	20.85
Mean [Sm] (ppm)	65.23
Analyst Initials	pos